Fluctuations of dynamic systems

James Cowie Reid

BSc. (Hons.), LLB (Hons.)

A thesis submitted for the degree of Doctor of Philosophy of
The Australian National University

August 2006

Research School of Chemistry

Australian National University

Statement of Originality

This thesis represents my own original work. Where the work of others has been used, it is cited appropriately. In a few sections, collaborations may make it unclear where work is not by the author. In Chapter 4, the deterministic results, and the experimental data for the three optical trapping systems were primarily the work of D.M. Carberry, G.M Wang and others. The stochastic analysis of the theoretical and experimental data in this chapter are mine. In Chapter 5, I undertook the original experiments for the ramp system, however the final data set used was generated by G.M. Wang using my experimental parameters. All data analysis of the experiment, and all other results in the chapter, and in the rest of the thesis are my own work.

....

James Reid Date

Acknowledgements

A PhD feels less like a qualification and more like a lifestyle: I would like to take the opportunity to thank those people who supported mine. Without these people and organisations the work may have turned into a lifetime.

- My supervisory pannel: E. Sevick, D. Evans, and D. Searles.
- Those who helped me with the experiments: G. Wang and D. Carberry.
- Those in my group who helped me over the years: S. Williams, E. Mittag and J. Bright.
- Members within the school who provided much needed support: C. Delfs, G. Lindsell, P. Cohen, A. Heerdegan.
- Those organisations that provided money or support, both directly and indirectly: APS, ARC, CosNET, RACI.
- The Research School of Chemistry and its staff, and the Australian National University.

I would also like to thank those who provided inspiration and encouragement outside of my PhD that enabled me to finally complete it.

- To my parents for all of their support and love in the past and present.
- To my friends, a list too long to place of people who have believed in me through good and through bad. You know who you are, and what you have given, and I thank you.
- To those teachers and lecturers who provided me the skills I needed to achieve.

Finally, I would like to thank my wife, Chantelle for taking this journey with me.

Abstract

The fluctuation theorem quantifies the distribution of reversible and irreversible system trajectories, while the work relation connects a weighted average of the work with the free energy change for a system. Both are unusual in that they apply exactly to non-equilibrium thermodynamic systems. The aim of this work is to study the connection between these two theorems, both in theory and application.

First, a general derivation of the fluctuation theorem and work relation is developed and a mathematical connection is made between their arguments, dissipation and work. We then use this approach to apply these relations to a system based on optical tweezers trapping a colloid in solution. This system is well described using both deterministic and stochastic dynamics, and enables us to undertake a number of different experiments that explore the relationship between these two theorems. These experiments verify the fluctuation theorem and work relation, but also show how the details of the experiment and the dynamics used to analyse it affect the application of these theorems and the information they provide.

Contents

List of Figures

Chapter 1

Introduction

There are some ideas that are so fundamental to a field that we take them for granted. In thermodynamics, one such concept is equilibrium. A system in equilibrium with its surroundings has the same properties regardless of how it was made or when we observe it. Equilibrium systems therefore act as a reference point for a variety of thermodynamic properties. When one examines systems out of equilibrium, there are still quantities that can be measured, but few theorems to describe their behaviour, and fewer still that are exact. In the last decade however, a number of exact non-equilibrium theorems have been developed: the fluctuation relations. These relations provide useful information about experimental systems, and answer lingering theoretical questions in thermodynamics. Surprisingly, these non-equilibrium relations can also provide information about the properties of systems in equilibrium. It is the theory and application of these relations that shall be the focus of this dissertation.

Thermodynamics seems to give a directionality to time that is absent in simple mechanics. Under classical mechanics, the equations of motion for an object are symmetric in that they are the same going forwards in time as going backwards; or to put it another way, you cannot tell whether time is flowing forwards or backwards just by looking at the motion of an object. Thermodynamics however is not symmetric with regards to the directionality of time: entropy increases going forwards in time, and decreases going backwards in time. Entropy corresponds to the dissipation of usable energy into heat. With a thermodynamic process, such as tea exchanging heat with the air, we can see the direction of time as the tea will always cool if time

flows forwards, and always warm if time flows backwards, with the work available due to the temperature difference between the tea and the air lost. This is embodied in the second law of thermodynamics: the overall entropy change for a process is always greater or equal to zero.

In the late nineteenth century, a number of physicists, most notably Boltzmann, Gibbs, and Maxwell, developed a statistical approach to thermodynamics. [1] Under statistical mechanics, we represent a thermodynamic system as a collection of objects (usually atoms or molecules) that move according to classical mechanics. In 1876, Loschmidt observed that this creates a paradox in thermodynamics: the individual motion of the particles is governed by classical mechanics and is symmetric in time, but we never see time symmetric behaviour in the overall system. [2] The development of a complete answer to this question will lead us to the first of our non-equilibrium relations.

The starting point to answering Loschmidt's paradox lies in the construction of statistical mechanics. Statistical mechanics treats a system as a set of indistinguishable components with a set of discrete states, a good example being a set of coin tosses. Each configuration of component states represents a microstate of the system, and the sum or average of the component states represents the macrostate of the system. Macrostates represent the observables of the system, and each macrostate of the system can correspond with a number of different microstates. For example, if we take a system of two coin tosses, each coin can be heads or tails, and so there are four possible microstates and three possible macrostates. As the size of the system increases, the number of microstates of the system increases much faster than the number of macrostates, and the distribution becomes more and more peaked around the most likely value. Taking our coin example, if we increase the number of coins to four, we have 16 microstates and only 5 macrostates, and the most likely outcome, half heads and half tails, is six times more likely then all heads. As the system gets bigger and bigger, extreme behaviour becomes less and less likely. In the thermodynamic limit, that is for a system of infinite size over infinite time, there is no extreme behaviour. What this means for Loschmidt's paradox is that for a system in the thermodynamic limit, we don't observe anti-entropic results because

they are statistically insignificant compared to the entropic outcome. We will always see the system dissipate energy to heat, never observe the system turn heat directly into work. However, for finite-size systems, this is an incomplete solution.

In 1994, over a century after the development of statistical mechanics, the fluctuation theorem provided a complete mathematical solution to Loschmidt's paradox, [3] that generalised the statistical solution to finite size systems. Rather than look at the average over all the system trajectories over a system change, it explicitly compares the probability of trajectories with a particular entropic result with the probability of trajectories exhibiting the equivalent anti-entropic result in finite size, non-equilibrium systems. What Evans and others discovered was that the entropic changes were always more probable than the anti-entropic changes in the distribution of results, [3, 4] and the difference in probability is exponentially connected to the magnitude of the entropy. This means that as systems get larger, and the average system change becomes more entropic, the relative likelihood of seeing anti-entropic behaviour decreases. The answer to Loschmidt's paradox is therefore that we can observe anti-entropic behaviour, but the larger the system or the more anti-entropic the behaviour, the less likely we are to see it. This is interesting, as it means that if we study finite size systems, we will not only observe unusual behaviour, but be able to quantify how often we will see it using the fluctuation theorem. What the fluctuation theorem does not answer is the question of causation: why does this entropy imbalance exist going forward in time? [5]

The fluctuation theorem quantifies the behaviour of a system over time. Often with thermodynamic systems, if we change the state of a system away from equilibrium, it will relax to a new equilibrium state over a period of time. In this case, we are often interested in the difference in properties of the initial and final equilibrium states, rather than the distribution of trajectories between them. Our second non-equilibrium relation, the work relation, uses the distribution of work due to this change of state to measure the difference in the free energy between the two states. The free energy is of great practical importance as it is a measure of the relative stability of the two equilibrium distributions.

The traditional method for measuring the free energy difference between two

equilibrium states is to measure the work done over a reversible path. [1] A reversible path is created by changing the system of interest infinitely slowly, so that the system is always in equilibrium. This is not always practical for an experimental system; however if a system is changed in a non-reversible manner, the value of the work measured will vary from measurement to measurement, and not be directly comparable to the free energy. In 1997, Jarzynski proposed the work relation to relate the distribution of work values with the change in free energy over an irreversible system change. [6, 7] It relates the average of the exponential of the work to the exponential of the free energy. This means that rather than sample one infinitely long system trajectory, the fluctuations of a number of finite length trajectories can be measured.

Both the fluctuation theorem and the work relation are applicable to finite size non-equilibrium systems. Both represent important advances in thermodynamics. Interestingly, they are also deeply connected. In 1999, Crooks showed that a rearrangement of the work relation, the Crooks relation, was equivalent to the fluctuation theorem under certain circumstances. [8] Subsequent work has generalised this connection. [9] The primary purpose of this thesis is to explore this connection between these two relations, and to test them on small, non-equilibrium systems. Along the way we will briefly discuss other fluctuation relations.

The experimental system we have chosen to study with our fluctuation relations is the optical tweezers system. Optical tweezers use laser beams to move and manipulate physical objects. [10–14] This is possible because light carries a small amount of momentum that can be imparted to matter. The particular system we will study uses a laser to constrain an extremely small latex particle ($\sim 6\mu$m) that is suspended in water. The laser exerts a harmonic potential on the particle tying it loosely to a point in space. Experiments can be undertaken by manipulating the laser and measuring the particle position.

The optical trapping experiment is a very simple system to treat theoretically: the equilibrium states of this system are well known and can be easily moved between. More importantly, it has a couple of traits that make it particularly suitable for study of the fluctuation relations. In an optical trapping system, the particle

exhibits Brownian motion, the spontaneous movement of the particle due to fluctuations in the water. These spontaneous fluctuations can display the anti-entropic behaviour that can be quantified by the fluctuation theorem. In addition, because the equilibrium states are well known, the differences in free energy between them are well known. This provides an easy check for testing the work relation.

Optical trapping experiments are also interesting in that they can be described with two different sets of dynamics. The first approach, deterministic dynamics, represents every component in the optical tweezers system, the latex particle and all of the water molecules, and traces their movement using standard equations of motion. This approach is the same approach that statistical mechanics is based upon, and the original dynamic framework under which the fluctuation relations were proven. The second approach, stochastic dynamics, represents only the colloid particle explicitly, and represents the water molecules as a drag term and a random term in the equations of motion. This description was developed to simplify the treatment of Brownian systems, such as the optical tweezers system, by reducing them to a one body problem.

The actual experiments we will approach in this work break into two categories. The first set are experiments designed to test the fluctuation theorem. Optical tweezers were used in the first experimental demonstration of the fluctuation theorem, [15] and subsequently to improve upon the results. [16, 17] We will treat these experiments using both stochastic and deterministic dynamics and it will also be noted how the work relation applies to these relations. The second category is the ramp experiment. This is an experiment designed to test the work relation, that can also be used to test the fluctuation theorem and some miscellaneous relations.

As can be seen, the overall aim of this project is an investigation of the fluctuation relations. Within this there are a number of distinct threads of work that span a variety of interests. We will examine the fluctuation theorem from a general theoretical framework, and in application to experiment. We will treat the experiments both deterministically and stochastically. While these areas of interest are often segregated, we use all of them to elucidate these relations.

Bibliography

[1] P. Atkins, *Physical Chemistry, Fifth Edition* (Oxford University Press, 1994).

[2] E. Broda, *Ludwig Boltzmann, Man-Physicist-Philosopher* (Ox Bow Press, 1983).

[3] D. J. Evans, D. J. Searles, *Phys. Rev. E* **50**, 1645 (1994).

[4] D. J. Evans, E. G. D. Cohen, G. P. Morriss, *Phys. Rev. Lett.* **71**, 2401 (1993).

[5] D. J. Evans, D. J. Searles, *Adv. Phys.* **51**, 1529 (2002).

[6] C. Jarzynski, *Phys. Rev. E* **56**, 5018 (1997).

[7] C. Jarzynski, *Phys. Rev. Lett.* **78**, 2690 (1997).

[8] G. Crooks, *Phys. Rev. E* **60**, 2721 (1999).

[9] J. C. Reid, E. M. Sevick, D. J. Evans, *Europhysics Letters* **72**, 725 (2005).

[10] A. Ashkin, *Phys. Rev. Lett.* **24**, 156 (1970).

[11] A. Ashkin, J. M. Dziedzic, J. E. Bjorkholm, S. Chu, *Opt.Lett.* **11**, 288 (1986).

[12] A. Ashkin, *Proc. Nat. Acad. Sci. USA* **94**, 4853 (1997).

[13] D. G. Grier, *Nature* **424**, 810 (2003).

[14] S. B. Smith, Y. Cui, C. Bustamante, *Science* **271**, 795 (1996).

[15] G. M. Wang, E. M. Sevick, E. Mittag, D. J. Searles, D. J. Evans, *Phys. Rev. Lett.* **89**, 050601 (2002).

[16] D. M. Carberry, J. C. Reid, G. M. Wang, E. M. Sevick, D. J. Searles, D. J. Evans, *Phys. Rev. Lett.* **92**, 140601 (2004).

[17] G. M. Wang, J. C. Reid, D. M. Carberry, D. R. M. Williams, E. M. Sevick, D. J. Evans, *Phys. Rev. E* **71**, 046142 (2005).

Chapter 2

The Fluctuation Relations

The fluctuation theorem (FT) and work relation (WR) are called fluctuation relations because they measure and quantify fluctuating quantities for non-equilibrium systems. These two relations otherwise seem to have little in common: the FT quantifies the entropic behaviour of individual system trajectories, while the WR measures the free energy change for a system by taking a biased average of the work over an ensemble of system trajectories. When the derivations for these relations are looked at together, they are striking similar. In this chapter, we will define these relations, and then we will rigorously derive these relations in the most general way for a dynamical thermodynamic system. This will provide an opportunity to discuss the application of the two relationships, as well as demonstrating the intimate connection between them.

It is important to note that the derivations presented in this chapter are not the original derivations of these fluctuation relations. The FT was originally derived in 1994 by Evans and Searles for thermostated deterministic systems. [1] The work relation was first developed and demonstrated by Jarzynski in 1997, [2,3], and later proved by Evans for the same systems as the FT. [4] Subsequent proofs for a variety of different systems have been developed, such as for other deterministic systems, [5], stochastic systems, [6–8] and quantum systems. [9] The method presented in this chapter follows on from the derivations of Evans, but is for non-specific dynamics and systems.

2.0.1 The Fluctuation Theorem

The FT quantifies the fluctuations in a thermodynamic system via a dissipation function, Ω. [1, 5] The dissipation function is a novel quantity that does not correspond strictly with either work or heat. [5,14–16] It is a dimensionless energy quantity, similar to entropy production, that is measured along a system trajectory over time.* This means that rather than get the same value whenever we measure the system, as we would for an ensemble quantity, we instead get a distribution of values for the dissipation function for the system.

The FT shows that the probabilities of trajectories with opposite values of the dissipation function are related in an exponential fashion,

$$\frac{P(\Omega)}{P(-\Omega)} = e^{\Omega}. \tag{2.1}$$

The FT describes the relationship between the positive and negative sides of the distribution of the dissipation function, that is the symmetry of the distribution. It does not however, fully define this distribution: the overall shape will depend on the details of the system, figure 2.1. The FT can also be expressed in terms of an ensemble average, known as the partition identity (PI), [10–13]

$$\langle e^{-\Omega} \rangle = 1. \tag{2.2}$$

The FT provides information about the distribution of the trajectories, rather than the average of the trajectories. However, if we take the ensemble average of the dissipation function, we derive an expression similar to the Second Law of Thermodynamics, [17]

$$\langle \Omega \rangle \geq 0. \tag{2.3}$$

The relationship between the FT and this average means that individual system trajectories can exhibit positive or negative dissipation, but the behaviour of the ensemble will tend to be positive. In order to understand what this means in terms of the evolution of a system, we need to have a physical understanding of what

*Indeed, in the weak field regime near equilibrium, the ensemble average of the dissipation function and the entropy production are the same, $\langle \Omega \rangle = \langle \Sigma \rangle$.

the dissipation function is, and we will be exploring this in more detail later in the chapter, Section 2.1. However, what the FT does tell us is that an individual trajectory will not always exhibit the same characteristics as the ensemble behaviour, but the odds of observing these unusual trajectories are lower than observing the expected behaviour.

2.0.2 The Work Relation

The WR predicts that the difference in the free energy, between two system states is related to the distribution of a fluctuating thermodynamic variable, work, over a transformation between those system states. [2,3] The distribution of work is related to the free energy change by a weighted ensemble average:

$$\langle e^{-\beta \Delta W} \rangle = e^{-\beta \Delta A}, \tag{2.4}$$

where $\beta = 1/k_B T$, T is the temperature the system is thermostated to, ΔW is the work done, and ΔA is the Helmholtz free energy change. The WR is interesting because it gives information about the equilibrium states of a system from the non-equilibrium trajectories between them. This is in contrast with the traditional methods of measuring free energy using work, which require equilibrium at all times. In the quasi-static approach a path between states is chosen such that the system is always in equilibrium, usually by changing the system infinitely slowly, and the work done is equal to the free energy change. An alternative approach is the instantaneous sampling method, where an ensemble average is taken over an initial equilibrium distribution of the exponential of the work required to instantly change between the initial and final state of the system. The WR bridges the gap between these two approaches by allowing the choice of any path to analyse the free energy change.

We can also express the work relation in a form more like the FT, known as the Crooks relation (CR), [16, 18]

$$\frac{P_{\lambda(t)}(\beta \Delta W)}{P_{\lambda^*(t)}(-\beta \Delta W)} = e^{\beta \Delta W - \beta \Delta A}. \tag{2.5}$$

Figure 2.1: **Two figures that show the relationship between the system distribution and the fluctuation theorem.** In figure 2.1a, we plot probability density, p, vs dissipation, Ω for a Gaussian distribution (**black**) and an exponential distribution (blue) that obey the FT. The FT describes the relationship between the positive and negative halves of a distribution, but as can be seen, more than one distribution can satisfy this relationship. If two relations obey the FT, and the probability density of the distributions is equal at a positive value of the dissipation, such as at $\Omega = 0.5$ (red) in figure 2.1a, then from the definition of the FT the probability density of the distributions must also be equal at the negative of that dissipation value, $\Omega = -0.5$ (green). In figure 2.1b, we plot probability density, p, vs dimensionless scale for negative exponential function comparing distribution probability densities in figure 2.1a at $\Omega = 0.5$ (red) and $\Omega = -0.5$ (green). To obey the FT the probability density at a positive value of the dissipation such as at $\Omega = 0.5$ must be connected to the value of the probability density at the corresponding negative value, $\Omega = -0.5$ by the negative exponential of the positive value of the dissipation, $p(\Omega = 0.5)\exp(-0.5) = p(\Omega = -0.5)$.

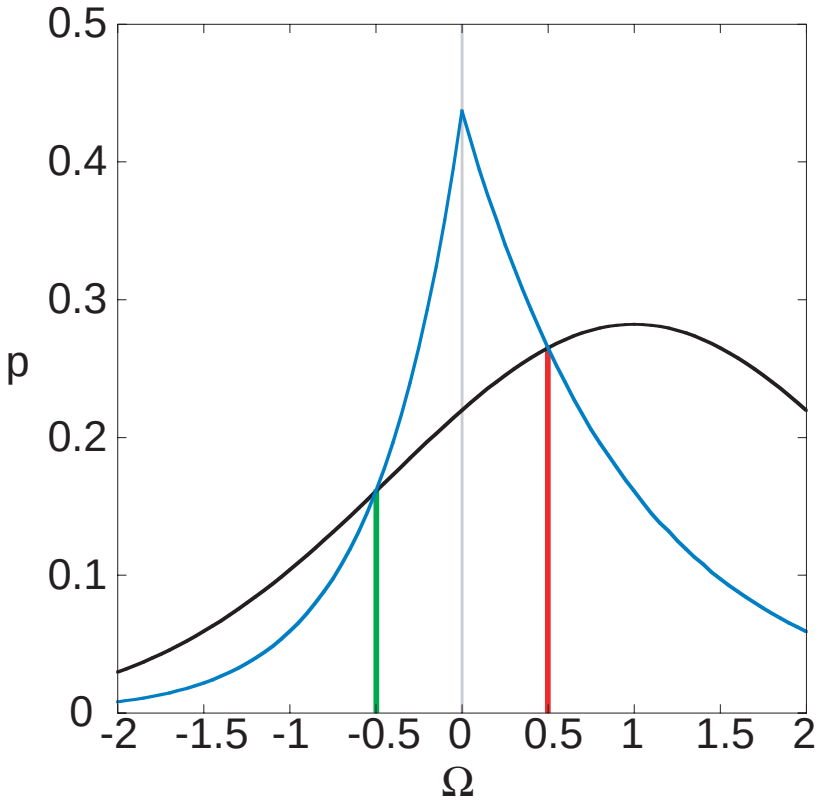
0.5
0.4
0.3
p
0.2
0.1
0
-2
-1.5
-1
-0.5
0
0.5
1
1.5
2
Ω

(a)

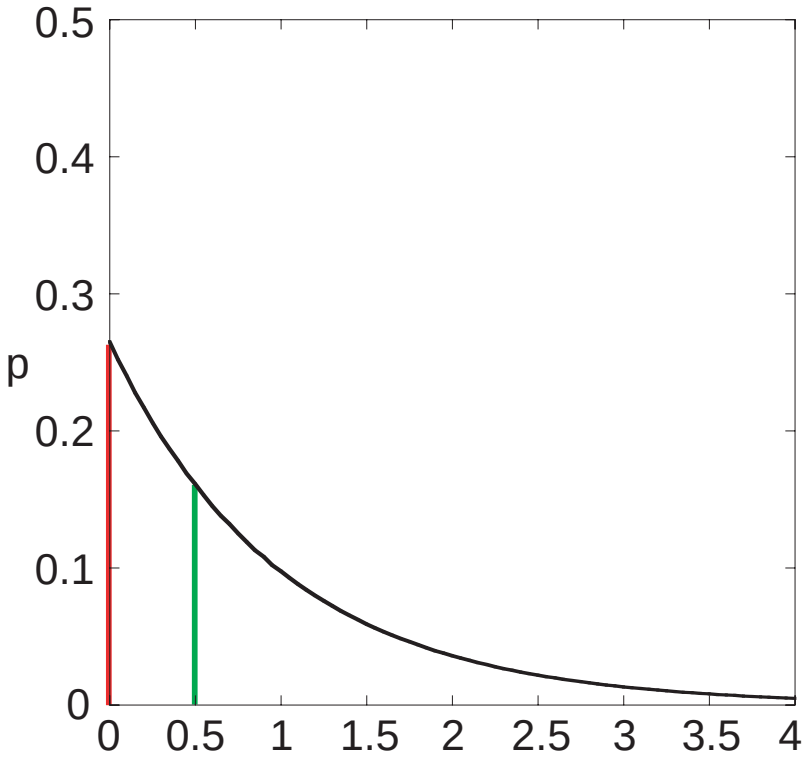
0.5
0.4
0.3
p
0.2
0.1
0
0
0.5
1
1.5
2
2.5
3
3.5
4

(b)

Figure 2.1

We define an ensemble of system trajectories in terms of $\lambda(t)$, the time dependent external parameter(s) that drive the system from an initial state defined by $\lambda(0)$ to its final state with $\lambda(\tau)$. We can then define a conjugate ensemble of system trajectories in terms of $\lambda^*(t)$, which represents the time dependent external parameters that would drive a system from its initial state governed by $\lambda(\tau)$ to a final state with $\lambda(0)$ over the time reverse set of external parameters, $\lambda^*(t) = \lambda(\tau - t)$. The FT and CR differ in that for the FT, both trajectory probabilities are evaluated over the same ensemble of trajectories, while in the CR, one is measured going "forwards" and the other is measured going in "reverse". The CR therefore quantifies reversibility in a different way: it defines the balance between positive and negative work over time reversed system changes, see figure 2.2.

2.0.3 The Fluctuation-Dissipation Theorem

In addition to the FT and WR, there is a relation quantifying fluctuations that we will not be discussing in this work, the fluctuation-dissipation theorem. The fluctuation-dissipation theorem relates the fluctuations of a system property at equilibrium to the system's dissipative linear response to that property. Examples of this theorem include the relationship between the diffusion co-efficient at equilibrium and the drag co-efficient for a Brownian particle, and the relationship between the equilibrium voltage fluctuations and the resistance in an electrical circuit. [19]

The fluctuation-dissipation theorem is an extremely important result in statistical mechanics, and represents the first use of system fluctuations to characterise system properties, an essential feature of the fluctuation relations. The fluctuation-dissipation theorem differs from the FT and WR in one important aspect however, it is a theorem of equilibrium statistical mechanics. The dissipative properties it quantifies apply to non-equilibrium processes only when they are close to equilibrium in the linear regime, where the behaviour of the system is fundamentally the same as it is in equilibrium. The aim of this work is to study exact, non-equilibrium relations, and as such, we will not be examining the fluctuation-dissipation theorem.

2.1 A general approach to Fluctuation Relations

The FT and WR exploit the statistics of individual trajectories to provide information about a thermodynamic system. To apply these relations we need to characterise these trajectories by either dissipation or work. So far we have simply described the dissipation function as a dimensionless energy, we will now demonstrate this by deriving it as a statistical quantity. Work, on the other hand, is a fluctuating variable of classical thermodynamics; [20] however for the purposes of the WR it can also be derived as a statistical quantity. By using the same approach to derive these quantities we can show that they are important measures of individual system trajectories, and that their associated fluctuation relations provide information about the behaviour of the overall system, and that these arguments and fluctuation relations are intimately related.

To derive the FT and WR, we first need to define a general thermodynamic system. Let ξ_t be a co-ordinate vector that describes a system or micro-state at some time t. This could be a list of heads and tails for a set of coin tosses, the velocity of a pendulum, or the position and momentum for every particle in a system. We can represent the external constraints on the system as λ, and for a dynamic system we can make them time dependent $\lambda(t)$. The external parameters are the macroscopic variables that define the thermodynamic state of the system. For a traditional thermodynamic system, like an ideal gas in a container, the external parameters would be the number of gas particles, the temperature, and the volume. For a set of coins, these parameters might be the number of coins and the relative likelihood of heads versus tails.

For a dynamic system, we wish to examine the transformation between two states of the system. We can define a "forward" ensemble of trajectories for a system as one that starts in a time invariant distribution of co-ordinates $f_e(\xi, \lambda(0))$ under a constant external field $\lambda(0)$, and evolves under a time dependent external parameter, $\lambda(t)$, for $0 \leq t \leq \tau$, to a new distribution $f(\xi, \lambda(\tau), \tau)$. Initially, the system need only be in a time-invariant state, either an equilibrium state, or a non-equilibrium steady-state. The "reverse" ensemble corresponds to the same system starting with a time invariant distribution $f_e(\xi, \lambda(\tau))$ and evolving under $\lambda^*(t)$ for $0 \leq t \leq \tau$ to

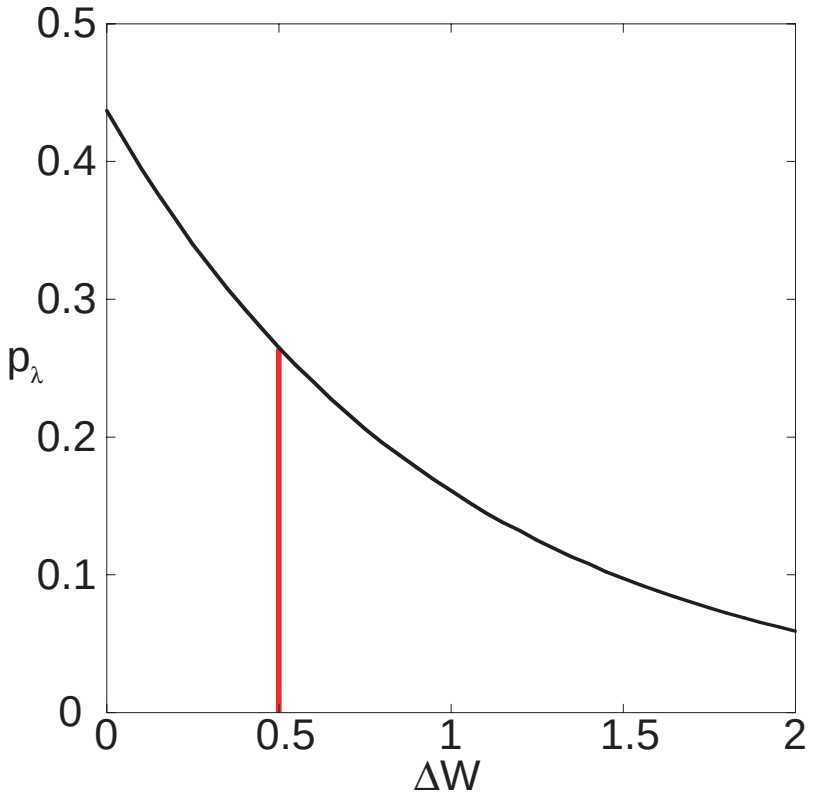

(a)

Figure 2.2: **Three figures that show the relationship between the "forward" and "reverse" system distributions and the Crooks relation.** In figure 2.2a, we plot probability density, p, vs work, ΔW for an ensemble of trajectories subject to a change in external parameters $\lambda(t)$, and in figure 2.2b we plot probability density, p, vs work, ΔW for an ensemble of trajectories subject to a change in external parameters $\lambda^*(t)$. The CR describes the relationship between the probability density of values of work in the ensemble of trajectories defined by $\lambda(t)$, such as at $\Delta W = 0.5$ (red), figure 2.2a, and the probability density of the opposite value of work in the ensemble of trajectories defined by $\lambda^*(t)$ such as at $\Delta W = -0.5$ (green), figure 2.2b. In figure 2.2c, we plot probability density, p, vs dimensionless scale, Θ for negative exponential function (**black**), $\exp(-\Theta)$, and negative exponential modified by the free energy (blue), $\exp(-\Theta + \Delta A)$, comparing distribution probability density in figure 2.2a at $\Delta W = 0.5$ (red) and probability density in figure 2.2b $\Delta W = -0.5$ (green). The CR requires the two probabilities to be related by the modified exponential, $p(\Delta W = 0.5)\exp(-0.5 + A) = p(\Delta W = -0.5)$.

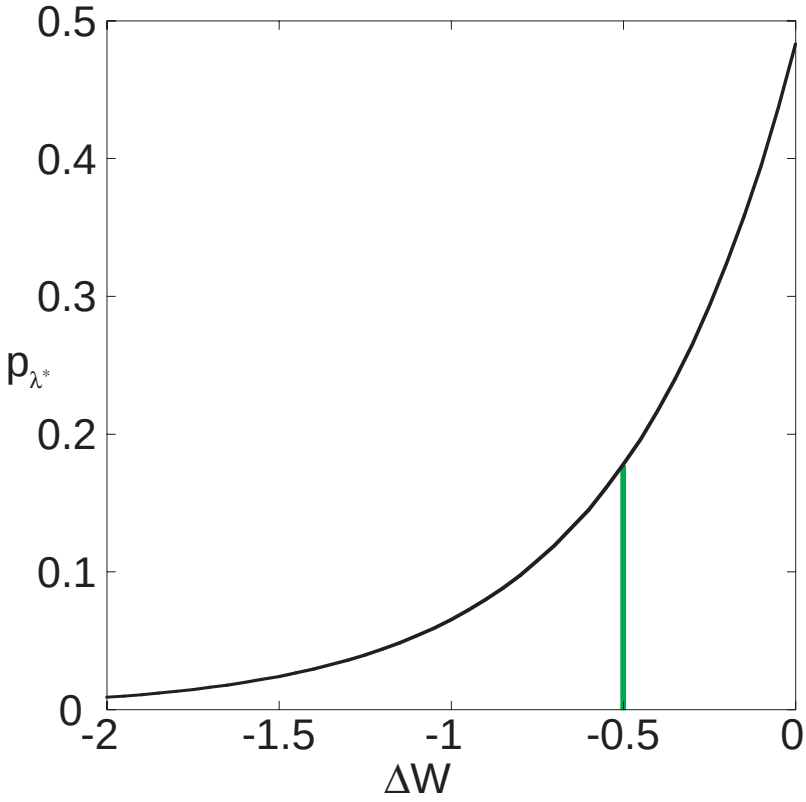
0.5
0.4
0.3
p_{λ^*}
0.2
0.1
0
-2
-1.5
-1
-0.5
0
ΔW

(b)

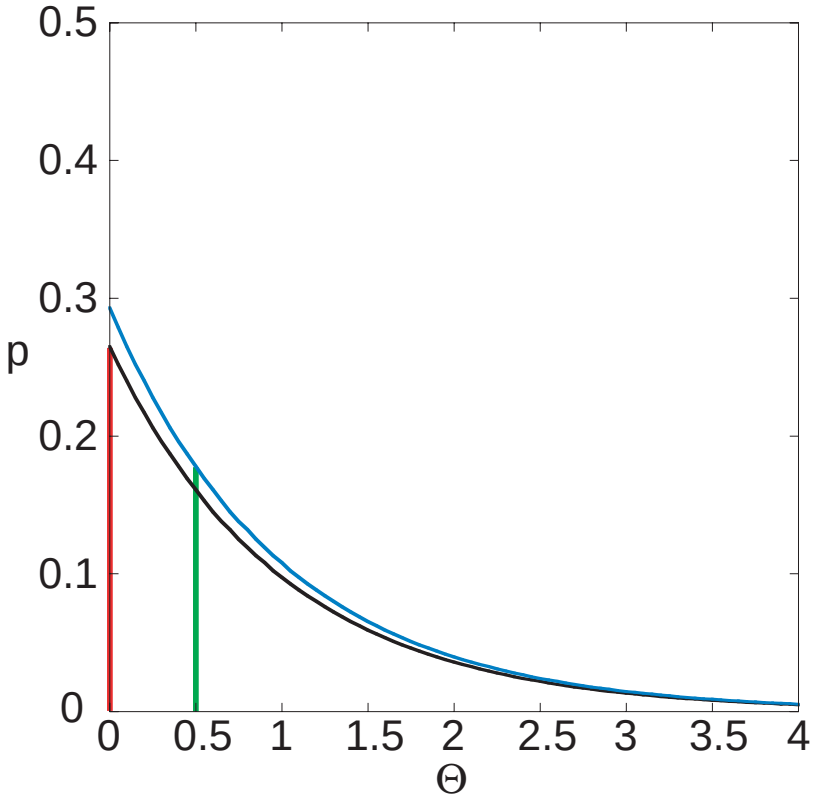
0.5
0.4
0.3
p
0.2
0.1
0
0
0.5
1
1.5
2
2.5
3
3.5
4
Θ

(c)

Figure 2.2

distribution $f(\xi, \lambda^*(\tau), \tau)$ where $\lambda^*(t)$ is defined such that $\lambda^*(t) = \lambda(\tau - t)$, that is it is the time reverse of $\lambda(t)$ over the period $0 \leq t \leq \tau$.

A system trajectory represents the evolution of the system co-ordinates with time: let $\{\xi_0, \xi_\tau\}$ represent the complete set of system trajectories that evolve from an initial co-ordinate, ξ_0, to a final co-ordinate, ξ_τ, over a time τ. Depending on the dynamics and co-ordinates used to define the system, this set may represent a single trajectory, such as for deterministic dynamics, an infinite collection of trajectories, such as for stochastic dynamics, or some finite set.

For any set $\{\xi_0, \xi_\tau\}$, we can define a conjugate set of "anti-trajectories" or time-reverse trajectories denoted by $\{\xi_\tau^*, \xi_0^*]$. Here, the superscript $*$ represents a time reversal map of the system co-ordinate; this means that if there are any components in the vector ξ that would invert sign if time was reversed, that is they are functions that are time derivates such as momentum or acceleration, they are reversed in the conjugate trajectory, Figure 2.3. For example, under deterministic dynamics, we can define the system co-ordinate of a single particle in one dimension in terms of the particle's position and momentum, $\xi_0 = (\mathbf{q}(\mathbf{0}), \mathbf{p}(\mathbf{0}))$. When we apply the time reverse map to this co-ordinate, the position of the of particle is unchanged, but the momentum reverses due to it being a time derivative of the position: $\xi_0^* = (\mathbf{q}^*(\mathbf{0}), \mathbf{p}^*(\mathbf{0})) = (\mathbf{q}(\mathbf{0}), -\mathbf{p}(\mathbf{0}))$.

The relationship between a set and its conjugate set is that of a system going forwards and backwards in time. However as Loschmidt pointed out, both of these trajectory sets can be valid solutions for the evolution of a thermodynamic system with time. By defining these trajectory sets independently of time, we can examine them both over the same change in external parameters λ, to try to address Loschmidt's paradox, or we can examine them in terms of conjugate changes in external parameters λ and λ^*, so we are looking at the time forward and time reverse behaviour of the system. As we manipulate these conjugate trajectories and conjugate system changes we will see that the arguments of the fluctuation relations will appear. It is important to note however that just because we have defined the conjugate set of trajectories does not mean that these trajectories will exist for a given system and change in external parameters.

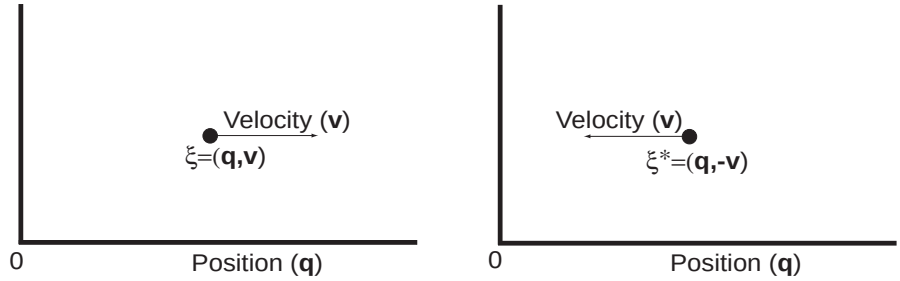

(a) (b)

Figure 2.3: **Two illustrations of a deterministic system co-ordinate and its conjugate.** In figure 2.3a we plot position, **q**, one-dimensional plot with illustration of velocity for an arbitrary deterministic system co-ordinate ξ, and in figure 2.3b we plot the same for the conjugate system co-ordinate ξ^* to the system co-ordinate in figure 2.3a. When we take the time-reverse of ξ, the position is unchanged, but the velocity changes sign.

We will start by constructing the dissipation function for our general thermodynamic system. Let $P_{\lambda(t)}(\{\xi_0, \xi_\tau\})$ represent the probability distribution of trajectories over the forward ensemble, $\lambda(t)$. Furthermore, let $dv(\{\xi_0, \xi_\tau\})$ represent the infinitesimal volume in the probability distribution centred on $\{\xi_0, \xi_\tau\}$. The dissipation function can be defined as the ratio of probability densities for an arbitrary trajectory set and its conjugate over the forward ensemble of trajectories:

$$\exp\left(\Omega_\tau(\{\xi_0, \xi_\tau\})\right) \equiv \frac{P_{\lambda(t)}(\{\xi_0, \xi_\tau\})}{P_{\lambda(t)}(\{\xi_\tau^*, \xi_0^*\})} \frac{dv(\{\xi_0, \xi_\tau\})}{dv(\{\xi_\tau^*, \xi_0^*\})}, \tag{2.6}$$

see figure 2.4.

The dissipation function is a measure of the relative likelihood of a trajectory compared to its conjugate from Loschmidt's paradox. It works on a different scale to quantities like entropy and is more analogous to heat or work, focussing on individual system trajectories rather than thermodynamic ensembles. A trajectory with a large positive dissipation is heavily favoured over its time-reverse, while a trajectory with a large negative dissipation is unfavoured relative to its time-reverse. Positive dissipation trajectories therefore represent a change in the system that is statistically favoured and likely to be maintained, while negative dissipation trajectories represent unfavoured behaviour of the system.

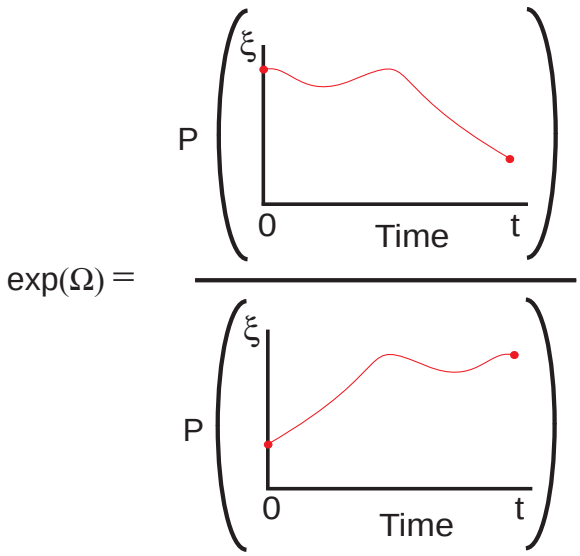

Figure 2.4: **Illustration of Ω in terms of the probabilities of conjugate trajectories.** On the top and bottom of the ratio we represent trajectories on system co-ordinate, ξ, vs time, plots. The bottom trajectory is the conjugate trajectory to the top trajectory, as the initial and final values of the system co-ordinate are reversed. The color of the system trajectories (red), indicates that these are evaluated over the same system change, $\lambda(t)$.

We can similarly define a work quantity; the normalised work function, ΔW_d,

$$\exp\left(\Delta W_d(\{\xi_0, \xi_\tau\})\right) \equiv \frac{P_{\lambda(t)}(\{\xi_0, \xi_\tau\})}{P_{\lambda^*(t)}(\{\xi_\tau^*, \xi_0^*\})} \frac{dv(\{\xi_0, \xi_\tau\})}{dv(\{\xi_\tau^*, \xi_0^*\})}, \tag{2.7}$$

see figure 2.5. Note that the denominator of this definition differs from that of Ω_τ, equation 2.6, in that it considers a distribution with a time-reverse application of the external parameters, $\lambda^*(t)$. Now we have a different measure of reversibility: one that compares a trajectory in an ensemble of trajectories with the time-reverse trajectory in the time reverse ensemble.

So far we have compared trajectories and their conjugates to express the dissipation function and normalised work function. We can derive a third function, the normalised conjugate work function, ω_d, if we evaluate the same set of trajectories over conjugate system changes,

$$\exp\left(\omega_d(\{\xi_\tau^*, \xi_0^*\})\right) \equiv \frac{P_{\lambda(t)}(\{\xi_\tau^*, \xi_0^*\})}{P_{\lambda^*(t)}(\{\xi_\tau^*, \xi_0^*\})} \frac{dv(\{\xi_\tau^*, \xi_0^*\})}{dv(\{\xi_\tau^*, \xi_0^*\})}, \tag{2.8}$$

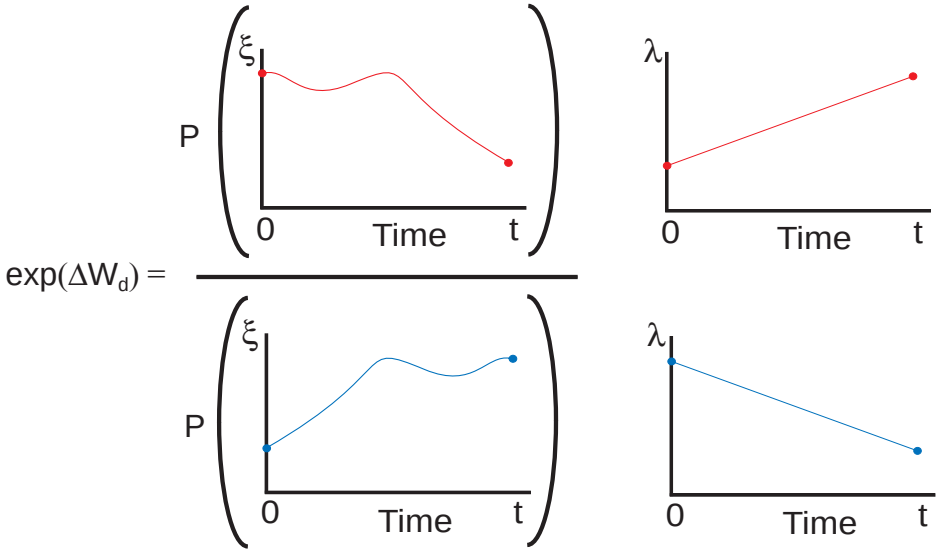

Figure 2.5: **Illustration of the normalised work, ΔW_d, in terms of the probabilities of conjugate trajectories from conjugate ensembles.** On the top and bottom of the ratio we represent trajectories on system co-ordinate, ξ, vs time, plots. The bottom trajectory is the conjugate trajectory to the top trajectory, as the initial and final values of the system co-ordinate are reversed. The colors of the trajectories represent the ensemble the trajectory is taken from, the top trajectory is (red), representing that it is from the ensemble $\lambda(t)$, and the bottom trajectory is (blue), representing that it is from the ensemble $\lambda^*(t)$.

see figure 2.6. It seems odd to define a function in terms of conjugate trajectories: it only makes sense to talk about conjugate trajectories, $\{\xi^*_\tau, \xi^*_0\}$, when comparing them to primary trajectories, $\{\xi_0, \xi_\tau\}$. Indeed, we can simply rewrite this expression in terms of ordinary trajectories,

$$\exp\left(\omega_d(\{\xi_0, \xi_\tau\})\right) \equiv \frac{P_{\lambda(t)}(\{\xi_0, \xi_\tau\})}{P_{\lambda^*(t)}(\{\xi_0, \xi_\tau\})} \frac{dv(\{\xi_0, \xi_\tau\})}{dv(\{\xi_0, \xi_\tau\})}. \tag{2.9}$$

We have chosen to use the conjugate or anti-trajectories, $\{\xi^*_\tau, \xi^*_0\}$, to define this function because we can then relate this function to the normalised work function and dissipation functions:

$$\Omega_\tau(\{\xi_0, \xi_\tau\}) = \Delta W_d(\{\xi_0, \xi_\tau\}) - \omega_d(\{\xi^*_\tau, \xi^*_0\}), \tag{2.10}$$

see figure 2.7.

The normalised conjugate work function compares the same trajectory between forward and reverse ensembles of trajectories. When the function is positive, it

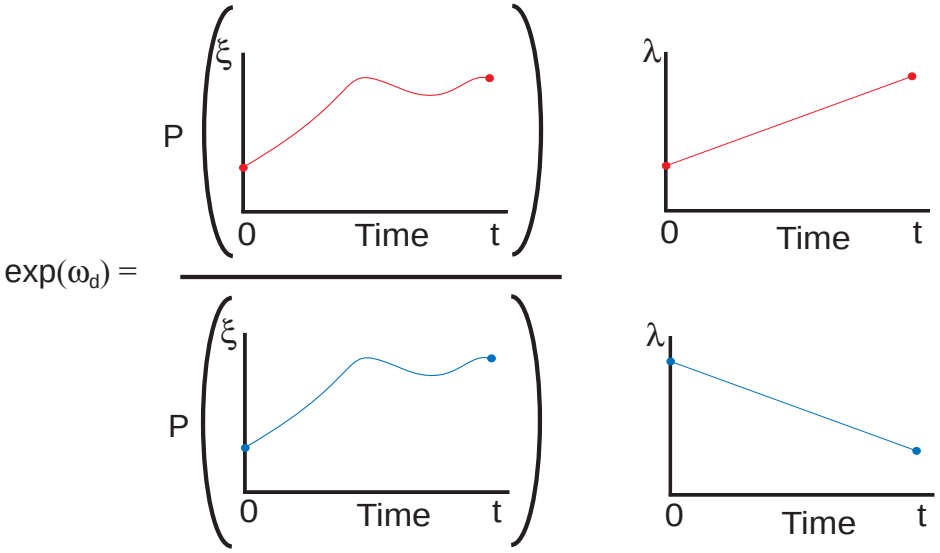

Figure 2.6: **Illustration of the normalised conjugate work, ω_d, in terms of the probabilities of trajectories from conjugate ensembles.** On the top and bottom of the ratio we represent trajectories on system co-ordinate, ξ, vs time, plots. The colors of the trajectories represent the ensemble the trajectory is taken from, the top trajectory is (red) representing that it is from the ensemble $\lambda(t)$, and the bottom trajectory is (blue) representing that it is from the ensemble $\lambda^*(t)$. It is important to note that the trajectories depicted on both the top and bottom of the fraction are the conjugate trajectories, $\{\xi^*_\tau, \xi^*_0\}$, to the trajectories on the top of the dissipation function, figure 2.4 and the normalised work function, figure 2.5.

means that the trajectory is more likely in the ensemble it was evaluated over then in the reverse ensemble. The normalised conjugate work function like the dissipation function can be described as a measure of reversibility: a trajectory with a negative value is one we would expect to see if we were performing the opposite (time reversal of external parameters) process to the one we are currently performing, and one with a positive value is one we would expect to see for the current process rather than the opposite.

From these simple arguments we can derive our fluctuation relations. As an example, we can derive the FT. If we start with the probability ratio for the FT:

$$\frac{P(\Omega = a)}{P(\Omega = -a)} = \frac{\int dv(\{\xi_0, \xi_\tau\})\delta(\Omega - a)P_{\lambda(t)}(\{\xi_0, \xi_\tau\})}{\int dv(\{\xi_0, \xi_\tau\})\delta(\Omega + a)P_{\lambda(t)}(\{\xi_0, \xi_\tau\})}, \tag{2.11}$$

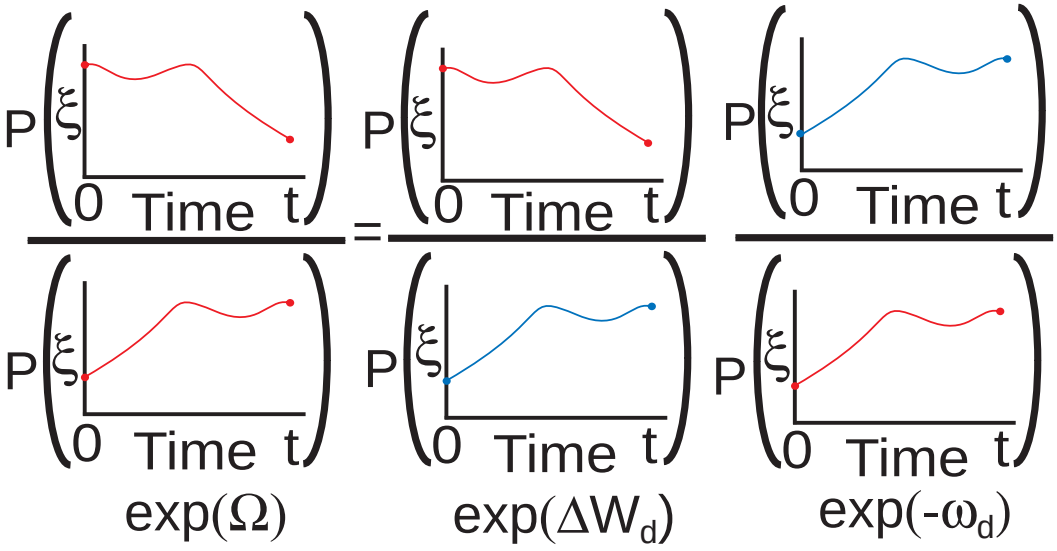

Figure 2.7: **Illustration of the relationship between the dissipation function, figure 2.4, the normalised work function, figure 2.5, and the normalised conjugate work, figure 2.6.** This illustration is equivalent to equation 2.10.

and substitute our definition of the dissipation function, equation 2.6,

$$\frac{P(\Omega = a)}{P(\Omega = -a)} = \frac{\int dv(\{\xi_0, \xi_\tau\})\delta(\Omega - a)P_{\lambda(t)}(\{\xi_0, \xi_\tau\})}{\int dv(\{\xi^*_\tau, \xi^*_0\})\delta(\Omega - a)P_{\lambda(t)}(\{\xi^*_\tau, \xi^*_0\})} \tag{2.12}$$

$$= \frac{\int dv(\{\xi_0, \xi_\tau\})\delta(\Omega - a)P_{\lambda(t)}(\{\xi_0, \xi_\tau\})}{\int \exp(-a)dv(\{\xi_0, \xi_\tau\})\delta(\Omega - a)P_{\lambda(t)}(\{\xi_0, \xi_\tau\})}, \tag{2.13}$$

$$= \exp(a). \tag{2.14}$$

We can then take an ensemble average of this quantity in the forward direction to derive the PI:

$$\langle e^{-\Omega} \rangle = \int dv(\{\xi_0, \xi_\tau\})P_{\lambda(t)}(\{\xi_0, \xi_\tau\} \exp(-\Omega), \tag{2.15}$$

$$= \int \frac{dv(\{\xi_0, \xi_\tau\})P_{\lambda(t)}(\{\xi_0, \xi_\tau\}dv(\{\xi^*_\tau, \xi^*_0\})P_{\lambda(t)}(\{\xi^*_\tau, \xi^*_0\})}{dv(\{\xi_0, \xi_\tau\})P_{\lambda(t)}(\{\xi_0, \xi_\tau\}}, \tag{2.16}$$

$$= \int dv(\{\xi^*_\tau, \xi^*_0\})P_{\lambda(t)}(\{\xi^*_\tau, \xi^*_0\}), \tag{2.17}$$

$$= 1. \tag{2.18}$$

We can derive similar relations for the normalised work and the normalised conjugate

work functions:

$$\begin{aligned}
\langle \exp(-\Delta W_d) \rangle &= 1, && (2.19)\\
\frac{P_{\lambda(t)}(\Delta W_d = a)}{P_{\lambda^*(t)}(\Delta W_d = -a)} &= \exp(a), && (2.20)\\
\frac{P_{\lambda(t)}(\omega_d(\{\xi_\tau^*, \xi_0^*\}) = a)}{P_{\lambda^*(t)}(\omega_d(\{\xi_\tau^*, \xi_0^*\}) = a)} &= \exp(a), && (2.21)\\
\langle \exp(-\omega_d) \rangle &= 1. && (2.22)
\end{aligned}$$

These relations are all similar; only the arguments differ between them. What we are lacking are relations that provide us with information about the overall system change, such as the work relation. To develop these relations we need to redefine our arguments.

The work relation measures the free energy change between two time-invariant equilibrium states, characterised by $\lambda(0)$ and $\lambda(\tau)$, the beginning and end points of our change in system parameters. Let $z_{\lambda(0)}$ and $z_{\lambda(\tau)}$ represent the partition functions of the equilibrium states associated with external fields $\lambda(0)$ and $\lambda(\tau)$. A partition function is a thermodynamic function that is the sum of the probabilities of all the micro states in the ensemble. It is important to make a distinction between the distribution of system states ξ, and the distribution of trajectories $\{\xi_0, \xi_\tau\}$ when defining our partition functions for equilibrium. When constructing the arguments of our fluctuation relations, we use distributions of trajectories, $P_{\lambda(t)}(\{\xi_0, \xi_\tau\})$. This distribution is dependent on both the initial equilibrium distribution of states and the change in external system parameters. When comparing equilibrium systems, we are only interested in the difference between the ensemble of system states and our partition function is the sum of these states,

$$z_{\lambda(0)} = \int d\xi f_e(\xi, \lambda(0)). \tag{2.23}$$

We can use these partition function to define the thermodynamic work, ΔW, in terms of probability functions,

$$\exp(\Delta W(\{\xi_0, \xi_\tau\})) \equiv \frac{P_{\lambda(t)}(\{\xi_0, \xi_\tau\})}{P_{\lambda^*(t)}(\{\xi_\tau^*, \xi_0^*\})} \frac{dv(\{\xi_0, \xi_\tau\})}{dv(\{\xi_\tau^*, \xi_0^*\})} \frac{z_{\lambda(0)}}{z_{\lambda(\tau)}}. \tag{2.24}$$

Partition functions represent the statistical size of an ensemble. In statistical thermodynamics the ratio of partition functions is related to the free energy change for a thermodynamic system:

$$e^{\Delta F} = \frac{z_{\lambda(0)}}{z_{\lambda(\tau)}}, \tag{2.25}$$

where ΔF is the difference in dimensionless free energy between the stationary state associated with $\lambda(0)$, and the stationary state associated with $\lambda(\tau)$. The partition functions are independent of the other terms in our expressions, and are the only terms left when we average over the exponential of the work, leaving the WR,

$$\langle e^{-\Delta W} \rangle = e^{-\Delta F} \tag{2.26}$$

We can similarly define a conjugate work function ω, and derive analogues to the WR and CR which we call the Conjugate work relation and conjugate CR:

$$\exp\left(\omega(\{\xi^*_\tau, \xi^*_0\})\right) \equiv \frac{P_{\lambda(t)}(\{\xi^*_\tau, \xi^*_0\})}{P_{\lambda^*(t)}(\{\xi^*_\tau, \xi^*_0\})} \frac{dv(\{\xi^*_\tau, \xi^*_0\})}{dv(\{\xi^*_\tau, \xi^*_0\})} \frac{z_{\lambda(0)}}{z_{\lambda(\tau)}}, \tag{2.27}$$

$$\frac{P_{\lambda(t)}(\omega(\{\xi^*_\tau, \xi^*_0\}) = a)}{P_{\lambda^*(t)}(\omega(\{\xi^*_\tau, \xi^*_0\}) = a)} = \frac{z_{\lambda(\tau)}}{z_{\lambda(0)}} \exp(a), \tag{2.28}$$

$$\langle \exp\left(-\omega(\{\xi^*_\tau, \xi^*_0\})\right) \rangle = \frac{z_{\lambda(\tau)}}{z_{\lambda(0)}}. \tag{2.29}$$

Note that in the FT, both the top and bottom of the expression start in equilibrium with the same state, and the partition functions will simply cancel out.

In these relations we have defined a work and a free energy for the system. In classical thermodynamics, both of these terms are associated with specific expressions that are dependent on the system chosen. As we will see in later sections, for example section 3.2, our definitions of these terms will reduce to these classical definitions if applied to an appropriate thermodynamic system.

There are some caveats on the applicability of these various relations. The first is that a number of assumptions have been made about the general system in deriving these relations, such as the system being defined by external parameters and there existing some time invariant probability distributions under those parameters. These features are required in a system for this approach to be valid. Second, since all of the functions defined in this chapter are based on ratios, it is important that the

denominator of these fractions is non-zero. In other words, whichever conjugate is chosen to the original trajectory, it must exist, and vice versa.

In the dissipation function, it is necessary that for every forward trajectory $\{\xi_0, \xi_\tau\}$ in the ensemble of trajectories that evolve over $\lambda(t)$, the conjugate trajectory $\{\xi_\tau^*, \xi_0^*\}$ must exist in the ensemble of trajectories over $\lambda(t)$ as well. This means that the time reversal map, ξ^*, of every point in the final distribution of co-ordinates that has non-zero probability, $f(\xi, \lambda(\tau), \tau) \neq 0$, must have non-zero probability in the initial distribution of co-ordinates for the system, $f_e(\xi^*, \lambda(0)) \neq 0 \ \forall \ \xi^*$, and the same is true for time reversal maps of points in the initial distribution and points in the final distribution of the system. If this is not satisfied, the dissipation function, and therefore the FT, cannot be applied to a system.

For the work function, it is necessary that for every trajectory $\{\xi_0, \xi_\tau\}$ in the ensemble of trajectories that evolve over $\lambda(t)$, the conjugate trajectory $\{\xi_\tau^*, \xi_0^*\}$ exists in the time reverse system change $\lambda^*(t)$. This means that the time reversal map, ξ^*, for every point in the final distribution of co-ordinates with non-zero probability, $f(\xi, \lambda(\tau), \tau) \neq 0$, must have non zero probability in the time invariant distribution for the external parameters at the end of the experiment, $f_e(\xi^*, \lambda(\tau)) \neq 0 \ \forall \ \xi^*$. This difference between the requirements of the work and dissipation to be properly defined for a system means that it is possible for one to be applicable to a system but not the other. Finally, for the conjugate work, we have to have all of the trajectories that exist in the forward ensemble exist in the reverse ensemble.

In addition to these theoretical difficulties in applying the fluctuation relations, there can be practical difficulties. The FT and CR are both expressed as probability ratios. To evaluate these probability ratios in an experiment, we have to repeat the experiment a number of times and construct a distribution of the relevant argument. Unfortunately, not all fluctuations are equal in probability, and therefore not all fluctuations are equally sampled. This causes a variety of problems. When discussing these problems, the relations we will treat can be separated into average relations, such as the WR and PI, and ratio relations, such as the FT and CR.

When constructing the ratio type relations, we talk about comparing the probability of a trajectory of value A with $-A$. To be mathematically precise, we are

actually comparing the probability over the trajectory sets within an infinitesimal volume, dv, of trajectories with value A and $-A$, so we are actually looking at values of $A \pm \delta A$, where δA is an infinitesimal amount. The reason for this is that in a continuous distribution, the probability of any point or set of points is always 0.

To generate a distribution in an experiment we need to bin the data. We start by dividing the results by their values into a series of evenly sized bins that are symmetrically arranged around 0. Each bin will have a value at its centre A, and the bin size is ΔA. The probability of the infinitesimal region around A, δA, will therefore be approximated by averaging over the finite size region ΔA. The accuracy of this approximation will be strongly dependent on the number of repetitions we undertake: the larger the number of samples taken, the narrower the bins will be able to be, reducing the averaging and improving the agreement with FT and CR. This creates difficulties where there is a limit in an experiment to the number of repetitions that can be made.

In addition, more probable regions of a distribution will be better sampled then less probable regions, as more samples will land in their bins. This is a particular problem with the FT, as negative values of the dissipation function are exponentially less probable than positive regions. This means negative dissipations will be sampled less often than positive ones, and since the FT is a ratio of the two, this can lead to large uncertainties.

To maximise the number of samples available for testing the FT, we can apply the integrated form of the FT: [5]

$$\frac{P(\Omega < A)}{P(\Omega > A)} = \langle \exp(-a) \rangle_{\Omega > A} \tag{2.30}$$

The integrated FT compares the ratio of negative to positive dissipation against the ensemble average over the positive dissipations. By increasing the number of samples we look at, we decrease the sampling error. In addition, the form of the integrated FT means that we can plot the two sides of the expression against time, allowing us to test the FT at intermediate times.

All of this creates problems in measuring the error in the results for a ratio type relations. As the values of the argument move to less probable regions of the

distribution, the sampling error will dominate the ratio. This will mean that for these relations, agreement will be strong in the regions where the probability of the numerator and denominator are high, and poor in other regions. The uncertainty in the relation varies with the range of values tested.

When measuring the ensemble averages we have an even bigger problem with uncertainties. These relations are weighted averages in the exponential. This means that results on the edge of the distribution, which is often the least sampled region, will contribute proportionately more to the average than the centre of the distribution, see figure 2.8. This makes estimating the deviation of these results from the expected value extremely difficult.

Despite the caveats placed on these theorems, they are applicable to a wide variety of physical systems. The FT provides information on the reversibility of a system change while the WR can measure its free energy change. We will demonstrate this utility over a number of physical systems.

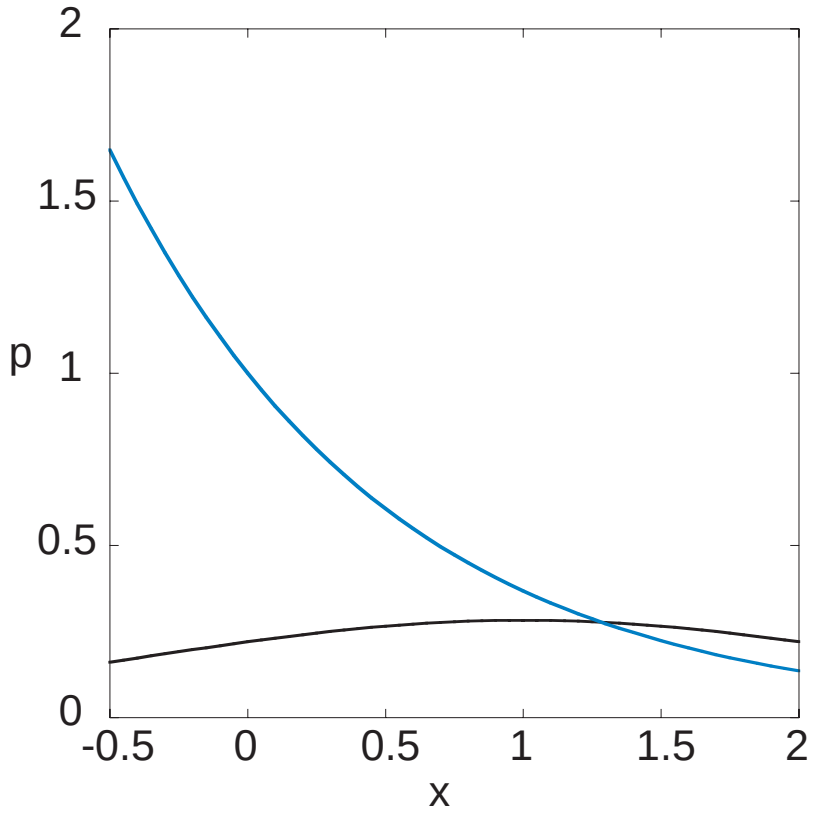

Figure 2.8: **Figure showing an arbitrary distribution function and its negative exponential weighting.** Probability density, p, vs an arbitrary variable, x, for a Gaussian distribution function (**black**) with a negative exponential function $\exp(-x)$ (blue) superimposed. The Gaussian distribution represents a common experimental distribution, while the negative exponential represents the weighting of a variable in a relation such as the PI or WR. This shows that for some distributions, low probability parts of the distribution will dominate the exponential average.

Bibliography

[1] D. J. Evans, D. J. Searles, *Phys. Rev. E* **50**, 1645 (1994).

[2] C. Jarzynski, *Phys. Rev. E* **56**, 5018 (1997).

[3] C. Jarzynski, *Phys. Rev. Lett.* **78**, 2690 (1997).

[4] D. J. Evans, *Molecular Physics* **101**, 1551 (2003).

[5] D. J. Evans, D. J. Searles, *Adv. Phys.* **51**, 1529 (2002).

[6] J. Kurchan, *J. Phys. A* **31**, 3719 (1998).

[7] J. L. Lebowitz, H. Spohn, *J. Stat. Phys.* **95**, 333 (1999).

[8] J. Reid, D. Carberry, G. M. Wang, E. M. Sevick, D. J. Searles, D. J. Evans, *Phys. Rev. E* **70**, 16111 (2004).

[9] T. Monnai, *Phys. Rev. E* **72**, 027102 (2005).

[10] T. Yamada, K. Kawasaki, *Prog. Theor. Phys.* **38** (1967).

[11] G. P. Morriss, D. J. Evans, *Mol. Phys.* **54** (1985).

[12] D. Evans, G. Morriss, *Statistical Mechanics of Nonequilibrium Liquids* (Academic Press, 1990).

[13] D. M. Carberry, S. R. Williams, G. M. Wang, E. M. Sevick, D. J. Evans, *J. Comp. Phys.* **121**, 8179 (2004).

[14] R. van Zon, E. G. D. Cohen, *Phys. Rev. Lett.* **91**, 110601 (2003).

[15] R. van Zon, E. G. D. Cohen, *Phys. Rev. E* **67**, 046102 (2003).

[16] G. Crooks, *Phys. Rev. E* **60**, 2721 (1999).

[17] D. J. Searles, D. J. Evans, *Aust. J. Chem.* **57**, 1119 (2004).

[18] G. Crooks, *Phys. Rev. E* **61** (2000).

[19] J. McLennan, *Introduction to Non-Equilibrium Statistical Mechanics* (Prentice-Hall, 1989).

[20] P. Atkins, *Physical Chemistry, Fifth Edition* (Oxford University Press, 1994).

Chapter 3

Optical Trapping: Experimental and Theoretical

One of the major advances in physics was the realisation that light carries momentum and can therefore exert force upon matter. [1] In 1970, Ashkin showed that this radiation pressure could be used to manipulate microscopic objects, [2] and subsequent developments led to the development of optical tweezers. [3] This technique has found a number of practical applications, [4] particularly in biology, where it can be used to manipulate cells and organelles. [5]

In an optical tweezers apparatus, a laser beam is focused through a lens to a point in space, Figure 3.1a, to create an intensity gradient. When the laser beam interacts with a transparent object that has a different index of refraction to its surroundings, the light will refract through the object, Figure 3.1b. Due to the intensity gradient, the amount of light refracted varies over the volume of the particle, creating an imbalance of the forces on the particle in the direction of the focal point. This force creates the optical 'trap' that can be manipulated by changing the focal point.

For our experiments, we will be studying a latex sphere in solution that is trapped by optical tweezers. A latex sphere suspended in solution is subject to Brownian motion, a process where the thermal fluctuations in the solvent cause the object to start and stop moving through the solution at random intervals. Brownian motion is of interest because it exhibits anti-entropic behaviour: heat can be taken directly from the solution and converted into work on the particle.

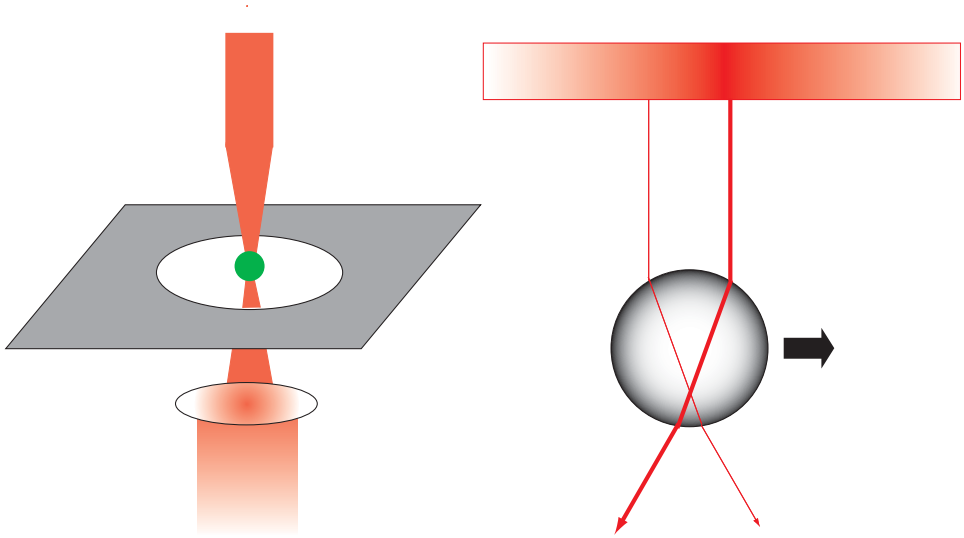

(a) (b)

Figure 3.1: **Two illustrations of the optical trapping experiment.** In figure 3.1a we present an illustration of the creation of an optical trap using a lens. The laser is focused through a tight focus lens to capture a particle at the focal point. In figure 3.1b we present an illustration of optical trapping with a ray diagram. As the light refracts through the colloid (parallel rays used for simplicity), it imparts momentum to the particle. High intensity parts of the beam carry greater momentum, and this causes a net force on the particle in the direction of highest intensity.

If we have an unconstrained Brownian particle, it will slowly diffuse through the solution. Such behaviour does not violate the Second Law of Thermodynamics as the process is reversible, with the particle stopping and the solution heating again, giving no net entropy change.

In our experiments the particle is constrained using a trap with a potential energy on the same order as the thermal fluctuations in the solution. This gives a system where the sphere is localised around the trap centre, but is still able to exhibit Brownian motion. For our system, that is a Gaussian beam focused onto a spherical particle, the laser potential is approximately harmonic, that is the force is of the form: [6]

$$\mathbf{F}_{opt} = -k\mathbf{x}, \tag{3.1}$$

where $\mathbf{F}_{opt}$ is the optical force, k is the force constant for the trap, and $\mathbf{x}$ is the displacement of the centre of the sphere from the focal point. This means we can represent an optically trapped latex sphere as a simple harmonic oscillator coupled to the solution: a system that is well characterised, but that has fluctuations that

can be studied with the fluctuation relations.

3.1 Experimental set up for optical trapping.

To generate an optical trap, all that is required is a light source and a lens; to perform the experiments required to test the fluctuation relations, a more complicated set up was required. In this section we will describe the setup of our optical tweezers, the trapping of a colloid in an optical trap and discuss the difficulties associated with this system.

The optical trap is generated by focusing a laser through a high numerical aperture lens of an inverted microscope. The focal point of the microscope is directed into a sample cavity containing a dilute mixture of latex spheres in water. The laser has a frequency in the infra-red ($\lambda = 1064$nm, 4W max output), and the strength of the laser is controlled by a laser stabiliser mounted between the laser and the sample. The sample holder itself can be translated by piezo-electric servo motors with a claimed accuracy of 1.2 nm. The tight focus of the laser means that the trap is significantly stronger in the beam direction than in the plane perpendicular to the beam, localising trapped particles in the focal plane of the lens. Finally, the position of a particle is measured by illuminating the particle with visible light and using a quadrant photodiode to measure the shadow position, with an accuracy of approximately 15nm. [7] The equipment list for the experimental apparatus is contained in table 3.1. Note that for experiments before 2004, a Cell Robotics laser was used, with a wavelength of 985nm. This laser produced an asymmetric beam, limiting analysis to one dimension, before failing and being replaced. Experiments in chapter 4 use the original laser, experiment in chapter 5, use the newer laser. The specific laser used does not affect the analysis of the experiments however.

To undertake an experiment, an extremely strong trap is used to capture a single latex sphere so that it does not exhibit any measurable position fluctuation due to thermal noise. The sample holder is then translated so that the sphere is well separated from any others in the solution. The photodiode is calibrated by displacing the detector by fixed amounts and measuring the change in signal output. Finally, the laser power is lowered to its experimental power, a level where the thermal motion

Table 3.1: List of experimental equipment for optical trapping. [7]

Item	Manufacturer	Model
Microscope	Nikon	DIAPHOT 300
Infra-red laser	Coherent Scientific	Compass-4000M
Laser Stabiliser	BEOC	LPC-NIR
Arbitrary Function Generator	Thurlby Thander Industries	TGA 1242
Piezo-electric servos	Physik Instrumente	P-814.40
Quadrant Photodiode	Hamamatsu	S4349

of the sphere is measurable.

To measure the trapping constant, the particle is allowed to equilibrate, and then its position is recorded over time. The strength of the trapping constant, k, can be found by sampling the position of the particle and applying equipartition theory:

$$\sigma^2(\mathbf{q}_1) = \frac{k_B T}{k}, \tag{3.2}$$

Where $\sigma(\mathbf{q}_1)$ is the standard deviation in the particle position.

We can control two parameters in an experiment with our optical tweezers; we can translate the sample holder, which is equivalent to dragging the particle through the solution, or we can vary the laser power to change the strength of the optical trap. We do this by feeding either our laser stabiliser or our servo motors a waveform generated on an arbitrary waveform generator, table 3.1. As we will see in subsequent chapters, these two parameters, trap strength and displacement, allow us to thoroughly study the fluctuation relations.

Associated with each of these parameters is a different difficulty. When translating the stage, the velocity can be set, but the acceleration to that velocity is uncontrolled and governed by the response of the servos. When manipulating the trap strength, there can be a small lag in the response, which imposes an upper limit on how fast the trap the trap strength can be varied.

There are a number of technical problems with the optical tweezers set up that cause difficulties or limit our experiments. The first of these problems is in the optics. In order to generate a tightly focused beam to create our trap, we use a high numerical aperture lens covered in oil. Over long periods of time, the oil can

deform or drift over the lens slightly, changing the point and depth of focus and invalidating the calibration of the system. The second problem is that in order to trap a particle in the solution, we have to seed a reasonable number of the colloidal particles into the solution, so that we can find one using our microscope. Even after finding a clear region of the sample holder to carry out our experiment, diffusion of the particles coupled to the attractive nature of the trap means that there is an increasing chance with time that a new particle will come in and replace our trapped particle, invalidating the calibration. Finally, the particles can sometimes sink in the solution, adhering to the sample holder and no longer in suspension. These factors conspire to limit the maximum number of repetitions we can perform in a given experiment.

In spite of these limitations, the optical trapping system is capable of producing useful experimental results. Each of the problems listed above produces distinct errors that can be checked for in the data, and stochastic simulations can provide reference data for diagnosing other problems. As we will show, the optical trapping system has provided a number of successful demonstrations of the fluctuation relations.

3.2 Theoretical representations of optical trapping

Optical trapping can be approached using a number of different theoretical approaches. It may seem odd that the same system in physics can be represented in a variety of different ways. Often in physics however, different levels of abstraction of a system may trade unnecessary accuracy for practical results. Strictly speaking there is only one thermodynamic system in physics, the entire universe. In practice we are more often concerned with a limited sub-system, such as an optical trapping experiment. For representing our optical trapping experiment, we will use two different representations: deterministic molecular dynamics and stochastic inertialess Langevin dynamics. Deterministic dynamics represents each molecule in our solvent bath and our latex sphere and treats their motion by evaluating the forces between them and applying Newtonian dynamics. Stochastic dynamics treats only the latex sphere and represents the solvent as a random force acting on the particle. Each

approach has its advantages and disadvantages for this system.

3.2.1 Deterministic Dynamics

Deterministic dynamics are Newton's dynamics: the simple equations of motion intuitive to our daily lives. Based on Newton's three laws of motion, objects only change their motion when subjected to a force, and the change in motion is related to the force and the mass of the object. While deterministic dynamics are strictly only an approximation for non-relativistic, non-quantum systems, the errors associated with this approximation are extremely small.

When we apply deterministic dynamics to a thermodynamic system we get what is termed molecular dynamics: we literally apply Newton's equations of motion to the molecules that make up a thermodynamic system. [8] Each molecule in a system is assigned a position, $\mathbf{q}_i$, and a momentum, $\mathbf{p}_i$, where i is an index number for each molecule from 1 to N, $i = 1, 2, 3...N$. We can then describe a system micro-state using a phase space vector $\mathbf{\Gamma}$, that represents the position and momentum of every particle in the system, $\mathbf{\Gamma} = \{\mathbf{q}_1, \mathbf{p}_1, \mathbf{q}_2, \mathbf{p}_2, \mathbf{q}_3, \mathbf{p}_3, ...\mathbf{q}_N, \mathbf{p}_N]$. For a three dimensional physical system, our phase space vector will have 6N dimensions, three dimensions for the position and three dimensions for the momentum of each particle. A thermodynamic system can be represented with a density function over this phase space, $f(\mathbf{\Gamma})$, determined by the forces and constraints upon the system.

Given a system co-ordinate defined in terms of positions and momenta, we expect equations of motion in terms of the change of these two quantities: [9]

$$\dot{\mathbf{q}}_i = \frac{\mathbf{p}_i}{m} + \mathbf{C}_i F_e, \tag{3.3}$$

$$\dot{\mathbf{p}}_i = \mathbf{F}_{int} + \mathbf{D}_i F_e, \tag{3.4}$$

where m is the mass of the particles, F_e is the external field on the system, $\mathbf{C}_i$ and $\mathbf{D}_i$ represent the coupling of the external field to the position and the momentum of particle i, and $\mathbf{F}_{int}$ are the internal forces of the system such as intermolecular

forces. Often these equations will be represented in terms of a Hamiltonian, H: [9]

$$\dot{\mathbf{q}}_i = \frac{\partial H(\mathbf{\Gamma})}{\partial \mathbf{p}_i},\ \dot{\mathbf{p}}_i = -\frac{\partial H(\mathbf{\Gamma})}{\partial \mathbf{q}_i}. \tag{3.5}$$

which is the sum of the kinetic, $K(\mathbf{p})$, and potential, $\Phi(\mathbf{q})$, energy terms of a system,

$$H(\mathbf{\Gamma}) = K(\mathbf{p}) + \Phi(\mathbf{q}). \tag{3.6}$$

Hamiltonian dynamics are a convenient way of representing the equations of motion for the system in a compact fashion, while the Newtonian expression is useful for actually evolving the phase space vector with time. Using Hamiltonian dynamics has an additional advantage: the distribution for a thermodynamic system in equilibrium within the canonical distribution, that is constant number of particles, volume, and temperature, is related to its Hamiltonian via the Boltzmann distribution, [9]

$$f(\mathbf{\Gamma}) = \frac{e^{-\beta H(\mathbf{\Gamma})}}{z}, \tag{3.7}$$

where z is the partition function for the system, that is $z = \int e^{-\beta H(\mathbf{\Gamma})}$.

It is at this point that the thermodynamic approach to mechanics takes a detour from classical mechanics. In classical mechanics, when we wish to constrain a system, we generally want the constrained system to exhibit Hamiltonian dynamics, as the underlying dynamics of real systems are Hamiltonian. Such constraints are holonomic, that is when they are applied to the unconstrained Hamiltonian of the system, the constrained equations of motion for the system are also in terms of a Hamiltonian. [9] In thermodynamics, a lot of the constraints we can impose are holonomic in form: volume, number of particles, energy, and bond length. These constraints only constrain the position co-ordinate of the system with time. There are however a number of non-holonomic constraints we may wish to impose upon a system such as pressure or temperature, which are associated with the momenta of the particles, that will lead to non-Hamiltonian dynamics.

An approach using non-Hamiltonian dynamics was developed simultaneously but independently by Evans and Hoover. [10, 11] This approach involves adding a term

to the equations of motion that impose the thermodynamic constraint directly upon the system of interest. In using the constraint to effectively remove a part of the real system from the equations of motion, the remaining equations become non-Hamiltonian. The nature of the term is dependent on the quantity constrained.

In order to have a constant temperature system using Hamiltonian dynamics, we would have to include the equations of motion of a much larger thermal reservoir, so that the reservoir plus system were at constant energy. This would massively increase the overall size and complexity of our system, while not providing much in the way of useful information. Furthermore, if we wanted to simulate this system on a computer, we would spend most of our resources simulating the heat bath, and very little on the system we were interested in. The Evans and Hoover approach is preferable.

In this thesis, the quantity we wish to constrain is the temperature. Temperature is a thermodynamic variable that connects the infinitesimal change in energy to that in entropy for a system. To measure the temperature for a deterministic system we generally relate it to the average kinetic energy per particle of the system in each dimension, a relation known as the equipartition theorem: [12]

$$< KE >= \frac{1}{2} k_B T, \tag{3.8}$$

but there are a number of different expressions for the temperature, such as the configurational temperature, [13] that can be used that will correspond to the thermodynamic temperature in equilibrium. Out of equilibrium however, the thermodynamic definition of temperature is not clearly defined, and each of these different measurements can produce different results when applied to a system.

To thermostat a system out of equilibrium, we need an expression for the temperature. We define the temperature of the system out of equilibrium in terms of one of the expressions for the system at equilibrium. We will use equation 3.8 to define an out of equilibrium temperature, the kinetic temperature. The correspondence of the kinetic temperature and the thermodynamic temperature at equilibrium means that if a system relaxes to equilibrium with a thermostat set by kinetic temperature, it will be at the desired thermodynamic temperature. To constrain the kinetic tem-

perature of the system, we can add a thermostating term to the expression for the change in momentum of the particles, α:

$$\dot{\mathbf{q}}_i = \frac{\mathbf{p}_i}{m} + \mathbf{C}_i F_e, \tag{3.9}$$

$$\dot{\mathbf{p}}_i = \mathbf{F}_{int} + \mathbf{D}_i F_e - \alpha \mathbf{p}_i. \tag{3.10}$$

There are an infinite number of constraints that could be added to the equations of motion that would constrain the temperature; how do we choose an appropriate constraint? The first consideration is that the constraint will maintain the temperature of the system. A second concern in thermodynamics is that the constraint will generate an equilibrium state in the absence of any time dependent fields:

$$\frac{\partial f(\mathbf{\Gamma}, t)}{\partial t} = 0. \tag{3.11}$$

This is important in thermodynamics as a constant temperature system should come to equilibrium.

The two most commonly used thermostats that satisfy these properties are the Gaussian and Nose-Hoover thermostats. The Gaussian isokinetic thermostat, proposed by Evans and Hoover, constrains the system such that the system temperature is a constant of the equations of motion: [10, 11]

$$\frac{\partial T}{\partial t} = 0. \tag{3.12}$$

This is equivalent to fixing the kinetic energy of the system. In contrast, the Nose-Hoover thermostat constrains the system by relating the thermostat term to the difference in temperature between the system and the thermostat, $T - T_{therm}$. [14, 15] This means that the Gaussian isokinetic thermostat will keep the system at a constant temperature for all times, while the Nose-Hoover thermostat will allow the system temperature to fluctuate around the thermostated temperature. When applying our equations we will use a Nose-Hoover thermostat, however we would get equivalent results from using a Gaussian isokinetic thermostat.

These temperature constraints are artificial, that is they are not present in any

physical process. Surprisingly, as long as we choose a sensible thermostat, such as those discussed above, we can still accurately model a physical system that interacts with a thermostat: the details of the thermostat are unimportant. [16] Indeed, as we will see when we apply these thermostats to the fluctuation relations, the details of the thermostat will cancel out, and it is only the temperature they introduce that matters.

Complications arise however due to the non-Hamiltonian nature of the thermostated dynamics. The choice of thermostat will affect the distribution function of the system: the Boltzmann distribution will be modified by the thermostat term chosen. Under Hamiltonian dynamics, volumes of phase space flow with time like an incompressible fluid: if we take an infinitesimal volume around a phase point and follow that volume in time, it will extend in some directions and compress in other so that its shape may change, but its volume in phase space will not. For a constrained system, it is as if we have a much larger system and have thrown away most of it: while phase space might be incompressible for the full system, it is not for the subsystem, for example Figure 3.2. We measure the distortion over time of an infinitesimal volume centred on $\mathbf{\Gamma}$ with the phase space contraction factor, Λ: [9]

$$\frac{d}{dt} ln[f(\mathbf{\Gamma}, t)] = -\Lambda(\mathbf{\Gamma}). \tag{3.13}$$

For a Hamiltonian system, Λ is 0, and there is no phase space contraction. [9]

With the equations of motion plus the thermostats we can describe the dynamics of our optical trapping system. Our system is in the thermostated canonical distribution, that is it has a constant number of particles, a fixed volume, and a Nose-Hoover thermostat constraint applied to a subset of the particles in the system that act as a wall. In addition, the first particle in the system, $\mathbf{q}_1$ is the colloid particle, and is subject to an external potential generated by the optical trap. Combining these

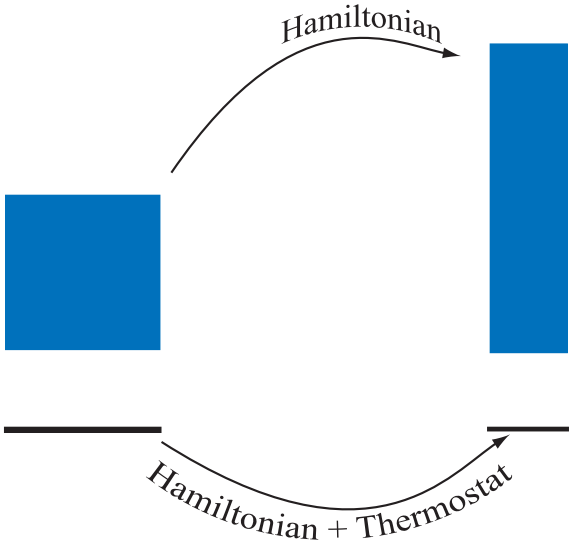

Figure 3.2: **Illustration of phase space contraction in thermostated systems arising from the reduction in dimensionality.** If we take a volume in phase space, such as the box, and let it evolve in time under Hamiltonian dynamics, then it will change shape but preserve its volume. When we introduce a constraint, such as a thermostat, we are effectively reducing the degrees in freedom in phase space. In this illustration the system goes from two dimensions (boxes) to one dimension (**lines**), and the phase space volume is not conserved in the reduced space.

expressions we get these equations of motion: [17]

$$\dot{\mathbf{q}}_i(t) = \frac{\mathbf{p}_i(t)}{m_i}, \tag{3.14}$$

$$\dot{\mathbf{p}}_i(t) = \mathbf{F}_{int} - \delta_{i1} k \mathbf{q}_i(t) - S_i \zeta(t) \mathbf{p}_i(t), \tag{3.15}$$

$$\dot{\zeta} = \frac{3k_B}{Q}(T_{therm} - T), \tag{3.16}$$

where S_i is a function that equals 1 for the wall particles and 0 for the non-wall particles, N_w is the number of the wall particles, Q is a scaling term for the thermostat, d is the number of spatial dimensions the experiment is carried out in (it will be between 1 and 3), and T_{therm} is the kinetic temperature of the wall particles. For a system in equilibrium with the optical trap, we get the following distribution phase co-ordinates:

$$f(\mathbf{\Gamma}) = \exp\left(-\beta[K(\mathbf{p}) + \Phi(\mathbf{q}) + \Phi_{trap}(\mathbf{q}_1, k_0) + \frac{1}{2}Q\zeta^2]\right)/z.$$

For the purposes of the fluctuation relations, we need to be able to define our

trajectory sets. The deterministic nature of the dynamics means that a single point in phase space defines an entire trajectory. We can therefore define our trajectory $\{\xi_0, \xi_\tau\}$ at any point along the trajectory $\mathbf{\Gamma}(t), 0 \leq t \leq \tau$: $\mathbf{\Gamma}(t) \equiv \{\xi_0, \xi_\tau\}$. To assign the time reverse trajectory $\{\xi^*_\tau, \xi^*_0]$, we must take the phase point with the same position elements, but reversed momenta, $\mathbf{\Gamma}^*$.

For most deterministic systems the only analytic distribution known will be that at equilibrium. Substituting our distribution functions into equations. 2.6, 2.24, we can derive our work and dissipation functions in terms of equilibrium distribution functions:

$$\Omega(\mathbf{\Gamma}) = \ln\big(\frac{f(\mathbf{\Gamma}(0),\lambda(0))}{f(\mathbf{\Gamma}^*(0),\lambda(0))}\frac{\partial V(\mathbf{\Gamma}(0))}{\partial V(\mathbf{\Gamma}^*(0))}\big), \tag{3.17}$$

$$\Delta W(\mathbf{\Gamma})) = \ln\big(\frac{f(\mathbf{\Gamma}(0),\lambda(0))}{f(\mathbf{\Gamma}^*(0),\lambda(\tau))}\frac{\partial V(\mathbf{\Gamma}(0))}{\partial V(\mathbf{\Gamma}^*(0))}\big). \tag{3.18}$$

For equilibrium canonical distributions, the phase space distribution is symmetric in momentum, $f(\mathbf{\Gamma}(\mathbf{q},\mathbf{p})) = f(\mathbf{\Gamma}(\mathbf{q},-\mathbf{p}))$. This means that the probability density for the time reverse phase, $\mathbf{\Gamma}^*$, will be the same as that for the final point of the forward trajectory in the same distribution, $\mathbf{\Gamma}(\tau)$: $p(\mathbf{\Gamma}^*(0),\lambda(0)) = p(\mathbf{\Gamma}(\tau),\lambda(0))$, $p(\mathbf{\Gamma}^*(0),\lambda(\tau)) = p(\mathbf{\Gamma}(\tau),\lambda(\tau))$. [18] We can then substitute our expression for the equilibrium distribution functions in terms of the modified Hamiltonians:

$$\Omega(\mathbf{\Gamma}) = \beta\int_0^\tau dt\big[\frac{dH(\mathbf{\Gamma}(t),\lambda(0))}{dt} - Q\zeta(t)\dot{\zeta}(t) - \Lambda(\mathbf{\Gamma}(t))\big], \tag{3.19}$$

$$\Delta W(\mathbf{\Gamma})) = \beta\int_0^\tau dt\big[\frac{dH(\mathbf{\Gamma}(t),\lambda(t))}{dt} - Q\zeta(t)\dot{\zeta}(t) - \Lambda(\mathbf{\Gamma}(t))\big]. \tag{3.20}$$

It is possible to take the expression for the work, equation 3.20, and expand the term in the integral,

$$\frac{dH(\mathbf{\Gamma}(t),\lambda(t))}{dt} = \frac{\partial H}{\partial \mathbf{q}}\frac{d\mathbf{q}}{dt} + \frac{\partial H}{\partial \mathbf{p}}\frac{d\mathbf{p}}{dt} + \frac{d\lambda}{dt}\frac{\partial H}{\partial \lambda} + \frac{d\zeta}{dt}\frac{\partial H}{\partial \zeta}, \tag{3.21}$$

which, we can simplify by substituting equation 3.5, subject to the extra constraint of the thermostat,

$$\frac{dH(\mathbf{\Gamma}(t),\lambda(t))}{dt} = \frac{d\lambda}{dt}\frac{\partial H}{\partial \lambda} + Q\zeta(t)\dot{\zeta}(t) + \Lambda(\mathbf{\Gamma}(t)). \tag{3.22}$$

Which means in practice that these functions can be solved in the canonical ensemble by ignoring the contribution of the thermostat/phase space compression. This is particularly important when applied to the work, as cancelling these terms when taking the derivative leads to this expression:

$$\Delta W = \beta \int_0^\tau dt \frac{d\lambda}{dt} \frac{\partial H(\mathbf{\Gamma}(t), \lambda(t))}{\partial \lambda}. \tag{3.23}$$

This is important as the mechanical work, w, is an energy, and it is related to this dimensionless work function through this expression, $\Delta W = \beta \mathrm{w}$, where $\beta = 1/k_B T$.

The mechanical work is a well defined quantity of physics. When a thermodynamic system undergoes a change in its internal energy, it exchanges energy with its surroundings in the form of work and heat. Changes in work correspond to the change in external parameters of the system, and heat corresponds to the exchange of thermal energy. Heat has a well understood connection with the entropy of a system; when a system is changed reversibly, the change in entropy is related to the heat transferred, $\Delta S = \beta q$.

When we compare our expression relating the mechanical work and thermodynamic work, we see a correlation between our thermodynamic work and the entropy. Both are related to energy quantities, but are statistical in nature. Thermodynamic work differs from entropy in that our thermodynamic work is a measure of an individual trajectory, while entropy is a measure over the ensemble. We connect the heat and entropy in a reversible system, because the heat transferred is the same over any trajectory in the ensemble. For an irreversible system, the equality breaks down, as the heat differs from trajectory to trajectory. The work equality is always true because it only describes the behaviour of individual trajectories. This implies that the thermodynamic work is a quantity similar to the entropy production for a given trajectory, but tied to work rather than heat. It is important to note that when non-deterministic dynamics are used, the relationship between the mechanical work and the thermodynamic work will differ.

Both the fluctuation theorem (FT) and work relation (WR) were originally proven using thermostated deterministic dynamics. [19, 20] Using our general approach, we reproduce the form of the dissipation, equation 3.17, and the form of the

work, 3.20, used in these derivations. This is important in confirming the utility of the general approach, and relating it to body of previous work on the fluctuation relations.

3.2.2 Stochastic Dynamics

In 1828, Brown noticed that particles suspended in solution would start and stop moving at random intervals and in random directions. [21] This random motion is fascinating as the motion comes not from the particles themselves, but from the thermal fluctuations of the solvent. This idea of random forces acting on a particle led directly to stochastic dynamics, that is dynamics driven by randomness. Interestingly, if we look at the motion of the solvent and the suspended particle together, we can represent the motion deterministically, while if we narrow our focus to just the particle, the motion becomes random. The choice of what dynamics to apply to a system is therefore one of scale.

The latex sphere used in an optical trapping experiment is significantly larger and more massive than the water molecules surrounding it. If we begin with a stationary sphere then we can imagine that at some point a solvent molecule will collide with the latex sphere. Due to the mass difference between the two particles, the latex sphere will only move very slightly. As time passes more and more solvent molecules will interact with the latex sphere, each one applying a very little bit of force, see Figure 3.3a. For an isotropic solution we would expect the average of the forces to be zero, however thermal fluctuations mean that there can be an imbalance in the impacts on each side of the sphere, leading to a significant net force. Langevin dynamics therefore work by using a course graining approximation, that is it averages the solvent interaction with the sphere over a short period of time, so for each time step there is a random but significant force, $g(t)$, exerted by the solvent on the sphere. In addition to this random force, there is a viscous component to particle's interaction with the solvent. If we look at a particle moving through the solvent over a short time interval, it is more likely to hit particles in its direction of movement rather than the opposite direction, and this will act to slow the particle down or "damp" its motion. The faster the particle is travelling, the more solvent particles it will hit, and

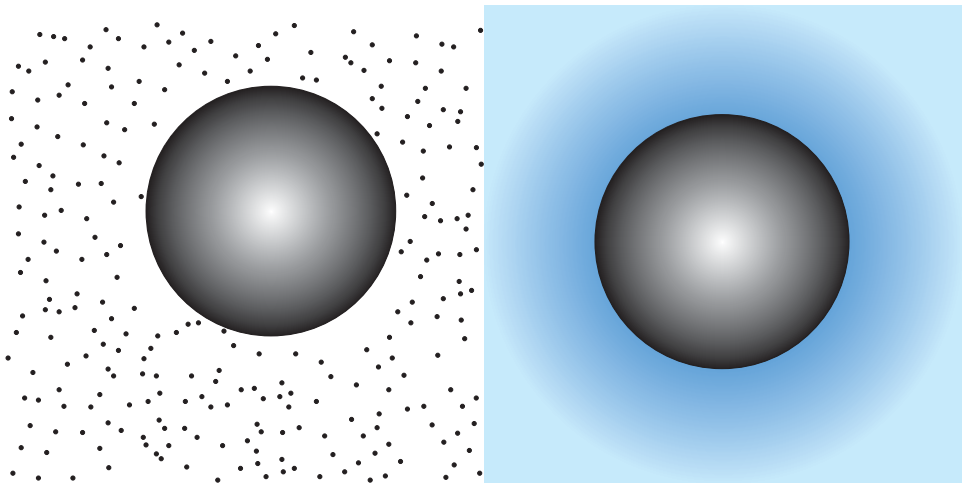

(a) (b)

Figure 3.3: **Two illustrations representing a a colloid in solvent using deterministic and stochastic dynamics.** In figure 3.3a we present an illustration of a colloid suspended in fluid as represented by deterministic dynamics, and in figure 3.3b we present an illustration of colloid suspended in fluid as represented by stochastic dynamics. Under deterministic dynamics, the solvent molecules are explicitly modelled, while under stochastic dynamics the solvent molecules are represented by a continuous force field.

the stronger the drag will be: the force exerted on the particle will be proportional to the velocity.

To produce the Langevin equation, we simply start with Newton's first law of motion,

$$m\ddot{\mathbf{r}} = \mathbf{F}, \tag{3.24}$$

in terms of the acceleration of the colloid particle, $\ddot{\mathbf{r}}$, and replace the interaction of the solvent with the sphere with the random force and the drag force:

$$m\ddot{\mathbf{r}} = F_{ext} - \zeta\dot{\mathbf{r}} + g(t), \tag{3.25}$$

where ζ is the friction co-efficient that relates the velocity to the drag force, and F_{ext} represents any non-solvent forces on the particle. For our work, we wish to make an additional approximation to simplify the dynamics, the inertialess approximation, $m = 0$. If the inertial term, $m\ddot{\mathbf{r}}$, of the particle is very small, relative to the force terms, the left hand side of the equation will go to zero, and we can rewrite our

equations of motion: [22]

$$\zeta \dot{\mathbf{r}} = F_{ext} + g(t). \tag{3.26}$$

In traditional mechanics, the velocity of an object depends upon its previous velocity and the forces exerted upon it. Under inertialess dynamics, the velocity only depends upon the force; the previous velocity of the particle has no bearing on the current velocity. Physically, this represents the drag on the particle stopping the particle, and the random force kicking it in another direction, all over a time scale smaller than our course graining scale.

The external force for the system is again our harmonic potential. For a viscous solvent such as water, the random force is an average, and therefore the central limits theorem tells us that it must be Gaussian distributed, as it is with these properties: $\langle g(t) \rangle = 0$, $\langle g(t)g(t') \rangle = 2\zeta k_B T \delta(t - t')$. [22] Combining these we can derive our equilibrium distribution function for an optically trapped colloid, which is a Boltzmann distribution (for one dimension):

$$P(\mathbf{r}) = \sqrt{\frac{k}{2\pi k_B T}} \exp\left(-\frac{k\mathbf{r}^2}{2k_B T}\right). \tag{3.27}$$

It should come as no surprise that this distribution for the particle position is the same as it would be under deterministic dynamics: they describe the same system of a particle in a harmonic potential.

To generate our stochastic fluctuation relations, we map our trajectory $\{\xi_0, \xi_\tau\}$, to our position space $\{\mathbf{r}_0, \mathbf{r}_\tau]$, and our transition will depend on how we vary the system. Unlike deterministic dynamics, knowing $\mathbf{r}_0$ does not define the whole trajectory, we have to define the end point as well. It is therefore insufficient to express our arguments solely in terms of the initial distributions. To account for the evolution of the system, we define a Green's function $G(\mathbf{r}_\tau : \mathbf{r}_0, t, \lambda(s))$, which is the conditional probability function that the particle will be at $\mathbf{r}_\tau$ given it was at $\mathbf{r}_0$ a time τ earlier and was acted upon by by a time dependent external parameter $\lambda(s)$. For the optical trapping system, we will be varying the velocity of the trap, v_{opt}, or the trapping constant k over time, and the final form of the Green's function will reflect this. Combining our expression for the initial probability P, and our Green's function G,

into equations. 2.6, 2.24, we can express our dissipation and work functions under stochastic dynamics: [23]

$$\Omega = \ln(\frac{P(\mathbf{r}_0, \lambda(0))G(\mathbf{r}_\tau : \mathbf{r}_0, \tau, \lambda(t))}{P(\mathbf{r}_\tau, \lambda(0))G(\mathbf{r}_0 : \mathbf{r}_\tau, \tau, \lambda(t))} \tag{3.28}$$

$$\Delta W_d = \ln(\frac{P(\mathbf{r}_0, \lambda(0))G(\mathbf{r}_\tau : \mathbf{r}_0, \tau, \lambda(t))}{P(\mathbf{r}_\tau, \lambda^*(0))G(\mathbf{r}_0 : \mathbf{r}_\tau, \tau, \lambda^*(t))} \tag{3.29}$$

We define the normalised work, rather than the work for the stochastic expression under optical trapping because our partition functions are trivial additions to the expression: they are the normalisation factor to the Boltzmann distribution,

$$z_{\lambda(0)} = \sqrt{\frac{k(\lambda(0))}{2\pi k_B T}}. \tag{3.30}$$

Indeed, we can calculate the change in the free energy by simply taking the ratio of these normalisation terms. The stochastic WR is therefore unnecessary to calculate free energy differences: all of the information is contained in our probability distributions that we would use to derive the work. It is also worth noting that the free energy change calculated using stochastic dynamics is the free energy change associated with the particle degrees of freedom, as this is the thermodynamic system of interest under these dynamics.

In addition to the standard fluctuation relations, under stochastic dynamics we have an additional fluctuation relation, the Hatano-Sasa relation: [24, 25]

$$\langle e^{-Y} \rangle = 1, \tag{3.31}$$

where the argument in the expression is,

$$Y = \int_0^\tau dt \frac{d\lambda(t)}{dt} \frac{\partial(-\ln(P(\mathbf{r}(t), \lambda(t))))}{\partial \lambda}. \tag{3.32}$$

The relationship of this to the other fluctuation relations is interesting. It represents the stochastic analogy to the deterministic expression in equation. 3.23, but for the normalised work function, W_d. It cannot however be related back to a ratio of

probability functions:

$$\exp(Y) \neq \frac{P_{\lambda(0)}(r(0))}{P_{\lambda^*(0)}(r(t))}. \tag{3.33}$$

The reason for this discrepancy is due to the properties of the two differentials. If we take the differential of the log of the probability function under stochastic dynamics, we get an additional contribution from the position:

$$\frac{d\ln(P(\lambda(t),\mathbf{r}(t))}{dt} = \frac{d\lambda}{dt}\frac{\partial\ln(P(\lambda(t),\mathbf{r}(t))}{\partial\lambda} + \frac{d\mathbf{r}}{dt}\frac{\partial\ln(P(\lambda(t),\mathbf{r}(t))}{\partial\mathbf{r}}. \tag{3.34}$$

Under deterministic dynamics, the integral and ratio forms of the work are interchangeable as the terms in position, momentum, and the thermostat cancel out in the integral. Under stochastic dynamics, these expressions are different, but both obey fluctuation relations. Both the stochastic work function, and the Hatano-Sasa functions are stochastic analogues to the deterministic (mechanical) work function, one is the analogue if we compare probability ratios, and the other probability integrals.

Langevin dynamics produce easy to solve equations of motion that enable us to produce distributions for the system under both equilibrium and non-equilibrium distributions. The trade off for this is an inability to probe short time scales or inertial effects. The fluctuation relations derived under stochastic dynamics share these advantages and disadvantages, as we will show in our results.

3.3 Simulation of optical trapping

Computer simulation provides a valuable intermediate between theory and experimentation. By performing computer simulations for a system we can check for errors or problems and correct them before undertaking experiments. Simulations can also provide proof of concept through the use of extremely simple systems, or systems that are not experimentally realisable.

While we think of a computer simulation as a virtual representation of the physical world, we approach them as a numerical analysis of the dynamics of a system. An actual experiment can be represented by deterministic and stochastic dynamics, and therefore fluctuation relations derived for both dynamics can be applied. On the other hand, a computer simulation is a product of the dynamics used, and different

equations of motion will yield different simulations. Stochastic dynamics are an approximation of deterministic dynamics: under the hood of the Langevin equation are Newton's equations of motion. What this means is that if we perform a stochastic simulation, we can apply fluctuation relations derived using stochastic or deterministic dynamics, but for a deterministic simulation, we can only apply deterministic dynamic unless we fall into the region where the Langevin approximation applies. Unfortunately, the deterministic simulations we perform are incompatible with this approximation.

3.3.1 Molecular Dynamics Simulation

Molecular dynamics (MD) simulations solve Newton's equations of motion to model a system. In order to do this we need to fill in the details of our system. The first step to performing MD simulations is to fully detail our equations of motion for each particle. We do this by defining the intermolecular forces for the system $\mathbf{F}_{int}$ in equation 3.4. In an experimental system the intermolecular force between two particles $\mathbf{F}_{ij}$, is a complex expression that depends on the nature and relative geometry of the two particles. To simplify our treatment of the system, we model the particles in the system as spheres: this means the inter-particle force is modelled from a potential that depends only on the separation of the two particles. Spherical potentials can take two forms: hard sphere potentials and soft sphere potentials. Hard spheres are exactly that, spheres that only interact through elastic collisions at a distance of $2r$. Soft sphere potentials exert forces over a range of inter-particle distances. For our simulations, we have used soft sphere potentials.

Two soft sphere inter-particle potentials are commonly used in MD simulations, the Lennard-Jones potential and the Weeks, Chandler, Andersen (WCA) potential. [8] The Lennard-Jones potential tries to incorporate the features of a real particle potential: a short range repulsive component and a long range attractive component,

$$\Phi_{LJ}(r) = 4\epsilon((\frac{\sigma}{r})^{12} - (\frac{\sigma}{r})^{6}), \tag{3.35}$$

where ϵ is the minima of the potential, and σ is the distance at which the potential is zero. The WCA potential is a simplification of the Lennard-Jones potential by

cutting the potential at its minima, r_{min} and setting this equal to zero:

$$\Phi_{WCA} = \begin{cases} \Phi_{LJ} + \epsilon & r < r_{min}, \\ 0 & r \geq r_{min}. \end{cases} \tag{3.36}$$

This function is continuous, but the range of the potential is finite, simplifying computation. We use the WCA potential for our simulations.

The difficulty with using soft sphere potentials is that more than two bodies can interact at a time and the equations of motion will become intractable. In order to evolve the simulation with time we have to numerically integrate the equations of motion. There are many methods available to integrate these functions; we use a fourth order Runge-Kutta algorithm. [26] The Runge-Kutta algorithm solves the change in a variable by re-expressing it as an integral, and numerically approximating the integral in terms of a sum of functions at subintervals between the initial and final time point. If we take position for example, we can approximate the change in position over a small time to the position at the start of that time plus an approximation over the momentum integral for that time period:

$$\mathbf{q}_i(t) = \int_0^t ds \frac{\mathbf{p}_i(s)}{m_i}, \tag{3.37}$$

$$\mathbf{q}_i(t + \Delta t) \approx \mathbf{q}_i(t) + \Delta t \frac{\mathbf{p}_i(\mathbf{q}_i(t + \Delta t/2), t + \Delta t/2)}{m_i}. \tag{3.38}$$

The position of the particle at $t + \Delta t/2$ is unknown, and is generated by approximating from the momentum integral again using the Euler method:

$$\mathbf{q}_i(t + \Delta t/2) = \mathbf{p}_i(\mathbf{q}_i(t), t)\Delta t/2, \tag{3.39}$$

this is the second order Runge-Kutta. The forth order Runge Kutta algorithm adds

two more time steps:

$$\mathbf{q}_i(t+\Delta t) \approx \mathbf{q}_i(t) + \frac{\Delta t}{6}\frac{\mathbf{p}_{i,1}+2\mathbf{p}_{i,2}+2\mathbf{p}_{i,3}+\mathbf{p}_{i,4}}{m_i} \tag{3.40}$$

$$\mathbf{p}_{i,1} = \mathbf{p}_i(\mathbf{q}_i(t), t) \tag{3.41}$$

$$\mathbf{p}_{i,2} = \mathbf{p}_i(\mathbf{q}_i(t) + \Delta t\mathbf{p}_{i,1}/2, t + \Delta t/2)) \tag{3.42}$$

$$\mathbf{p}_{i,3} = \mathbf{p}_i(\mathbf{q}_i(t) + \Delta t\mathbf{p}_{i,2}/2, t + \Delta t/2)) \tag{3.43}$$

$$\mathbf{p}_{i,4} = \mathbf{p}_i(\mathbf{q}_i(t) + \Delta t\mathbf{p}_{i,1}, t + \Delta t)) \tag{3.44}$$

The uncertainty in the position is $O(\Delta t^5)$. One important feature of the Runge-Kutta integrator is that it is self starting, that is it only requires knowledge of the initial position, as opposed to many integrators which rely on expansions that include previous time points as well as future time points. This means that we can simply create a set of particles, assign them velocities and start the simulation.

To model our experiment we make a number of other approximations to limit the amount of time required to simulate our system. In our experiment, the colloid particle is orders of magnitude larger in both mass and radius than the surrounding fluid particles. This means that at a given temperature, the fluid particles are moving significantly faster than the colloid. If we simulate this system, a large number of time steps will be spent simulating the fluid motion while the colloid particle stays relatively stationary. To overcome this problem we treat the colloid as having the same size as the other fluid particles: the only difference is that it feels the harmonic potential.

Another consideration is the number of particles simulated, in a real system there are $O \sim 10^{23}$ particles, from a practical point of view we want to simulate tens to hundreds of particles. We can overcome this problem with periodic boundary conditions. [8] Under periodic boundary conditions, we create a box with a modest number of particles in it. We then create images of this box and translate them to the borders of the box, repeating this process with the new boxes until we have an infinite number of these identical boxes, figure 3.4. We now have a macroscopic number of particles created using a small repeated subset. In a simulation, we only need to generate the original box, and we can reproduce the behaviour of the tessellated

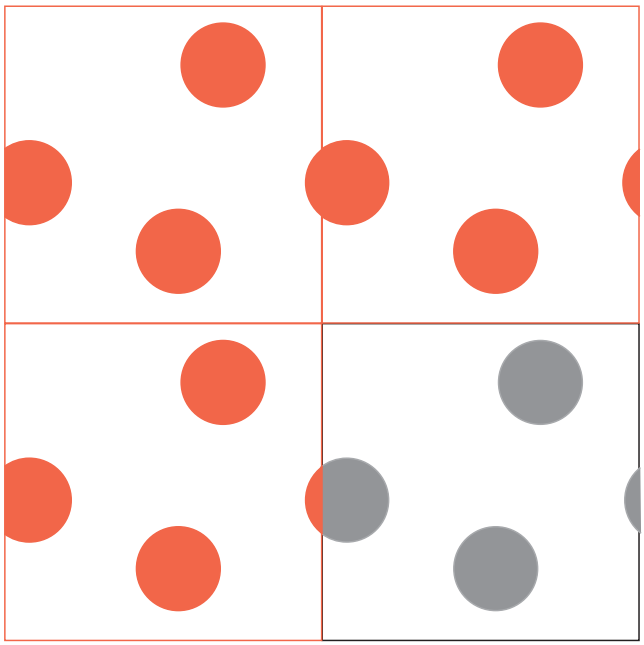

Figure 3.4: **Illustration of periodic boundary conditions.** Periodic boundary conditions represent a large system with an infinite number of repeated boxes of particles. To perform simulations, we only need to simulate one box (gray), and "wrap" potentials and particles that cross one side of the box to the other.

system by allowing particles and potentials that cross one boundary to appear on the opposite boundary. It is important when constructing periodic boundary conditions that each particle only interacts with only one copy of a given particle. This can be ensured by making r_{min} in the WCA potential less than half the box length.

To begin an experiment we start by arranging a set of particles in our box is a simple crystal lattice that is evenly spaced. We randomly assign momenta to the particles using the temperature distribution and then rescale the momenta so that there is a net momentum of zero in each dimension. The system is then allowed to run for a significant period of time so that it comes to equilibrium with the initial state for our simulations.

To avoid repeating this initial set up and equilibration, we rely on a branching approach to our simulation, figure 3.5. The first branch, known as the mother trajectory, will continue the simulation under the current conditions so that it remains in equilibrium. To generate an experimental trajectory, we pause our mother trajectory, perturb the system conditions in accordance with our experiment, and run off a new branch known as a daughter trajectory. We then return to the point

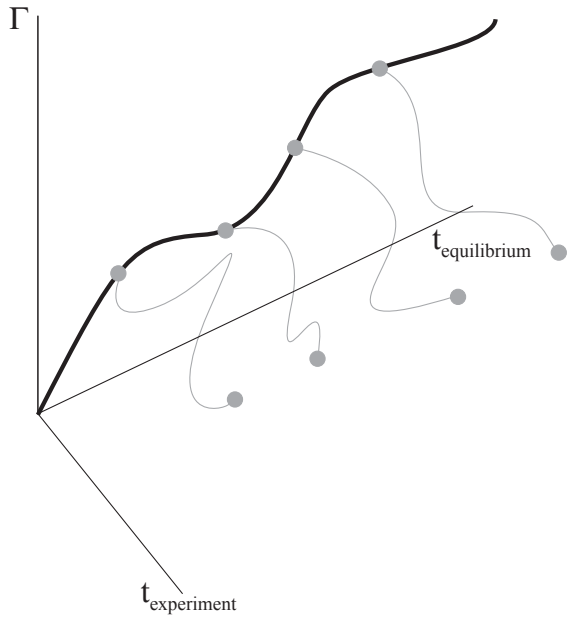

Figure 3.5: **Illustration of branching trajectories for MD simulations.** A single simulation trajectory (**black**) under equilibrium conditions is used to spawn many non-equilibrium experimental trajectories (gray) for an MD simulation.

where we paused the mother trajectory, and restart it under equilibrium conditions. If we let the mother trajectory evolve for long enough, its position in phase space will become independent of where we split the previous daughter trajectory. We can then split another daughter trajectory off, and repeat the process indefinitely to generate an ensemble of daughter trajectories, to represent performing an ensemble of experiments.

While MD simulations are somewhat abstracted from the real experimental system, they still provide an important test on the fluctuation relations. This is because MD simulations contain the fundamental features and dynamics that underlie an optical trapping experiment. If these simulations verify the fluctuation relations for a given system, then the experimental system should obey these relations as well.

3.3.2 Stochastic simulation

A Langevin dynamics simulation of an optical trapping experiment simulates the motion of the colloid particle by solving the Langevin equation. [22] These simulations produce results that are directly comparable with the optical trapping experiments, except over very short time scales. This makes Langevin simulations valuable for

assessing the feasibility of experiments, and trouble shooting problems.

Langevin dynamics are stochastic dynamics, that is they are driven by random forces. The key to running a Langevin simulation is producing random numbers. Unfortunately, computers, like people, are unable to produce truly random numbers. We instead rely on quasi-random numbers: numbers generated from a numerical algorithm or pattern. While not truly random, quasi-random numbers can be produced during a simulation and are repeatable, that is if we use the same algorithm with the same start point, we will generate the same set of random numbers.

When using quasi-random numbers two factors have to be taken into account. The first is that the random numbers must be evenly distributed over their range. This can be checked by producing a large quantity of numbers and analysing their distribution. The second factor to take into account is recurrence time.

Since we are using a numerical method to generate a sequence, when our random number generator repeats a number, the entire sequence of numbers following it will recur. It is important that the number of terms taken in the sequence before recurrence is larger than the number of random variables we are using in a simulation, otherwise we will keep using the same random number sequence over and over biasing the results. For our simulations we generate random numbers between 0 and 1 using a quasi-random number generator from Numerical Recipes (ran1) and then map the result to a Gaussian distribution. [27] The generator produces an unbiased Gaussian upon mapping and has a recurrence time of 2.1×10^9 samples. For the simulations in Chapter 5, we exceed this number of random numbers, and use a different generator (ran2), with a recurrence time of 2.3×10^{18} samples. [27]

For our simulations we are interested in the position of the colloid. Each simulation trajectory starts with a random number being used to pick a point from the initial position distribution, equation 3.27. To advance the simulation with time, we integrate the stochastic equations of motion and express in terms of position:

$$r(t) = r(0) + \frac{F_{opt}t}{\zeta} + R, \tag{3.45}$$

where R is the random force. We can build up a trajectory by sequentially advancing the position of the particle, and produce multiple trajectories to generate an

ensemble.

The advantage of performing Langevin simulations is that they can be directly compared with experimental results. If the fluctuation relations are verified for a Langevin simulation of an optical trapping system, they will work in the experiment.

3.3.3 Conclusion

Optical trapping is an excellent system to test the fluctuation relations. With a set of optical tweezers we can create interesting experiments with properties that are well characterised with theoretical models, allowing us to apply the fluctuation relations to these experiments in the next two chapters. In addition, the simplicity of this system makes it suitable for computer simulations to presage or bolster our experimental results.

Bibliography

[1] P. Tipler, G. Mosca, *Physics for scientists and engineers, Fifth Edition* (W.H. Freeman, 2004).

[2] A. Ashkin, *Phys. Rev. Lett.* **24**, 156 (1970).

[3] A. Ashkin, J. M. Dziedzic, J. E. Bjorkholm, S. Chu, *Opt.Lett.* **11**, 288 (1986).

[4] D. G. Grier, *Nature* **424**, 810 (2003).

[5] A. Ashkin, *Proc. Nat. Acad. Sci. USA* **94**, 4853 (1997).

[6] J. E. Molloy, M. J. Padgett, *Cont. Phys.* **43**, 241 (2002).

[7] D. M. Carberry, *Optical Tweezers: Experimental Demonstrations of the Fluctuation Theorem* (PhD Thesis: Australian National University, 2005).

[8] M. Allen, D. J. Tildesley, *Computer Simulation of Liquids* (Oxford University Press, 1987).

[9] D. Evans, G. Morriss, *Statistical Mechanics of Nonequilibrium Liquids* (Academic Press, 1990).

[10] D. J. Evans, *J. Comp. Phys.* **78**, 3297 (1983).

[11] W. G. Hoover, A. J. C. Ladd, B. Moran, *Phys. Rev. Lett.* **48**, 1818 (1982).

[12] P. Atkins, *Physical Chemistry, Fifth Edition* (Oxford University Press, 1994).

[13] O. Jepps, G. Ayton, D. Evans, *Phys. Rev. E* **62**, 4757 (2000).

[14] D. J. Evans, B. Hoilan, *J. Comp. Phys.* **83**, 4069 (1985).

[15] W. G. Hoover, *Phys. Rev. A* **31**, 1695 (1985).

[16] S. R. Williams, D. J. Searles, D. J. Evans, *Phys. Rev. E* **70**, 066113 (2004).

[17] G. M. Wang, E. M. Sevick, E. Mittag, D. J. Searles, D. J. Evans, *Phys. Rev. Lett.* **89**, 050601 (2002).

[18] D. J. Evans, D. J. Searles, *Adv. Phys.* **51**, 1529 (2002).

[19] D. J. Evans, D. J. Searles, *Phys. Rev. E* **50**, 1645 (1994).

[20] D. J. Evans, *Molecular Physics* **101**, 1551 (2003).

[21] J. McLennan, *Introduction to Non-Equilibrium Statistical Mechanics* (Prentice-Hall, 1989).

[22] M. Doi, S. F. Edwards, *The Theory of Polymer Dynamics* (Clarendon Press, 1988).

[23] J. Reid, D. Carberry, G. M. Wang, E. M. Sevick, D. J. Searles, D. J. Evans, *Phys. Rev. E* **70**, 16111 (2004).

[24] T. Hatano, S. Sasa, *Phys. Rev. Lett.* **86**, 3463 (2000).

[25] E. H. Trepagnier, C. Jarzynski, F. Ritort, G. E. Crooks, C. J. Bustamante, , J. Liphardt, *Proc. Nat. Acad. Sci. USA* **101**, 15038 (2004).

[26] D. Rapaport, *The Art of Molecular Dynamics Simulation, Second Edition* (Cambridge University Press, 2004).

[27] W. Press, S. Teukolsky, W. Vetterling, B. Flannery, *Numerical Recipes in Fortran 77, The Art of Scientific Computing, Second Edition* (Cambridge University Press, 2001).

Chapter 4

Experiments to test the Fluctuation Theorem

The optical trapping system was originally used to test the fluctuation theorem (FT) with arguments derived using deterministic dynamics. In this chapter we will discuss three optical trapping experiments, capture, drag, and steady state drag, that all test the FT. In particular, we will look at how the form and application of the dissipation function is affected by the choice of dynamics used to analyse each of these experiments.

4.1 Capture

In the capture experiment of Carberry and others, [1] a particle begins in equilibrium with a harmonic trap of force constant k_0, and at $t = 0$ the trap is increased instantaneously in strength to k_1, Figure 4.1. As the force on the particle towards the trap centre is increased for any given particle position, we would expect the particle to move towards the trap centre. However, the Brownian motion of the particle, coupled with the possibility of the particle starting extremely close to the trap centre make it possible for the particle to end further from the trap centre than it started, exhibiting statistically unlikely or anti-entropic behaviour that can be quantified by the FT.

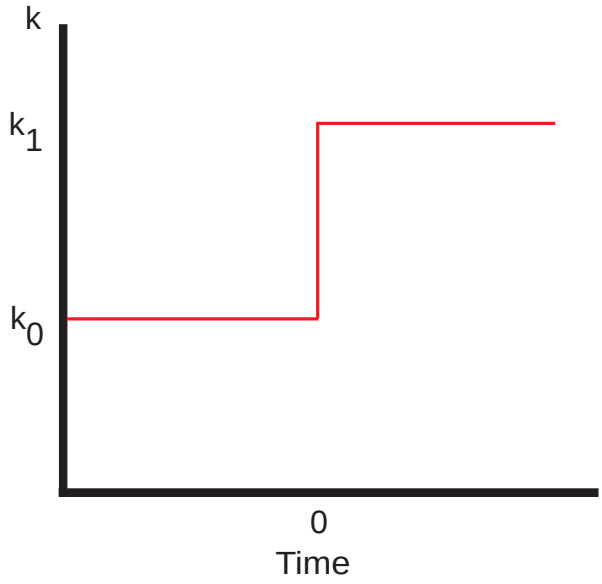

Figure 4.1: **Figure showing time dependent external parameter for the capture experiment.** Trapping constant, k, vs time, for capture experiment. The trap begins in equilibrium with trapping constant k_0, and at $t = 0$ the trap is discontinuously changed to k_1.

4.1.1 Deterministic

Under deterministic dynamics, the optical trapping system includes the trapped particle and the solvent, while the external parameters include the volume, the thermostat, and the optical trap. In the capture experiment we will be varying the trap strength: the initial system distribution will be governed by the initial trapping constant, k_0, while the equations of motion for the experiment are governed only by k_1, because the spring constant has changed before the system starts moving.

In section 3.2.1, we showed that the dissipation function for a deterministic system reduces to equation 3.19,

$$\Omega(\mathbf{\Gamma}) \quad = \quad \beta \int_0^\tau dt \big[\frac{dH(\mathbf{\Gamma}(t), \lambda(0))}{dt} - Q\zeta(t)\dot{\zeta}(t) - \Lambda(\mathbf{\Gamma}(t)) \big].$$

Expanding and solving we can derive our dissipation function:

$$\begin{aligned}\Omega(\mathbf{\Gamma}) &= \beta\int_0^t ds[\dot{K}(\mathbf{p}(s)) + \dot{\Phi}(\mathbf{q}(s)) + \dot{\Phi}_{trap}(\Gamma(s),k_0) - Q\zeta(t)\dot{\zeta}(t) - \Lambda(\mathbf{\Gamma}(t))],\\ &= \beta\int_0^t ds[(k_0-k_1)\mathbf{q}_1(s)\dot{\mathbf{q}}_1(s)],\\ &= \frac{1}{2}\beta(k_0-k_1)(\mathbf{q}_1^2(t)-\mathbf{q}_1^2(0)).\end{aligned} \tag{4.1}$$

The dissipation function will therefore be positive when the particle is closer to the trap centre at the end of the experiment than it was at the beginning, and negative if the particle ends further from the trap than it started. If we do the reverse experiment, and have our initial trap constant higher than our final trap constant, $k_0 > k_1$, then we would have the opposite behaviour: positive dissipation when the particle moved away from the trap centre and negative dissipation when it moved towards the trap centre. The dissipation function is a measure of physical expectation for the experiment, it is positive when the system does what we would expect it to do on average, and it is negative when it does not.

The capture experiment is best interpreted as a relaxation experiment. The system starts in a distribution that is not the equilibrium distribution for the external parameters, that is it starts in equilibrium with k_0 but the dynamics are governed by k_1, and relaxes over time towards equilibrium for k_1. All the work is done in changing the trap constant at $t = 0$, and afterwards the system is simply relaxing toward equilibrium. The net result of this is that the chance of negative dissipation does not go towards zero at long time. This is because even at long time, a particle that started close to the centre has the possibility of moving away from the trap centre.

Applying the work relation (WR) to this system is somewhat trivial. The change in the trap constant is carried out at $t = 0$, and the work function is simply the difference between the two trap constants at the same position:

$$\Delta W = \beta(k_1 - k_0)\mathbf{q}_1^2(0). \tag{4.2}$$

This corresponds to sampling the difference in the Hamiltonian due to the trap

change over the initial distribution function, the instantaneous sampling method, a well known result in equilibrium statistical mechanics:

$$\langle \exp(-\beta \Delta H(\mathbf{\Gamma}(0))) \rangle = \exp(-\beta \Delta A), \tag{4.3}$$

where $\Delta H(\mathbf{\Gamma}(0))$ is the difference between the final and initial Hamiltonians, $H(\mathbf{\Gamma}(0), t) - H(\mathbf{\Gamma}(0), 0)$.

Interestingly, the FT and WR are disjoint in their application to this system. When the work is done at $t = 0$, the value of dissipation is 0 for all trajectories. Once the system is dissipating, $t > 0$, the work is complete and the system is simply relaxing towards a new equilibrium under the new trapping constant.

4.1.2 Stochastic

The capture experiment was the first experiment to demonstrate the FT with a dissipation function derived from stochastic dynamics. Before the capture experiment the FT had been limited to deterministic systems and stochastic systems involving discontinuous dynamics. The capture experiment therefore represents the start of the development of the generalised definitions for the fluctuation relations.

From section 3.2.2, we define the stochastic dissipation function as:

$$\Omega = \ln\left(\frac{P(\mathbf{r}_0, \lambda(0)) G(\mathbf{r}_\tau : \mathbf{r}_0, \tau, \lambda(t))}{P(\mathbf{r}_\tau, \lambda(0)) G(\mathbf{r}_0 : \mathbf{r}_\tau, \tau, \lambda(t))}\right). \tag{4.4}$$

The starting distribution for the capture experiment is the Boltzmann distribution for a trap of strength k_0:

$$P(\mathbf{r}_0, k_0) = \sqrt{\frac{k_0}{2\pi k_B T}} \exp\left(-\frac{k_0 \mathbf{r}_0^2}{2 k_B T}\right). \tag{4.5}$$

The Green's function provides the probability of observing a particle at $\mathbf{r}_t$ in a trap of strength k_1, given its position $\mathbf{r}_0$ at time t earlier:

$$G(\mathbf{r}_t; \mathbf{r}_0, k_1, t) = \left[\frac{k_1}{2\pi k_B T (1 - \exp(-2t/\tau))}\right]^{\frac{1}{2}} \exp\left(-\frac{k_1 (\mathbf{r}_t - \mathbf{r}_0 \exp(-t/\tau))^2}{2 k_B T (1 - \exp(-2t/\tau))}\right). \tag{4.6}$$

where $\tau = \xi / k_1$ is the characteristic relaxation time of the particle residing in a

Table 4.1: Parameters for the capture experiment

k_0	$1.2pN/\mu m$
k_t	$2.8pN/\mu m$
Trajectories	3300

harmonic potential of strength k_1. In the limit of long time, $t \to \infty$, the Green's function reduces to the time-independent Boltzmann distribution for a particle in a well of strength k_1. Solving for the dissipation function, equation 3.28, we get:

$$\Omega = \frac{1}{2k_BT}(k_0 - k_1)(\mathbf{r}_t^2 - \mathbf{r}_0^2). \tag{4.7}$$

This expression is identical to the dissipation function derived from equation 3.19 using deterministic dynamics.

4.1.3 Experimental Capture

The parameters for the experiment are in table 4.1. [1] Given the identical forms of the dissipation function under both stochastic and deterministic dynamics, the experimental results demonstrate the FT for both sets of dynamics. The primary difficulty in this experiment was a slight lag in the power response of the laser: measurements were conducted at millisecond intervals, and the change in laser power took place over 2-3 ms, rather than instantly. This meant that for short system trajectories, $t \sim 10ms$, the change in laser power was a significant proportion of the trajectory time rather than the insignificant proportion assumed in describing the dynamics of the system. As the length of the trajectory in time is increased, an instantaneous transition becomes a better and better representation of the system. FT results are therefore presented at long times. In figure 4.2a, we present the FT and in figure 4.2b, we present the two sides of integrated form of the FT, for the capture experiment. Both of these figures show the experimental results to be consistent with the FT.

Figure 4.2: **Two figures showing FT and integrated FT results for the capture experiment.** In figure 4.2a we plot $\ln(P(\Omega = A)/P(\Omega = -A)$ vs Ω for the capture experiment at $t = 200$ms with the expected result for the FT (red), and in figure 4.2b we plot dimensionless value vs time, for $P(\Omega < 0)/P(\Omega > 0)$ $(+)$ and $\langle \exp(-\Omega) \rangle_{(\Omega>0)}$ $(\times)$ for the capture experiment. Both of these plots are constructed from 3300 trajectories. The points in figure 4.2a agree with the expected result for the FT. In figure 4.2b the two curves are co-incident, demonstrating the integrated form of the FT. [This data was originally presented in reference [1]].

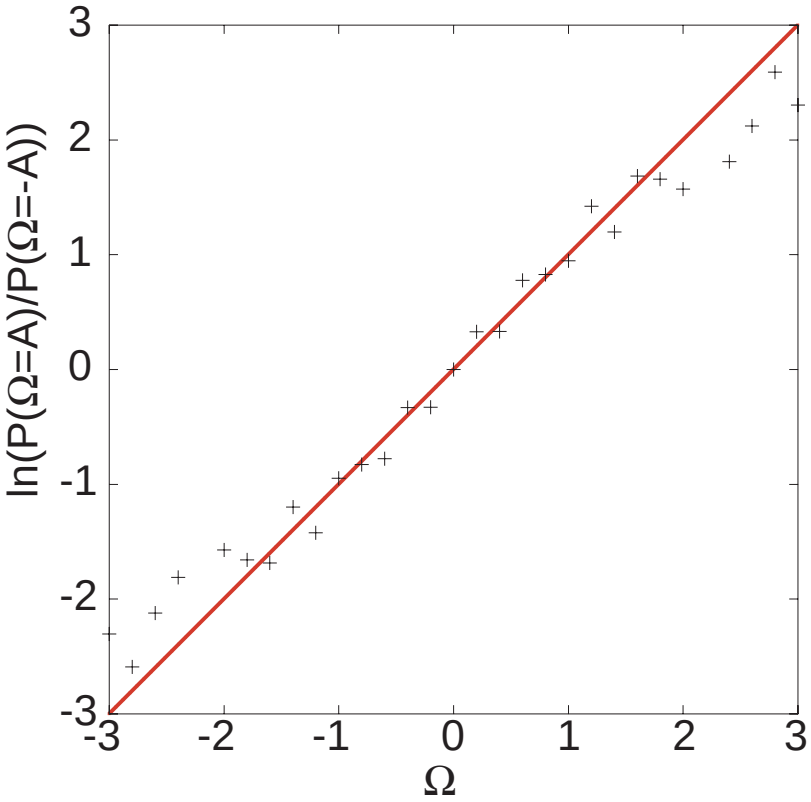
ln(P(Ω=A)/P(Ω=-A))
Ω
3
2
1
0
-1
-2
-3
-3
-2
-1
0
1
2
3

(a)

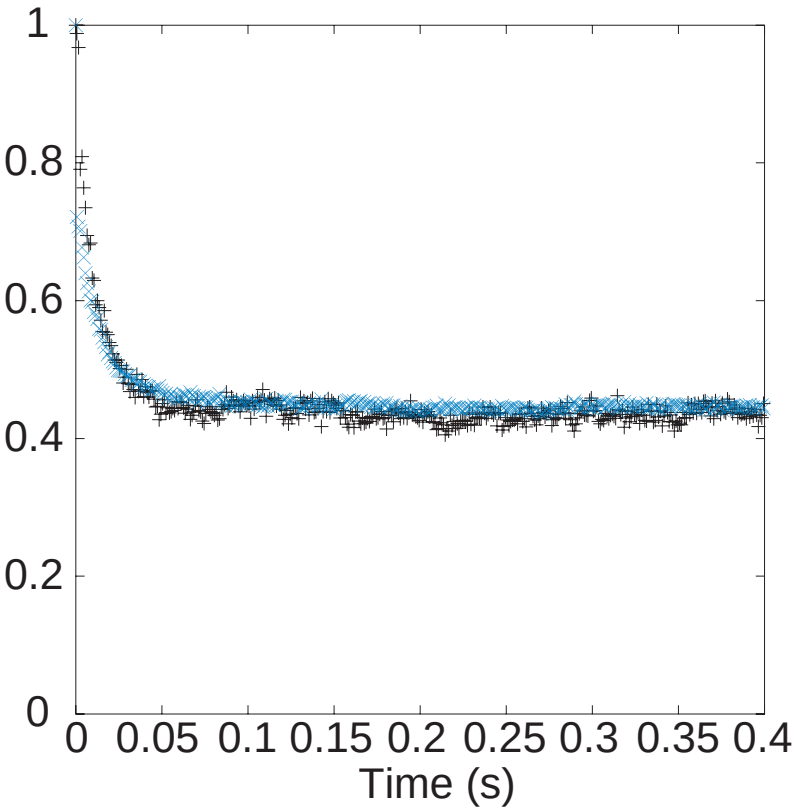
1
0.8
0.6
0.4
0.2
0
0
0.05
0.1
0.15
0.2
0.25
0.3
0.35
0.4
Time (s)

(b)

Figure 4.2

4.2 Drag

The drag experiment of Wang was the first experiment undertaken to test any of the fluctuation relations. [2] In this experiment, a particle begins in equilibrium with the trap, before the trap is displaced at a constant velocity, $\mathbf{v}_{opt}$, exerting a potential of:

$$\Phi(\mathbf{\Gamma}(t), t) = \frac{1}{2}k(\mathbf{q}_1(t) - (\mathbf{v}_{opt}t))^2. \tag{4.8}$$

During the experiment the particle feels the force of the optical trap balanced against the drag of the fluid as it moves through it. From this simple force balance, we expect the particle to continually lag behind the trap. Due to the thermal fluctuations in the liquid, it is possible for the particle to sometimes lead the trap, violating this expectation.

4.2.1 Deterministic

The drag paper of Wang and others provided the first experimental verification of the FT. [2] The capture and drag experiments are extremely similar under deterministic dynamics as both represent an optical trapping system in the same way, and both are subject to a discontinuous change in the system at the start of the experiment. The differences between the two are that in capture, we change the trapping constant from k_0 to k_1, while in the drag experiment there is just one trapping constant, k, and instead we give the optical trap a velocity of v_{opt} at $t = 0$. This makes the dissipation functions of the two experiments quite different.

The dissipation function for the experiment was derived differently from that of the capture experiment. If we apply equation 3.19, which we used for the capture experiment, and substitute in the potential for the drag experiment, equation 4.8, we derive this dissipation function:

$$\Omega = \beta k \int_0^\tau ds \frac{\mathbf{p}_i}{m}(\mathbf{q}_1(t) - (\mathbf{v}_{opt}t)). \tag{4.9}$$

The derivation of this function assumes that the particle feels the same force from the trap at $t = \tau$ as it would at $t = 0$ if the position of the particle is kept the same,

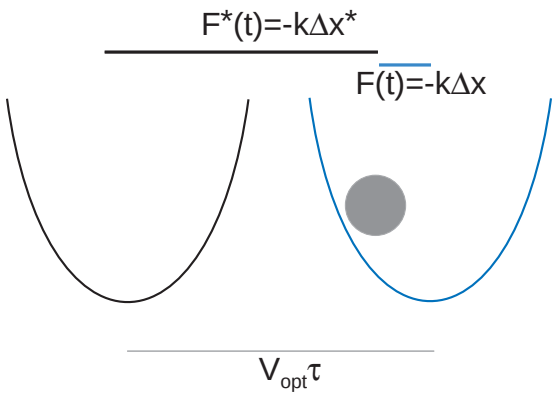

Figure 4.3: **Illustration of the difference in force exerted on a particle by the optical trap in its starting and finishing positions.** If the particle position is kept the same under the transformation from $\mathbf{\Gamma}(\mathbf{t})$, to $\mathbf{\Gamma}^*(\mathbf{t})$, then the force due to the optical trap will change as the distance and orientation to the trap centre will change, $\mathbf{F}(t)$ (**black**) vs $\mathbf{F}^*(t)$ (blue). The associated lines correspond to the different directions and magnitudes of the forces.

and its momentum reversed. At the end of an experimental run, $t = \tau$, the trap is displaced from the origin of the experiment, Figure 4.3. This means it exerts a different force on the particle, and we can not use this approach.

To solve this problem, we revert back to our general definition of the dissipation function, equation 2.6. To derive a valid dissipation function for this experiment, we need to choose a set of co-ordinates where conjugate trajectories exist for all forward trajectories. In the drag experiment, we can choose co-ordinates to be relative to the trap, and invert the position co-ordinate for the particle, such that $\mathbf{q}_1^* = \mathbf{q}_1(t) - \mathbf{v}_{opt}t$. This will create the correct force profile to generate the appropriate anti-trajectory. This gives us a dissipation function of

$$\Omega = \beta k \int_0^\tau ds \mathbf{v}_{opt}(\mathbf{q}_1(t) - (\mathbf{v}_{opt}t)). \tag{4.10}$$

This function provides a good illustration of how the dissipation function relates to our expectations of the system: it is positive when on average the particle is lagging the trap, the expected behaviour, and negative when the average is leading the trap, the anti-entropic behaviour.

It is interesting to note that this approach is exactly what would be done to generate the work, and as such, this dissipation function is equivalent to the work

for a system where the trap is displaced a fixed distance by translating at constant velocity. [3] Since the FT is satisfied, we know that the free energy change for this system is zero, equation 2.10, and the drag experiment represents a test of the WR. [3] This is the expected result for the displacement of the trap in an infinite solvent, as the two equilibrium states are indistinguishable.

4.2.2 Stochastic drag

With the realisation that the FT could be examined using stochastic dynamics, it was decided to revisit the drag experiment. The inertia-less Langevin equation governing the particle motion is:

$$\xi \frac{d\mathbf{r}}{dt} = -k(\mathbf{r} - \mathbf{v}_{opt}t) + \mathbf{g}(t). \tag{4.11}$$

We can transform this equation of motion into a different coordinate system, $\mathbf{x}$, that translates with constant velocity $\mathbf{v}_{opt}$ with its origin displaced by $\xi\mathbf{v}_{opt}/k$, using $\mathbf{r} = \mathbf{x} + \mathbf{v}_{opt}t - \xi\mathbf{v}_{opt}/k$. The equation of motion in the moving and displaced-coordinate frame, $\mathbf{x}$, is then

$$\xi \frac{d\mathbf{x}}{dt} = -k\mathbf{x} + \mathbf{g}(t). \tag{4.12}$$

This is the equation of motion of a particle in a stationary trap, for which we already have time-dependent distributions of the particle position, equations. 5.12 and 4.6.

As in the capture experiment, we can construct expressions for the distributions of forward and backward trajectories, and we can express the dissipation function as the ratio of these distributions. But unlike the capture experiment, there are two obvious coordinate frames, the fixed $\mathbf{r}$-coordinate and the moving $\mathbf{x}$-coordinate frame, in which we can cast the trajectories. We can express a set of forward trajectories using either coordinate frame ($\{\mathbf{r}_0, \mathbf{r}_t] \equiv \{\mathbf{x}_0, \mathbf{x}_t]$); however, because the displacement of the $\mathbf{x}$-coordinate frame from the $\mathbf{r}$-coordinate frame depends upon time, the corresponding sets of backwards trajectories are not identical ($\{\mathbf{r}_t, \mathbf{r}_0] \not\equiv \{\mathbf{x}_t, \mathbf{x}_0]$). That is, trajectories that are conjugate in $\mathbf{x}$-coordinate cannot be conjugate in $\mathbf{r}$, unless $\mathbf{v}_{opt} = \mathbf{0}$, Figure 4.4. Consequently, the dissipation function constructed from equation 3.28 depends upon the coordinate frame used to describe forward and backward

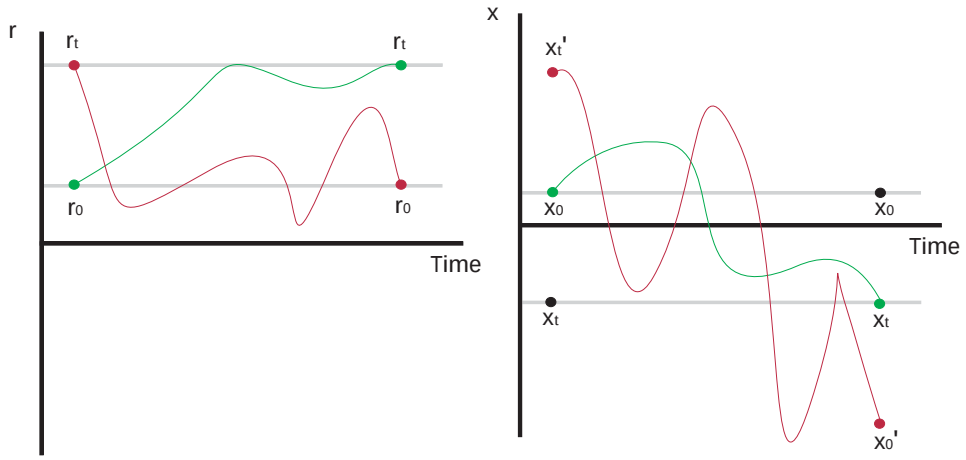

(a) (b)

Figure 4.4: **Two illustrations showing conjugate trajectories in different reference frames for the drag experiment.** In figure 4.4a we present an illustration of position, r, vs time, for an arbitrary trajectory (green) and its conjugate (red) in the **r** reference frame, and in figure 4.4b we present an illustration of position, x, vs time, for the same two trajectories, $\{\mathbf{r}_t, \mathbf{r}_0] \equiv \{\mathbf{x}'_t, \mathbf{x}'_0]$. The conjugate trajectory from the **r** frame is not the conjugate trajectory in the **x** frame: $\{\mathbf{x}'_t, \mathbf{x}'_0] \not\equiv \{\mathbf{x}_t, \mathbf{x}_0]$. The dissipation function is the probability ratio of a trajectory and its conjugate, and therefore we get different dissipation functions in the **r** and **x** frames.

trajectories.

First, let us consider the dissipation function generated by trajectories that are conjugate in the **x**-coordinate frame. This is a convenient coordinate frame as we can express the propagator distributions in the **x**-coordinate frame as simple Green's functions, as a consequence of equation 4.12. From equation 3.28, the dissipation function is

$$\Omega_x = -\frac{\xi \mathbf{v}_{opt}}{k_B T} \cdot (\mathbf{x}_t - \mathbf{x}_0), \tag{4.13}$$

where the subscript x indicates that the function was derived using Langevin trajectories that are conjugate in **x**,

$$\Omega_x = \ln\left(\frac{P(\mathbf{x}_0, \lambda(0))G(\mathbf{x}_\tau : \mathbf{x}_0, \tau, \lambda(t))}{P(\mathbf{x}_\tau, \lambda(0))G(\mathbf{x}_0 : \mathbf{x}_\tau, \tau, \lambda(t))}\right). \tag{4.14}$$

Similarly, Ω_r, the dissipation function constructed from trajectories that are conjugate in **r**,

$$\Omega_r = \ln\left(\frac{P(\mathbf{r}_0, \lambda(0))G(\mathbf{r}_\tau : \mathbf{r}_0, \tau, \lambda(t))}{P(\mathbf{r}_\tau, \lambda(0))G(\mathbf{r}_0 : \mathbf{r}_\tau, \tau, \lambda(t))}\right), \tag{4.15}$$

Table 4.2: Parameters for the drag experiment

k	$0.48pN/\mu m$
v_{opt}	$0.29\mu m/s$
Trajectories	400

is

$$\Omega_r = (\frac{k\mathbf{v}_{opt}t}{k_BT(1-\exp(-t/\tau))} - \frac{\xi\mathbf{v}_{opt}}{k_BT}) \cdot (\mathbf{r}_t - \mathbf{r}_0), \tag{4.16}$$

The reason we derive two expressions for the drag experiment is that our dynamics are inertialess. Generally in physics, we deal with inertial reference frames, that is we only treat the system in reference frames that move at a constant velocity. For an inertial system, the dissipation function in $\mathbf{x}$ would be the same as the dissipation function in $\mathbf{r}$, after applying the transformation between co-ordinates. In our system, the inertialess nature of the dynamics means these two expressions are different, but both of these different dissipation functions will satisfy the FT. In figure 4.5, we demonstrate this by presenting Langevin simulation results for the drag experiment that show the FT for these two dissipation functions.

4.2.3 Experimental drag

The Wang experiment was first carried out in 2001, [2] and again in 2004. [5] The results presented here are from the 2004 experiment where both deterministic and stochastic FT were tested. It is important to note that the experiment is carried out by translating the stage, rather than moving the trap. These two processes are physically equivalent for our experiment. The experimental parameters are in table 4.2. The integrated form of the FT was tested for the deterministic expression and for the $\mathbf{r}$ form of the stochastic dissipation function due to the small number of samples taken. As we can see from the experimental results, the integrated form of the FT is satisfied stochastically for all times. In the deterministic results, we see a small disagreement with the FT between 0.5s and 2s. The exact cause of this disagreement is unknown, but it likely due to the extremely small number of trajectories.

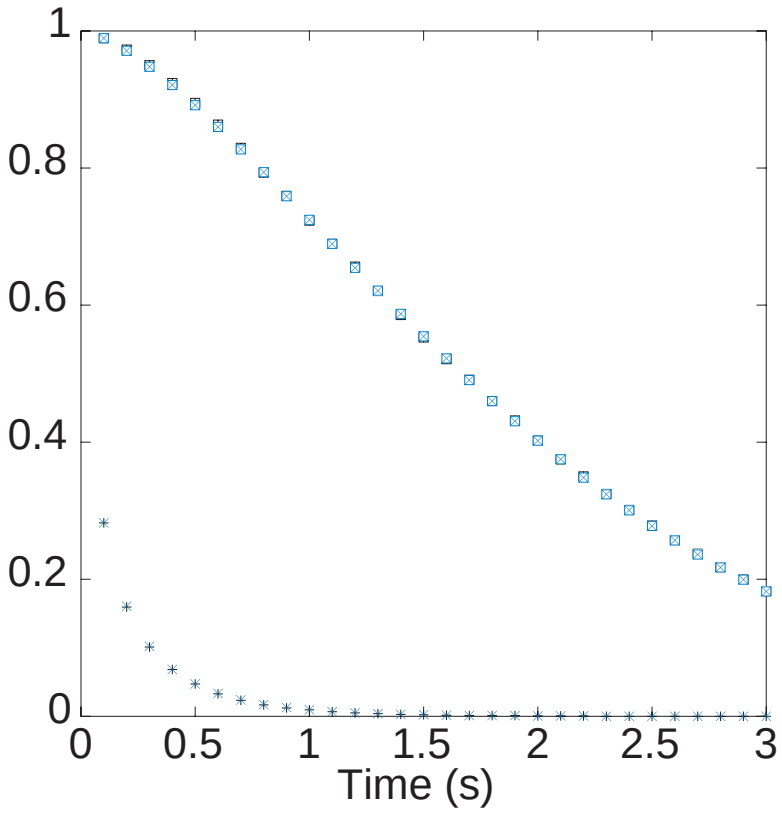

Figure 4.5: **Figure showing integrated FT results for stochastic simulations of the drag experiment.** Dimensionless value vs time, for $P(\Omega < 0)/P(\Omega > 0)$ $(+)$ and $\langle \exp(-\Omega) \rangle_{(\Omega>0)}$ $(\times)$ for the **x** frame stochastic dissipation function, and $P(\Omega < 0)/P(\Omega > 0)$ $(\oplus)$ and $\langle \exp(-\Omega) \rangle_{(\Omega>0)}$ $(\otimes)$ for the **r** frame stochastic dissipation function for a stochastic simulation of the drag experiment. Both dissipation functions satisfy the integrated FT for this simulation, despite their difference in form. [This data was originally presented in reference [4].]

Figure 4.6: **Two figures showing integrated FT results for the drag experiment.** In figure 4.3 we plot dimensionless value vs time, for $P(\Omega < 0)/P(\Omega > 0)$ $(+)$ and $\langle \exp(-\Omega) \rangle_{(\Omega>0)}$ $(\times)$ for the drag experiment with a deterministically derived dissipation function, and in figure 4.6b we plot the same for the drag experiment with a stochastically derived dissipation function in the **x** frame. The stochastic results are consistent with the integrated form of the FT at all times, while the deterministic results are generally consistent with the FT, however there is a discrepancy from 0.5s to 2s. [This data was originally presented in reference [5]]

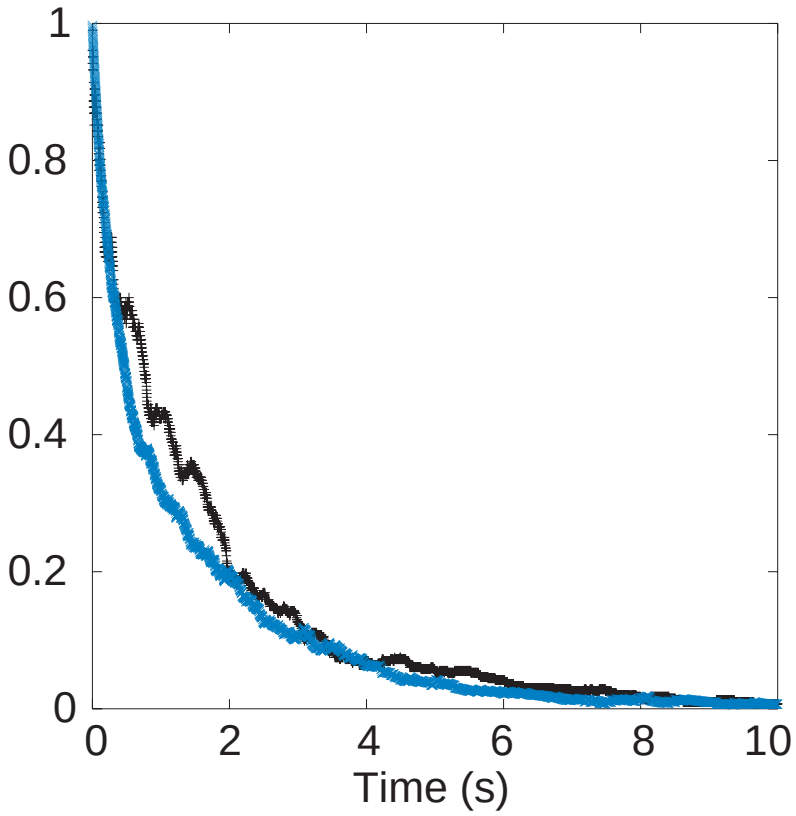

(a)

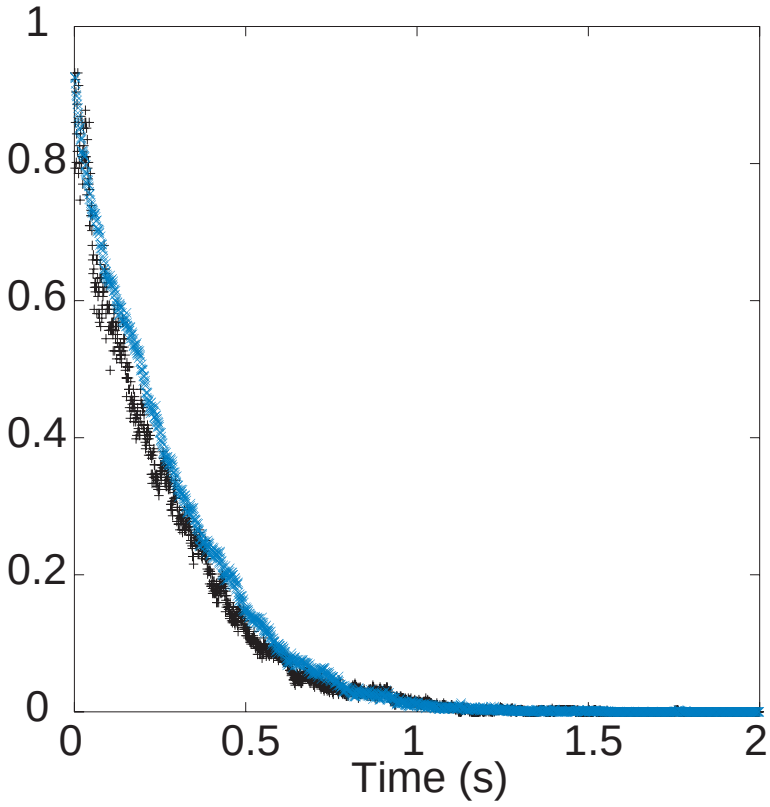

(b)

Figure 4.6

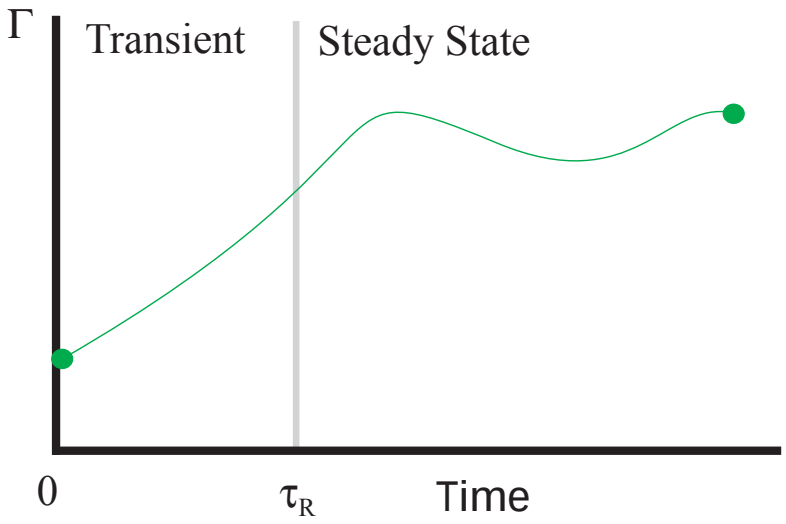

Figure 4.7: **Illustration to show the separation of the steady state and transient regions of the drag experiment.** An illustration of a phase space, Γ, vs time, plot to show the separation of the steady state and transient regions of the drag experiment. The steady state drag experiment is constructed by taking a system in equilibrium, beginning the drag experiment, and then continuing the drag experiment for a period sufficient for any transient behaviour to go to zero, τ_R. Once in the steady state, experimental measurements are undertaken.

4.3 Steady state drag

After the initial drag paper of Wang and others, the drag experiment was revisited in the context of non-equilibrium steady states. [5] Non-equilibrium steady states are one of the more difficult phenomena to categorise in thermodynamics. They possess some of the features of equilibrium, such as a time invariant behaviour and some of the features of a dissipative system, such as continuous dissipation of heat to the thermostat. The steady state can however exhibit fluctuations that are not present in an equilibrium system, and this makes the application of the FT to non-equilibrium steady states of particular interest.

To produce a non-equilibrium steady state in the drag experiment, we begin by conducting an ordinary drag experiment where we start translating the trap at $t = 0$. If we drag the particle for a long time, τ_R, then the transients from beginning the translation will have decayed to zero and we can treat our system as if it had always been translating, figure 4.7. This system is in a non-equilibrium steady state, and we can evaluate the FT for this system.

4.3.1 Deterministic steady state drag

Applying the FT to a non-equilibrium steady state is surprisingly difficult under deterministic dynamics. In order to derive the dissipation function, it is necessary to know the distribution function for the system at some point along the trajectory. The non-equilibrium steady state distribution function for the drag system is intractible under deterministic dynamics. [6] In order to apply the FT, we make the steady state approximation to the FT (SSFT). [5, 7, 8]

To make the steady state approximation, we begin with a known distribution, in this case the pre-translation, equilibrium distribution for the system. We then derive the dissipation function for this system, which is our original drag dissipation function:

$$\Omega = \beta k \int_0^\tau dt \mathbf{v}_{opt}(\mathbf{q}_1(t) - (\mathbf{v}_{opt}t)). \tag{4.17}$$

From the form of this expression, we can see that the dissipation function is extensive in time, that is on the average it increases with increasing time. If we split the dissipation function into the dissipation while the system is relaxing towards the steady state, known as the transient part, $\Omega_{\tau_R}, 0 \leq t \leq \tau_R$, and the dissipation in the steady state, $\Omega^{SS}, \tau_R \leq t \leq \tau$, then

$$\begin{aligned} \Omega &= \beta k[\int_0^{\tau_R} dt \mathbf{v}_{opt}(\mathbf{q}_1(t) - (\mathbf{v}_{opt}t)) + \int_{\tau_R}^{\tau} dt \mathbf{v}_{opt}(\mathbf{q}_1(t) - (\mathbf{v}_{opt}t))], \\ &= \Omega^{\tau_R} + \Omega^{SS}. \end{aligned}$$

As the time in the steady state goes to infinity, $\tau/\tau_R \to \infty$, the contribution from the transient relative to the steady state component will go to zero on the order of the limit, $1/\tau$.

To estimate the rate at which the fluctuations go to zero we need to estimate the spread in the value of the steady state dissipation function. In the steady state, the time average and the ensemble average are expected to be the same, that is the system is ergodic. If we re-express our steady state dissipation function as a sum of

time sequential dissipation functions of duration Δt, [5]

$$\Omega^{SS,\tau} = \sum_{i=1}^{\tau\Delta t} \Omega_i^{SS,\Delta t}, \tag{4.18}$$

and then take the time average,

$$\bar{\Omega}^{SS} = \frac{1}{t} \sum_{1}^{\tau\Delta t} \Omega_i^{SS,\Delta t}, \tag{4.19}$$

then as long as Δt is long enough for the trajectory segments to be independent, we can estimate the standard deviation in the time average, $\sqrt{1/t}$, and this will be the rate at which the fluctuations decay. Since the fluctuations in the dissipation function go to zero slower than the rate at which the transient goes towards zero, we can rewrite our FT as the SSFT:

$$\lim_{\tau/\tau_R \to \infty} \ln(\frac{p(\Omega^{SS} = A)}{p(\Omega^{SS} = -A)}) = A, \tag{4.20}$$

with the knowledge that Ω^{SS} is a good approximation of the real dissipation, and that there will be fluctuations to measure.

4.3.2 Stochastic steady state drag

The steady state drag experiment represents one of the more practical uses for the stochastic approach to the fluctuation relations. Under deterministic dynamics an approximation has to be made to derive arguments for this system, while under stochastic dynamics we simply apply the same approach as was used for the system starting in equilibrium. Indeed, as we will see, under stochastic dynamics, it can be argued that this system is in equilibrium.

We approach this system in exactly the same way as we approached the derivation for the drag experiment: we write down our equations of motion for the system in

the **x** and **r** co-ordinates:

$$\xi\frac{d\mathbf{r}}{dt} = -k(\mathbf{r}-\mathbf{v}_{opt}t)+\mathbf{g}(t), \tag{4.21}$$

$$\xi\frac{d\mathbf{x}}{dt} = -k\mathbf{x}+\mathbf{g}(t). \tag{4.22}$$

Looking at these equations, we see that in the **x** frame, we have a system that is indistinguishable from a stationary system in equilibrium. The dissipation function in this frame is

$$\Omega_x = 0, \tag{4.23}$$

that is, there is no dissipation in the **x** frame and the FT is trivially satisfied. The **r** frame is the experimental frame of reference, and the dissipation function is somewhat different:

$$\Omega_r = \frac{k\mathbf{v}_{opt}t}{k_BT}\frac{(\mathbf{r}_t-\mathbf{r}_0)}{(1-\exp(-t/\tau))}. \tag{4.24}$$

This was the stochastic dissipation function measured experimentally, and it was found to obey the FT at all time.

If we compare the dissipation functions for the drag and steady state drag we discover something interesting. We can rewrite our drag dissipation functions in terms of our steady state dissipation function;

$$\Omega_x = -\frac{\xi\mathbf{v}_{opt}}{k_BT}\cdot(\mathbf{x}_t-\mathbf{x}_0)+\Omega_x^{SS}, \tag{4.25}$$

$$\Omega_x = -\frac{\xi\mathbf{v}_{opt}}{k_BT}\cdot(\mathbf{x}_t-\mathbf{x}_0), \tag{4.26}$$

$$\Omega_r = -\frac{\xi\mathbf{v}_{opt}}{k_BT}\cdot(\mathbf{r}_t-\mathbf{r}_0)+\Omega_r^{SS}. \tag{4.27}$$

What we find is that the drag expressions have two, separable components. The first component is associated with moving the average position of the bead from the centre of the trap to a position behind the bead. The second component is the steady state dissipation, that is the dissipation associated with dragging it through the solution. In the **x** frame, the steady state component is zero. It is important to note that both the steady state and transient expressions obey the FT when

Table 4.3: Parameters for the steady state drag experiment

k	$0.12pN/\mu m$
v_{opt}	$0.18\mu m/s$
Trajectories	400

applied over the right time domains, in contrast with the approximation required by deterministic dynamics.

4.3.3 Experimental Steady State Drag

The optical trapping experiment was carried out using the apparatus detailed in chapter 3, by controlling the translation of the stage to drag the particles. The experimental parameters are listed in Table 4.3. To show the differing behaviour of the FT with stochastic and deterministic dissipation functions, we plot the integrated form of the FT. For the deterministic SSFT, we expect the FT to apply only asymptotically in time, and this is demonstrated in Figure 4.8a, where the two curves come together over a period of approximately 2 seconds. In contrast, for the stochastic expression, we expect agreement at all time, and we can see the two curves are co-incident in Figure 4.8b.

Figure 4.8: **Two figures of integrated FT results for the steady state drag experiment.** In figure 4.8a we plot dimensionless value vs time, for $P(\Omega < 0)/P(\Omega > 0)$ $(+)$ and $\langle \exp(-\Omega) \rangle_{(\Omega>0)}$ $(\times)$ for the steady state drag experiment with a deterministically derived steady state dissipation function and in figure 4.8a we plot the same with a stochastically derived dissipation function. The deterministic dissipation function is an asymptotic approximation, and only agrees with the FT at long time, here approximately 2s. In contrast, the stochastic FT in the steady state is exact, and agrees with the FT at all times. [This data was originally presented in reference [5].]

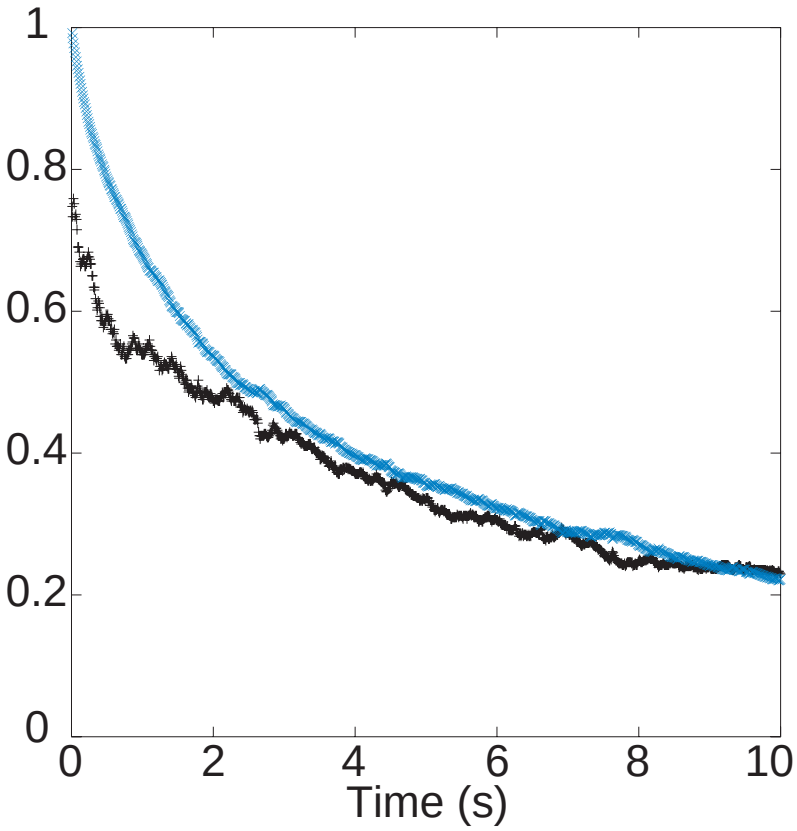

(a)

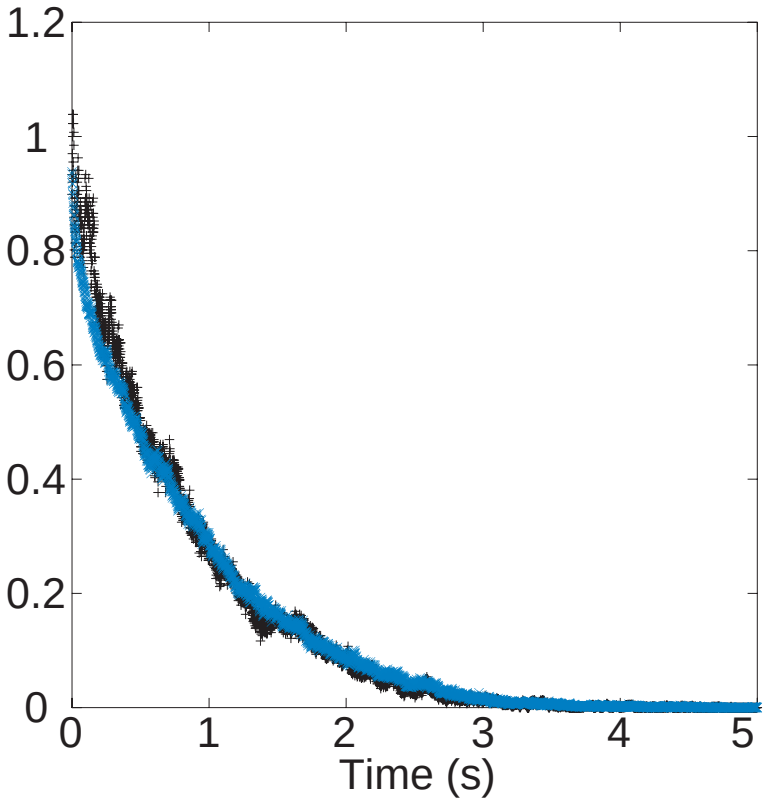

(b)

Figure 4.8

Bibliography

[1] D. M. Carberry, J. C. Reid, G. M. Wang, E. M. Sevick, D. J. Searles, D. J. Evans, *Phys. Rev. Lett.* **92**, 140601 (2004).

[2] G. M. Wang, E. M. Sevick, E. Mittag, D. J. Searles, D. J. Evans, *Phys. Rev. Lett.* **89**, 050601 (2002).

[3] O. Narayan, A. Dhar, *J. Phys. A: Math. Gen.* **37**, 63 (2004).

[4] J. C. Reid, D. M. Carberry, E. M. Sevick, D. R. M. Williams, D. J. Searles, D. J. Evans, *Phys. Rev. E* **70**, 016111 (2004).

[5] G. M. Wang, J. C. Reid, D. M. Carberry, D. R. M. Williams, E. M. Sevick, D. J. Evans, *Phys. Rev. E* **71**, 046142 (2005).

[6] D. Evans, G. Morriss, *Statistical Mechanics of Nonequilibrium Liquids* (Academic Press, 1990).

[7] D. J. Evans, E. G. D. Cohen, G. P. Morriss, *Phys. Rev. Lett.* **71**, 2401 (1993).

[8] D. J. Evans, D. J. Searles, *Adv. Phys.* **51**, 1529 (2002).

Chapter 5

The Ramp Experiment

The ramp experiment is based on the capture experiment of the last chapter. In the capture experiment a particle is held in equilibrium with a weak trap and then the trap strength is discontinuously increased. In the ramp experiment we replace this discontinuous increase with a linear increase of the trap strength with time. We then extend the experiment by allowing the system to relax at the new trapping constant, before returning the trap strength to its initial value over the same amount of time it was changed at the beginning of the experiment, Figure 5.1. This gives us a time dependent trapping constant, $k(t)$:

$$k(t) = \begin{cases} k_1 t/\tau + k_0(1 - t/\tau) & ,0 \leq t \leq \tau \\ k_1 & ,\tau \leq t \leq 2\tau \\ k_1(1 - (t - 2\tau)/\tau) + k_0(t - 2\tau)/\tau & ,2\tau \leq t \leq 3\tau \end{cases} \tag{5.1}$$

where τ is the time taken for the trapping constant to change between k_0, the initial trap strength, and k_1, the final trap strength.

The primary aim of the ramp experiment was to provide an unambiguous demonstration of the WR for a non-zero free energy change over non-equilibrium work paths of finite duration. Previous optical trapping experiments had technically tested the WR, but only where there was no change in the free energy, [1, 2] or the work paths were of infinitely short time. [3] In addition, two experiments have demonstrated the work relation for non-optical trapping systems.

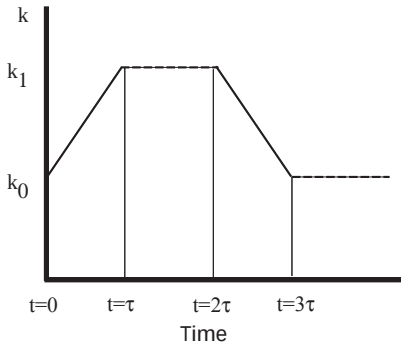

Figure 5.1: **Figure showing time dependent external parameter for the ramp experiment.** Trapping constant, k, vs time, for the ramp experiment. The optical trap begins in equilibrium with trapping strength k_0, before the trapping strength is linearly increased to k_1 over a period tau. From τ to 2τ the trap strength is held constant at k_1, and from 2τ to 3τ the trap strength is linearly decreased back to k_0. After each cycle of 3τ, the system is allowed a period to relax back to equilibrium. The primary focus of this chapter will be upon the up ramp, $0 \leq t \leq \tau$, however the full cycle from k_0 to k_1 and back again, $0 \leq t \leq 3\tau$, will feature in the deterministic discussion, and the down ramp will be analysed for the WR and Crooks, $2\tau \leq t \leq 3\tau$.

The experiment of Bustamante and others, [4] tested the work relation for the stretching of a polymer chain, and the experiment of Douarche and others, [5] tested the work relation for the thermal motion of a mechanical pendulum. The ramp experiment seeks to expand upon these two experiments. In the Bustamante experiment, the free energy change for stretching the polymer was not known analytically, and had to be measured by reversibly stretching the polymer. In the Douarche experiment, the WR was only verified where the distribution of work is Gaussian. The ramp experiment will test the WR for a known free energy change over non-Gaussian distributions of work. This is achieved by choosing appropriate values of k_0, k_1, and τ.

A second aim of the ramp experiment was to apply all the various relations described in this thesis to a single experiment. The application of the fluctuation theorem (FT) to the ramp experiment is of particular interest, as it demonstrates the conditions under which the dissipation function is and is not able to be defined for a system. In addition to the FT, we can also test the conjugate work relation (CWR) and the Hatano-Sasa relation. While these relations are not the primary focus of this work, it is still interesting to test them experimentally.

Table 5.1: Parameters for the ramp experiment

k_0	$1.10pN/\mu m$
k_t	$2.18pN/\mu m$
τ	1s
Trajectories	2000

The setup of the experiment is discussed in chapter 3 and the equipment used is listed in table 3.1. The experimental parameters are listed in Table 5.1. This experiment was used to study the fluctuation relations using both deterministic and stochastic dynamics, and the results are divided accordingly.

5.1 Deterministic

The ramp experiment was designed with deterministic systems in mind. The changes in trapping constants provide a robust test of the WR and CR, while the complete experiment tests the symmetry requirements of the FT. In addition, the ramp experiment provides an opportunity to test the CWR. The ramp experiment therefore provides a complete test of the fluctuation relations for deterministic dynamics.

We will start by defining our arguments in terms of the transition from k_0 to k_1 over the period of time $0 \leq t \leq \tau$. The only modification to our equations of motion is that the trapping constant k is explicitly time dependent:

$$k(t) = k_1 \frac{t}{\tau} + k_0(1 - \frac{t}{\tau}) \tag{5.2}$$

From equations 3.19 and 3.20 we can substitute $k(t)$ into our equations of motion and solve for dissipation and work:

$$\Omega = \beta \int_0^\tau dt(k_0 - k_1)\mathbf{q}_1(t)\dot{\mathbf{q}}_1(t)\frac{t}{\tau} \tag{5.3}$$

$$\Delta W(\tau) = \beta \int_0^\tau dt \frac{1}{2\tau}\mathbf{q}_1^2(t)(k_1 - k_0) \tag{5.4}$$

Both of these functions are interesting, but for different reasons.

Let us start by examining the work function. If we look at the form of this

function, we can see that it will always be positive where $k_1 > k_0$ and negative where $k_0 > k_1$. From the CR, we know that the positive values of work in one direction are related to the negative values of work in the other direction. This form of this work function is consistent with the CR, as if work in one direction is all positive the work in the other direction has to be all negative

What is also interesting about this function is its behaviour in the limits of the ramp time, τ. As $\tau \to 0$,

$$\lim_{\tau \to 0} \Delta W(\tau) = \beta \frac{1}{2} \mathbf{q}_1^2(t)(k_1 - k_0) \tag{5.5}$$

$$= \beta \Delta H(0) \tag{5.6}$$

we get the change in the Hamiltonian for the system at $t = 0$. From classical statistical mechanics, we know that the ensemble average of the exponential of this function is equal to the exponential of the free energy change,

$$\langle \exp(-\beta \Delta H(0)) \rangle = \exp(-\Delta F), \tag{5.7}$$

which is equivalent to the work relation in this limit. If we take the asymptotic limit in ramp time, $\tau \to \infty$, then we have a system that is in equilibrium at all times, known as a quasi-static system, and we know from classical thermodynamics that the work done for a system over a quasi-equilibrium path is equal to the change in free energy $\Delta W = \Delta A$. Therefore for the ramp experiment, classical thermodynamics recovers the WR for $\tau = 0, \infty$. We will therefore be studying paths over finite ramp times, $0 < \tau < \infty$.

Under deterministic dynamics, there is a problem in deriving the dissipation function for the ramp experiment. In section 3.2.1, the dissipation function was defined as the probability ratio between a trajectory and its conjugate:

$$\Omega(\mathbf{\Gamma}) = \ln \Big(\frac{\mathbf{p}(\mathbf{\Gamma}(0), \lambda(0))}{\mathbf{p}(\mathbf{\Gamma}^*(0), \lambda(0))} \frac{\partial V(\mathbf{\Gamma}(0))}{\partial V(\mathbf{\Gamma}^*(0))} \Big). \tag{5.8}$$

As was discussed, a necessary requirement for this expression to have a real value, and therefore for the FT to hold, is the requirement that for every phase space trajectory

$\mathbf{\Gamma}(0)$ there exists the associated anti-trajectory $\mathbf{\Gamma}^*(0)$ in the ensemble going forwards in time. For the initial (or final) ramp, the change in external parameters λ is not symmetric in time, that is the force constant goes from $k(0)$ to $k(\tau)$ if time goes from 0 to τ, and from $k(\tau)$ to $k(0)$ in time goes from τ to 0. A conjugate trajectory requires the time reverse force profile and so will not exist under deterministic dynamics, and we expect the FT to fail over these time periods.

If we extend the end point of our experiment out to the point where the trap constant returns to its original value, $t = 3\tau$, the change in external parameters will be even in time, that is the profile of the force constant is the same going forwards and backwards in time. This will have two effects: conjugate trajectories will now exist for all forward trajectories so that the dissipation function will be properly defined, and the free energy change over the system path will be 0 meaning that the work and dissipation are equal, see equation 2.10. It is therefore of interest to study the FT over the full range of time, with Ω as a piecewise function:

$$\begin{aligned}
\Omega(\mathbf{\Gamma}) &= \beta[\int_0^{\tau} dt(k_0 - k_1)\mathbf{q}_1(t)\frac{d\mathbf{q}_1(t)}{dt}\frac{t}{\tau} && (5.9)\\
&+ \int_{\tau}^{2\tau} dt(k_0 - k_1)\mathbf{q}_1(t)\frac{d\mathbf{q}_1(t)}{dt} && (5.10)\\
&+ \int_{2\tau}^{3\tau} dt(k_0 - k_1)\mathbf{q}_1(t)\frac{d\mathbf{q}_1(t)}{dt}\frac{1-(t-2\tau)}{\tau}] && (5.11)
\end{aligned}$$

If we follow the agreement of the FT with time, such as by plotting the integrated FT, then we will see that at times between 0 and 3τ, $0 < t < 3\tau$, the system will not obey the FT due to the lack of a properly defined dissipation function, while at the beginning and end of the experiment, $t = 0, 3\tau$, the FT will be obeyed.

The CWR is theoretically able to measure the difference in free energy, similar to the work relation. Its argument, the conjugate work function, is the difference between the work and the dissipation, equation 2.10. This means that this argument is subject to the same symmetry considerations as the FT, and will be undefined at the end of the change in trapping constant, $t = \tau$, the point at which the free energy change is measured, causing the CWR to fail. Over the period $t = 3\tau$, the argument will be defined, but zero. The CWR is therefore of limited use in the ramp experiment.

5.1.1 Experimental Results

The experimental results for the ramp experiment allow the testing a all of the fluctuation relations with deterministically derived arguments. In this section we present results that test the FT, partition identity (PI), WR, CR, and CWR, and compare them with our predictions.

From our derivation of the dissipation function, we expect the FT to fail for $0 < t < 3\tau$, but to be satisfied at $t = 3\tau$. In figure 5.2a we present the integrated FT result to show the agreement of the experiment with the FT over time. The two curves, $P(\Omega > 0)/P(\Omega < 0)$ and $\langle \exp(-a) \rangle_{\Omega>0}$, diverge over the up ramp, stay roughly parallel to each other through the plateau region, before converging again at 3τ. Since the FT can only be satisfied when these two curves are co-incident, the FT fails over $0 < t < 3\tau$, as predicted. Also of interest is the value at which the two sides of the inegrated form of the FT agree at 3τ: despite the trap constant returning to its original value, this value is no longer 1. This demonstrates that the path is dissipative or thermodynamically irreversible in nature.

In figure 5.2b, we present the FT at $t = 3\tau$ and show the expected trend. While there is quite a lot of noise in the data, probably due to the low number of samples, 2000 trajectories, the result is compatible with the FT. This combined with the integrated FT data suggests the FT is satisfied at $t = 3\tau$.

Looking at the other fluctuation relation based of the dissipation function, the PI, also presented in Figure 5.2a, we find that the value of the exponential average stays close to 1 throughout the path. With the FT breaking down at intermediate times, it might be expected that its value would diverge from 1 quite significantly, as it would be expected to be 1 only when the FT is satisfied, however this is not observed in the experiment.

In figures 5.3a, and 5.3b, the distributions of work on the up and down ramp are plotted. These distributions are clearly non-Gaussian and have non-zero mean and finite standard deviations, showing that both sets of data are neither in the quasi-static or instantaneous regime, as expected. This means that these experimental results are from work paths where the distribution of phase space is not always in equilibrium, which are the work paths this experiment was designed to study.

To test the work relation, we are interested in how well the average of the exponential of the work converges to the predicted exponential of the free energy change for the system. Figures 5.4a and 5.4b show the convergence of this average with number of trajectories relative to the analytic prediction and the equilibrium sampling method. Figure 5.4a presents the average over trajectories for the system change from low trap strength, $k(0) = 1.11$ pN/μm, to high trap strength, $k(t) = 2.177$ pN/μm, and figure 5.4b presents the average over the reverse system change, $k(0) = 2.177$ pN/μm to $k(t) = 1.11$ pN/μm. The WR and equilibrium sampling method both produce results within the uncertainty of our analytic prediction, $\exp(\Delta F) = \sqrt{k(t)/k(0)}$.

It is interesting to note that when going from a weak trap to a strong trap, the WR and equilibrium sampling method are comparable in number of trajectories required to accurately measure the free energy, while in going from a strong trap to a weak trap the WR measures the free energy with fewer trajectories. This difference is due to how the ensembles of trajectories sample the initial and final states. In this experiment the change in trap strength changes the distribution of the colloid particle positions, changing the free energy of the system. For the equilibrium sampling method, both states are sampled using the initial state's distribution. This means that if there are highly probable particle positions in the final state that have a low probability in the initial state, such as points distant from the mean under a weak trap compared to a strong trap, the final state will be poorly sampled and convergence slower, figure 5.5.

When the WR samples the two systems, it does so through a trajectory that evolves from one position in the initial distribution to a different position in the final distribution, allowing it to explore both states. However, how well it explores the two states will depend upon the rate of change between them. The equilibrium sampling method represents a set of WR trajectories taken over an infinitely fast transformation. At the other extreme, the quasi-static method, equivalent to an infinitely slow rate, always samples both states perfectly. For our finite paths, we see that there is a difference in the number of trajectories required to converge to the free energy between the two ramp directions, but it is less pronounced than for

Figure 5.2: **Two figures showing FT and PI results for the ramp experiment using a deterministically derived dissipation function.** In Figure 5.2a we plot dimensionless value vs time, for $P(\Omega < 0)/P(\Omega > 0)$ $(+)$, $\langle \exp(-\Omega) \rangle_{(\Omega>0)}$ $(\times)$, and $\langle \exp(-\Omega) \rangle$ $(\otimes)$ for the ramp experiment with a deterministically derived dissipation function, and in figure 5.2b, we plot $\ln(P(\Omega = A)/P(\Omega = -A)$ vs Ω for the ramp experiment at $t = 3\tau$ with the expected result for the FT (red) using the same dissipation function. These results were constructed with data from 2000 trajectories. The divergence between the two sides of the integrated FT, $P(\Omega < 0)/P(\Omega > 0)$ and $\langle \exp(-\Omega) \rangle_{(\Omega>0)}$, for times other than $t = 0, 3\tau$ is due to the lack of time reversal symmetry in the force. At $t = 3\tau$, there is a small separation between the two curves, but is close to the expected behaviour. This breakdown is not as visible in the PI, $\langle \exp(-\Omega) \rangle$, as the plot fluctuates close to 1 over the entire time. In figure 5.2b, the data generally follows the expected behaviour. Both figures suggest that the FT is obeyed at $t = 3\tau$, subject to the small number of samples.

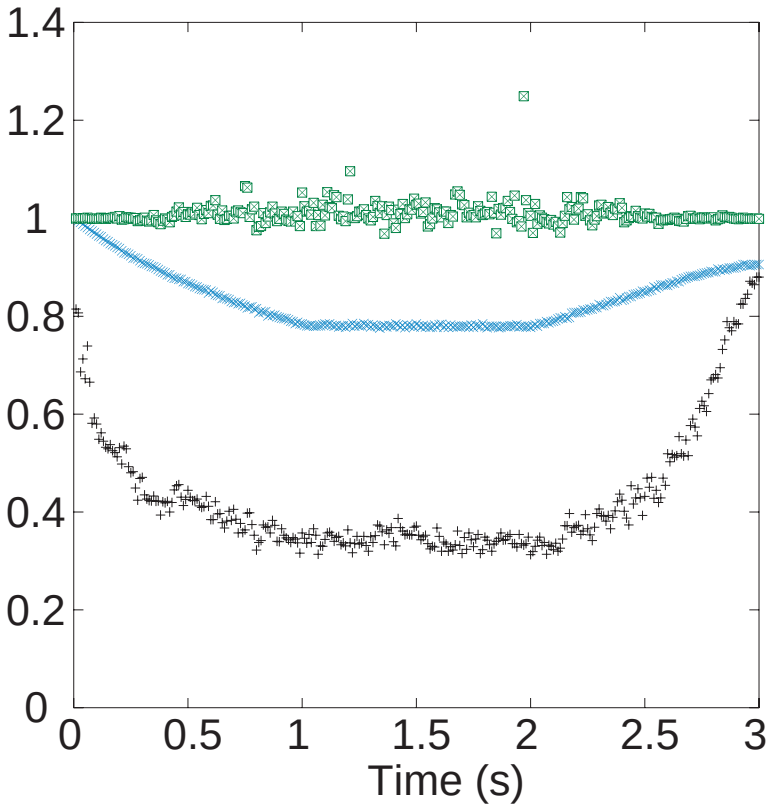
1.4
1.2
1
0.8
0.6
0.4
0.2
0
0
0.5
1
1.5
2
2.5
3
Time (s)

(a)

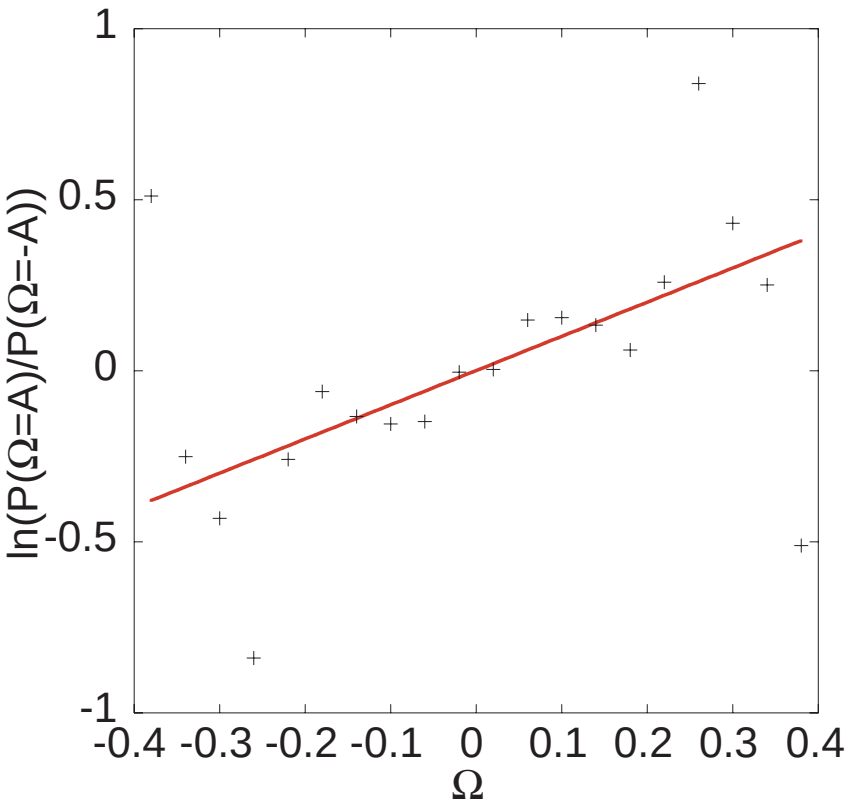
1
0.5
0
-0.5
-1
-0.4 -0.3 -0.2 -0.1 0 0.1 0.2 0.3 0.4
Ω
ln(P(Ω=A)/P(Ω=-A))

(b)

Figure 5.2

Figure 5.3: **Two figures showing the distribution of deterministically derived work for the ramp experiment.** In figure 5.3a we plot a histogram of deterministically derived work trajectories over a 1 second change in trapping constants from $k(0) = 1.11$ pN/μm to $k(t) = 2.177$ pN/μm for the ramp experiment and in figure 5.3b we plot a histogram of deterministically derived work trajectories over a 1 second change in trapping constants from $k(0) = 1.11$ pN/μm to $k(t) = 2.177$ pN/μm for the ramp experiment. Both histograms contain 2000 trajectories. These distributions are strongly asymmetric and non-Gaussian, with non-zero variance and maximum probability density. This demonstrates that the system is not in the quasi-static or instantaneous limit, but in the finite time, non-equilibrium range that we wished to study.

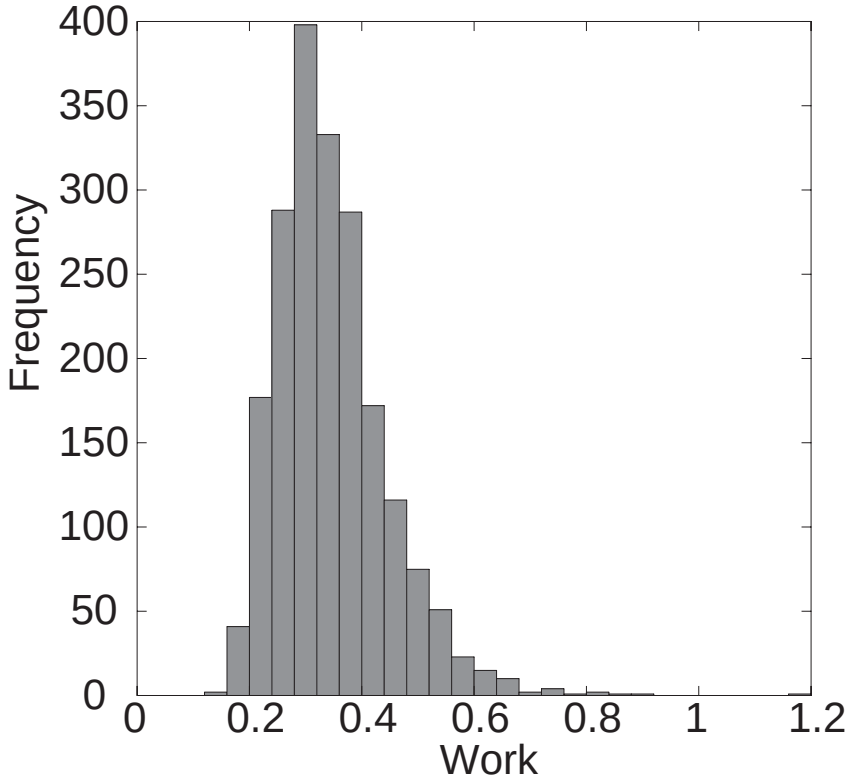
Frequency
Work
0
50
100
150
200
250
300
350
400
0
0.2
0.4
0.6
0.8
1
1.2

(a)

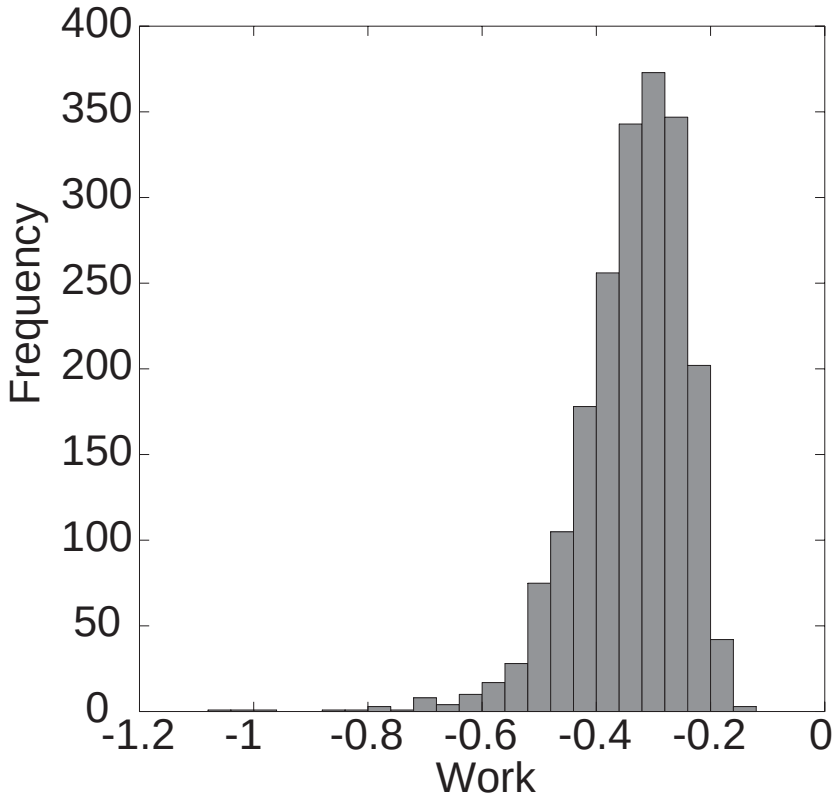
Frequency
Work
0
50
100
150
200
250
300
350
400
-1.2
-1
-0.8
-0.6
-0.4
-0.2
0

(b)

Figure 5.3

the equilibrium sampling method.

The WR requires less trajectories to reasonably estimate the free energy change between the two states in both directions. It should be noted however that each trajectory used in the work relation is 1s in duration, while samples at equilibrium could be taken every 100ms, which corresponds to the relaxation time of the system at equilibrium. This means that if we replotted figures 5.4a and 5.4b with the time required to collect each sample on the x-axis, rather than number of samples, the equilibrium sampling method would average to the free energy significantly faster.

In figure 5.6, the experimental results testing the CR are presented against the expected results. There is a large spread in the data is due to the limited number of samples taken, that broadens as we move towards the edges of the distributions. The trend of the data however is consistent with the CR.

Finally, figure 5.7 presents the average of the exponential of the conjugate work with number of samples for trajectories over the up ramp, $k(0) = 1.11$ pN/μm to $k(t) = 2.177$. As we can see, the CWR does not accurately measure the change in free energy between $k(0)$ and $k(t)$. This failure of the CWR is the expected behaviour over this time period. Over the full experimental time, $t = 3\tau$, the CWR is trivially satisfied, as the argument is uniformly 0.

5.1.2 MD simulation

The ramp experiment can be modelled using MD simulations. As discussed in section 3.3.1, to simplify the MD simulations, we make the colloid particle the same size as the solvent particles. In this section we will look at one of the relations, the FT, and demonstrate the difference this change of scale can have upon a system. The simulation parameters are contained in table 5.2. This system had a two particle thick wall surrounding the system, and the thermostat acted on the wall particles only.

We present the results for the integrated FT in figure 5.8a, and the results for the FT at $t = 3\tau$ in figure 5.8b. Fundamentally these results are the same as the experimental results. For the integrated FT, the two curves, $P(\Omega > 0)/P(\Omega < 0)$ and $\langle \exp(-a) \rangle_{\Omega>0}$, are only coincident at $t = 0$ and 3τ, due to the lack of a properly

Table 5.2: Parameters for MD simulations of the ramp experiment. N_{Sys} is the number of system particles, and N_{Wall} is the number of wall particles. All measurements are in reduced units. [6]

k_0	1
k_1	2
τ	1
Δt	10^{-3}
N_{Sys}	32
N_{wall}	24
T_{therm}	1.56
ρ	0.3
Trajectories	150,000

defined dissipation function at other times in the simulation. The FT plot for $t = 3\tau$ agrees with prediction, showing the FT is satisfied at this time.

The details of figure 5.8a, the integrated FT plot for the MD simulations, differ strongly from those of figure 5.2a, the integrated FT plot for the experiment. In the experimental plot, the behaviour of the two sides of the integrated FT with time are directly correlated to the behaviour of the trap constant in time. For $0 < t < \tau$, the two curves decrease in value linearly while the trap constant increases in value linearly, then at $t = \tau$, the curves flatten off significantly, corresponding with the region of constant trapping constant, before finally increasing linearly in value from $t = 2\tau$, corresponding with the final linear decrease in trapping constant. In contrast, the behaviour of the two curves in the simulations show a lag in responding to changes in the behaviour of the trapping constant.

The behaviour of the integrated FT is a reflection of the behaviour of the dissipation function. The dissipation function for the ramp is in turn a reflection of the behaviour of the particle position with time, equation 5.3. The difference between the simulations and the experiment are that both the size of the colloid and the times looked at in the simulation are shorter than those of the experiment. In the MD simulation we see the response of an undamped colloid particle, which manifests as a lag in response of the particle to a change in trapping constant. In the experiment, we see the response of a damped colloid particle, and this is what enables the experiment to be examined using stochastic dynamics.

Figure 5.4: **Two figures showing the WR results for the ramp experiment using a deterministically derived work function.** In figure 5.4a we plot dimensionless value vs number of trajectories for $\langle \exp(-\Delta W) \rangle$ ($\times$), $\langle \exp(-(\Delta k \mathbf{q}_1(0)) \rangle$ ($+$), and the analytic free energy prediction, $\sqrt{(}k(0)/k(t)))$ (red) over a 1 second change in trapping constants from $k(0) = 1.11$ pN/μm to $k(t) = 2.177$ pN/μm for the ramp experiment, and in figure 5.4b we plot the same over a 1 second change in trapping constants from $k(0) = 2.177$ pN/μm to $k(t) = 1.11$ pN/μm for the ramp experiment. The uncertainty in the analytic free energy prediction is 3%, and the work functions were derived using deterministic dynamics. The WR average, $\langle \exp(-\Delta W) \rangle$, converges to the analytic prediction in both figures, though it does so significantly faster going from a weak trap to a strong trap. This confirms the WR over the ramp experiment. The equilibrium sampling average, $\langle \exp(-(\Delta k \mathbf{q}_1(0)) \rangle$, takes more trajectories than the work relation going from a weak to strong trap, but still converges quickly. When going from a strong to weak trap, figure 5.4b, the equilibrium sampling method has converged around the correct value, but is still showing large fluctuations after 2000 trajectories.

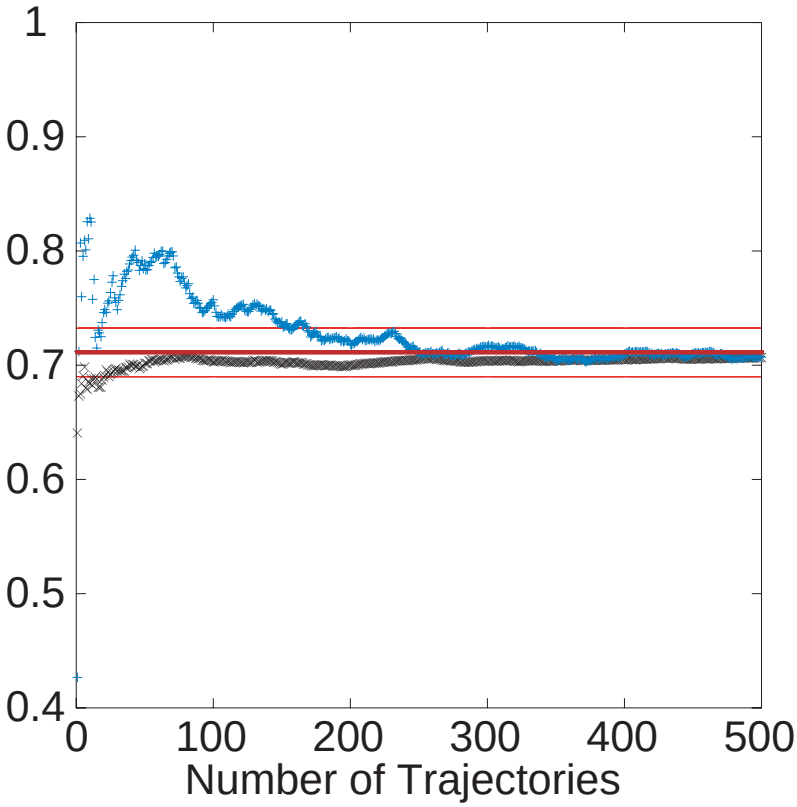
1
0.9
0.8
0.7
0.6
0.5
0.4
0
100
200
300
400
500
Number of Trajectories

(a)

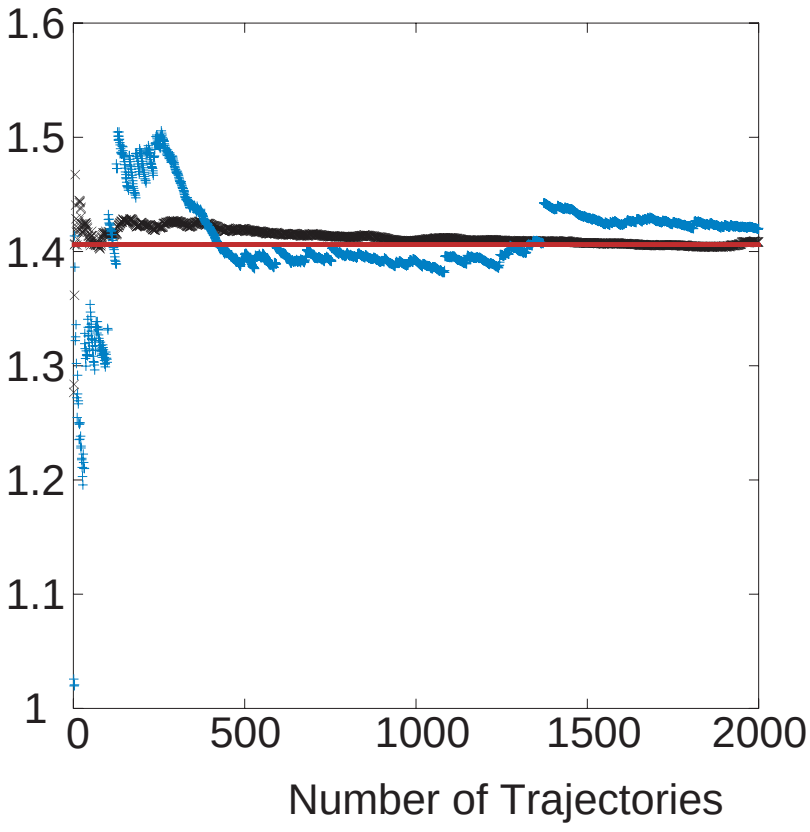
1.6
1.5
1.4
1.3
1.2
1.1
1
0
500
1000
1500
2000
Number of Trajectories

(b)

Figure 5.4

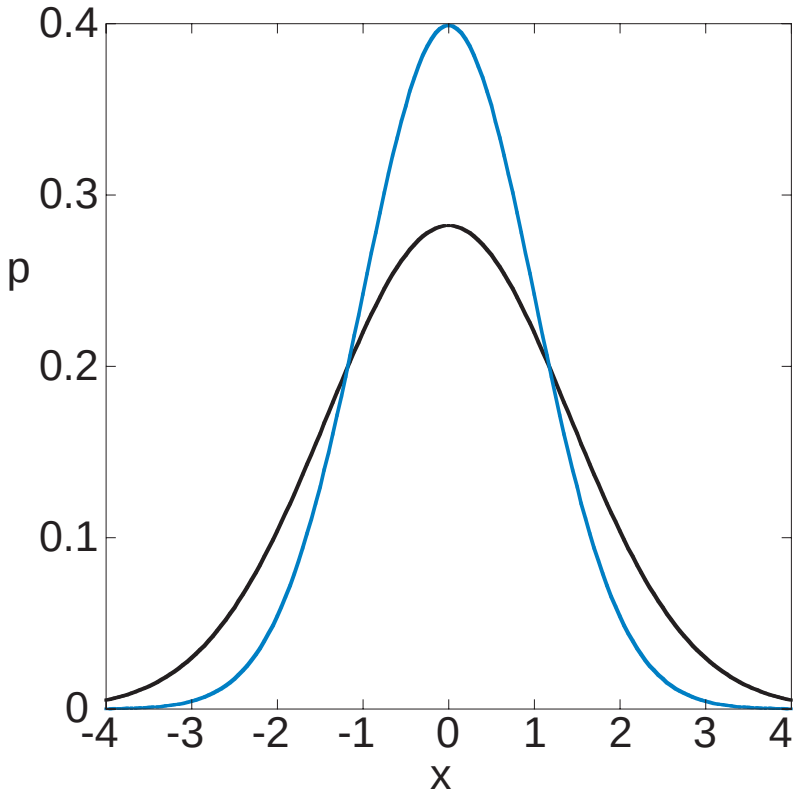

Figure 5.5: **Figure comparing two equilibrium distributions for optical trapping.** Probability density, p, vs displacement from the trap centre, x, for a particle in a weak (**black**) and strong (blue) optical trap. The distribution of the weak trap is broader in x than that of the strong trap. When using the equilibrium sampling method, the distribution of one trap is being used to sample both traps. The broad distribution of the weak trap means that it will sample both traps well, while the narrower distribution of the strong trap means that it will not sample the fringes of the weak distribution well. The equilibrium sampling method will therefore be expected to work best starting in equilibrium with a weak trap, see figure 5.4.

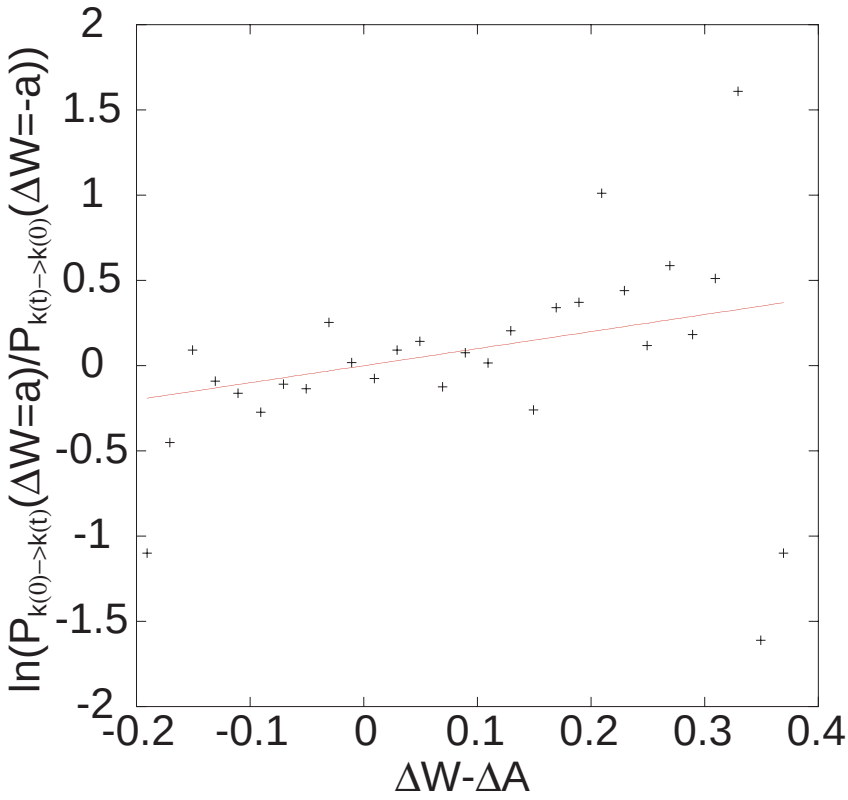

Figure 5.6: **Figure showing results for the CR for the ramp experiment using a deterministically derived work function.** $\ln[P_{k(0)\to k(t)}(\beta\Delta W = a)/P_{k(t)\to k(0)}(\beta\Delta W = -a)]$ vs $(\Delta W - \Delta A)$ with the expected result for the CR (red) for the ramp experiment using a deterministically derived work function over two 1 second ramps with $k(0) = 1.11$ pN/μm to $k(t) = 2.177$ pN/μm. These results were constructed with data from 2000 trajectories. The experimental results generally trend along the expected results, demonstrating the CR.

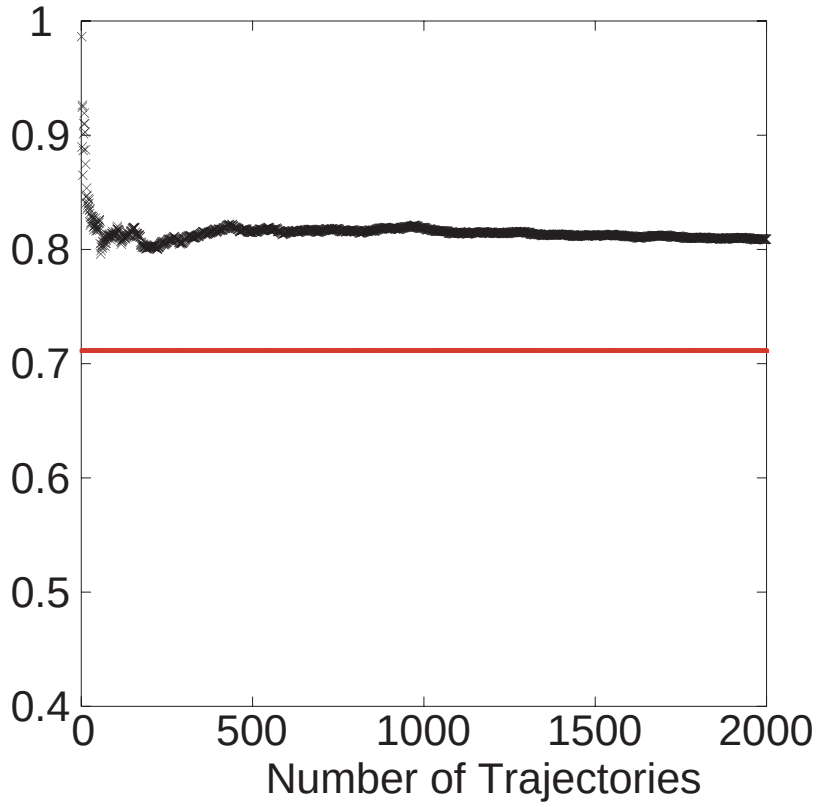

Figure 5.7: **Figure showing CWR results for ramp experiment using a deterministically derived conjugate work function.** Dimensionless value vs number of trajectories for $\langle \exp(-\omega) \rangle$ ($\times$), and the analytic free energy prediction, $\sqrt{(k(0)/k(t))}$ (red) over a 1 second change in trapping constants from $k(0) = 1.11$ pN/μm to $k(t) = 2.177$ pN/μm for the ramp experiment with a deterministically derived conjugate work function. These results were constructed with data from 2000 trajectories. The left hand side of the CWR fails to converge to the analytic prediction due to the lack of time symmetry in the force profile over this time.

5.2 Stochastic

The ramp experiment represents a significantly more difficult system to apply stochastic dynamics to then the cases of capture or drag. This added complexity comes from the necessity of deriving new Greens functions for the ramp. It still however provides some advantages over the deterministic approach in that all of the relations are applicable to the ramp system. In this section we will derive the various relations using stochastic dynamics, then demonstrate them using inertialess Langevin simulations.

The ramp experiment and the capture experiment both have the same external parameters at the beginning and end of the experiment. They therefore have the same equilibrium distributions for the particle in a one dimensional harmonic trap, the Boltzmann distribution:

$$P_B(\mathbf{r}_0, k_0) = \sqrt{\frac{k_0}{2k_BT}} \exp\left(-\frac{k_0\mathbf{r}_0^2}{2k_BT}\right). \tag{5.12}$$

The ramp experiment has equations of motion that are explicitly time dependent over the course of the experiment:

$$\xi\frac{d\mathbf{r}}{dt} = -[k_0(1-\lambda(t)) + k_1(\lambda(t))]\mathbf{r} + \mathbf{g}(t). \tag{5.13}$$

To derive the arguments to the fluctuation relations we need to derive a Greens function from our equations of motion, Appendix A:

$$\begin{aligned} G(\mathbf{r}_\tau : \mathbf{r}_0, \tau, \lambda(t)) \quad = \quad & \sqrt{\frac{\sqrt{\frac{\xi(k_0-k_1)}{\tau}}\exp(\frac{-\tau k_1^2}{\xi(k_0-k_1)})}{\pi^{\frac{3}{2}}k_BT(\mathrm{erf}(\frac{k_0}{\sqrt{\frac{\xi(k_0-k_1)}{\tau}}}) - \mathrm{erf}(\frac{k_1}{\sqrt{\frac{\xi(k_0-k_1)}{\tau}}}))}} \\ & \exp\Big(-(\frac{\sqrt{\frac{\xi(k_0-k_1)}{\tau}}\exp(\frac{-\tau k_1^2}{\xi(k_0-k_1)})}{\pi^{\frac{3}{2}}k_BT(\mathrm{erf}(\frac{k_0}{\sqrt{\frac{\xi(k_0-k_1)}{\tau}}}) - \mathrm{erf}(\frac{k_1}{\sqrt{\frac{\xi(k_0-k_1)}{\tau}}}))}) \\ & (\mathbf{r}_t - \mathbf{r}_0\exp(\frac{-\tau(k_0+k_1)}{2\xi}))^2\Big). \end{aligned}$$

Figure 5.8: **Two figures showing integrated FT and FT results for MD simulations of the ramp experiment with a deterministically derived dissipation function.** In figure 5.8a we plot dimensionless value vs time, for $P(\Omega < 0)/P(\Omega > 0)$ $(+)$ and $\langle \exp(-\Omega) \rangle_{(\Omega>0)}$ $(\times)$ for MD simulations of the ramp experiment with a deterministically derived dissipation function and in figure 5.8b we plot $\ln(P(\Omega = A)/P(\Omega = -A)$ vs Ω for MD simulations of the ramp experiment at $t = 3\tau$ with the expected result for the FT (red) for the same dissipation function. These plots use 150,000 trajectories, and $\tau = 1000$ MD steps for this simulation. These plots exhibits broadly the same behaviour as those from the experiment, figure 5.2, with the two curves in figure 5.8a converging at $t = 0, 3\tau$ and diverging at other times, and the results at 3τ obeying the FT, figure 5.8b. The response of the two curves in figure 5.8a to changes in the rate of $\dot{k}$ is very different to that of the experiment however.

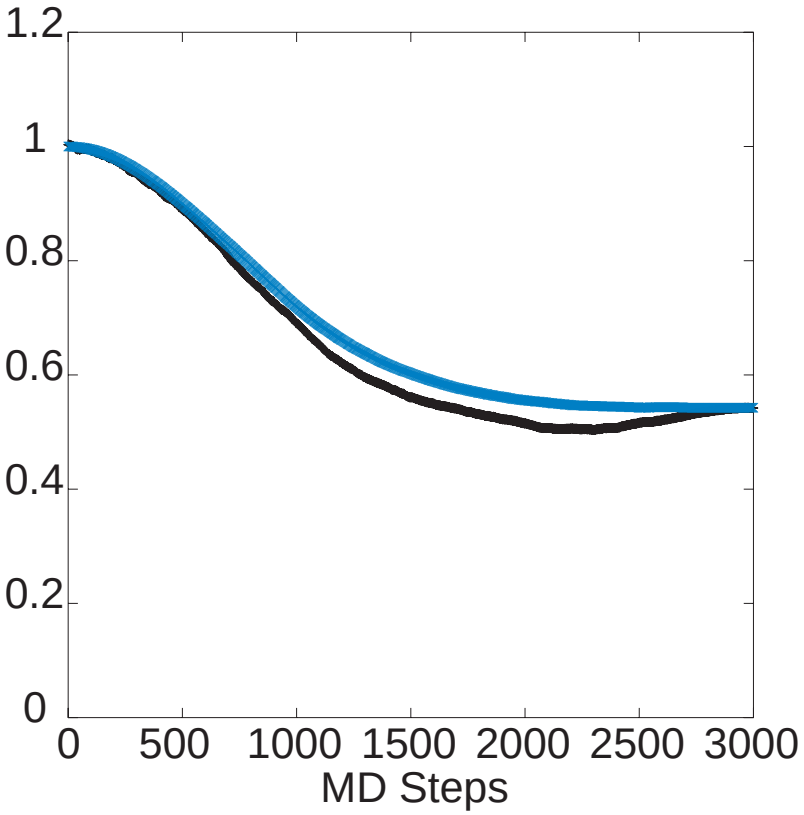
1.2
1
0.8
0.6
0.4
0.2
0
0 500 1000 1500 2000 2500 3000
MD Steps

(a)

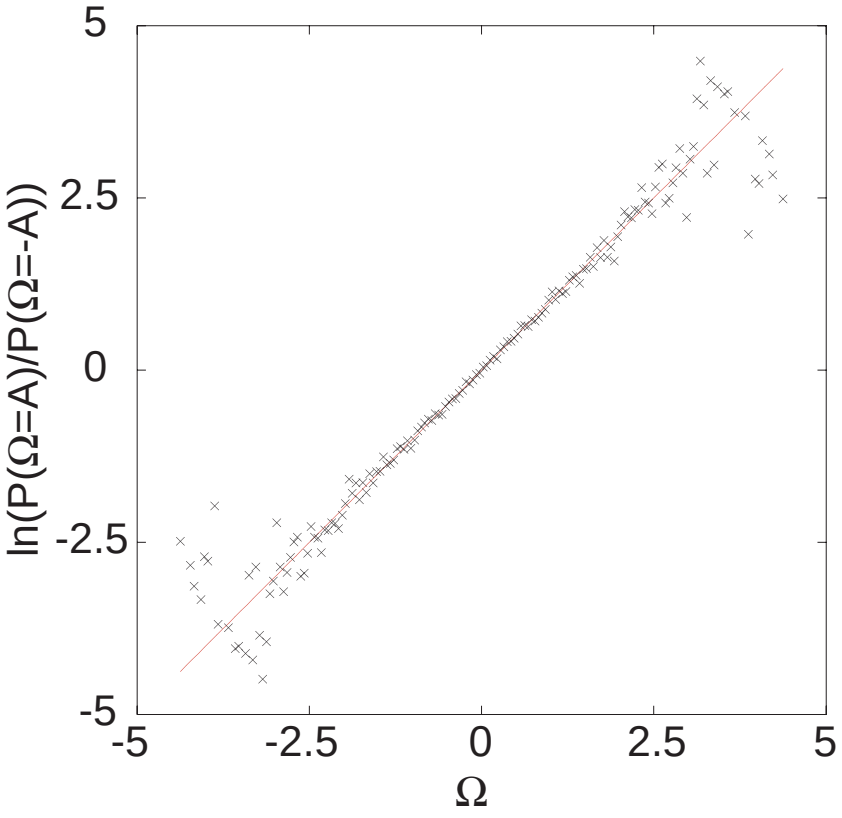
5
2.5
0
-2.5
-5
-5 -2.5 0 2.5 5
ln(P(Ω=A)/P(Ω=-A))
Ω

(b)

Figure 5.8

To derive the dissipation function, we apply equation :

$$\Omega = \frac{(x_t^2 - x_0^2)}{2k_BT}\sqrt{\frac{(k_0-k_1)\xi}{\tau\pi}}\exp(\frac{k_0^2\tau}{\xi(k_0-k_1)})(\frac{\exp(\frac{\tau(k_0+k_1)}{\xi})-1}{\mathrm{erf}(\frac{k_0}{\sqrt{\frac{(k_0-k_1)\xi}{\tau}}})-\mathrm{erf}(\frac{k_1}{\sqrt{\frac{(k_0-k_1)\xi}{\tau}}})}) \tag{5.14}$$

While this expression may look complicated, we see that for a set of values of k_0, k_1, ξ and τ, we can re-express it as;

$$\Omega = \frac{1}{2k_BT}[\mathbf{r}_t^2 - \mathbf{r}_0^2]\kappa(k_0, k_1, \tau, \xi) \tag{5.15}$$

which is very similar to the capture dissipation function.

Similarly, we can calculate the work function from equation ;

$$\begin{aligned}
W_d &= \ln(\sqrt{\frac{-\mathrm{i}k_0\exp(\frac{-\tau(k_0^2+k_1^2)}{\xi(k_0-k_1)})}{k_1}\frac{\mathrm{erf}(\frac{k_1}{\sqrt{\frac{\xi(k_1-k_0)}{\tau}}})-\mathrm{erf}(\frac{k_0}{\sqrt{\frac{\xi(k_1-k_0)}{\tau}}})}{\mathrm{erf}(\frac{k_0}{\sqrt{\frac{\xi(k_0-k_1)}{\tau}}})-\mathrm{erf}(\frac{k_1}{\sqrt{\frac{\xi(k_0-k_1)}{\tau}}})}}) \\
&+ \frac{1}{2k_BT}[k_1\mathbf{r}_t^2 - k_0\mathbf{r}_0^2 + \sqrt{\frac{\xi(k_0-k_1)}{\tau\pi}} \\
&\quad (\frac{(r_t\exp(\frac{\tau(k_1+k_0)}{2\xi})-r_0)^2\exp(-\frac{k_0^2\tau}{\xi(k_0-k_1)})}{\mathrm{erf}(\frac{k_1}{\sqrt{\frac{\xi(k_0-k_1)}{\tau}}})-\mathrm{erf}(\frac{k_0}{\sqrt{\frac{\xi(k_0-k_1)}{\tau}}})} \\
&+ \frac{\mathrm{i}(r_0\exp(\frac{\tau(k_1+k_0)}{2\xi})-r_t)^2\exp(\frac{k_1^2\tau}{\xi(k_0-k_1)})}{\mathrm{erf}(\frac{k_1}{\sqrt{\frac{\xi(k_1-k_0)}{\tau}}})-\mathrm{erf}(\frac{k_0}{\sqrt{\frac{\xi(k_1-k_0)}{\tau}}})})]
\end{aligned}$$

This expression does not simplify as easily as the dissipation function, but is still able to be evaluated.

Finally, we can derive the argument for the Hatano-Sasa relation. The Hatano-Sasa relation is much simpler to evaluate than the other fluctuation relation arguments under stochastic dynamics, as it does not require knowledge of the Greens function:

$$\begin{aligned}
Y &= \int_0^\tau dt\frac{d\lambda(t)}{dt}\frac{\partial(-\ln(P(\mathbf{r}(t),\lambda(t))))}{\partial\lambda}, &(5.16)\\
&= \int_0^\tau dt\frac{(k_1-k_0)}{2\tau}[\frac{r^2(t)}{k_BT} - \frac{1}{k_0(1-t/\tau)+k_1t/\tau}]. &(5.17)
\end{aligned}$$

This ease of derivation of the argument makes the Hatano-Sasa relation an attractive

fluctuation relation to apply to the ramp experiment. This function will obey the same relation as the normalised work relation: the ensemble average of its negative exponential will equal 1.

5.2.1 Experimental Results

The first results we present are for the fluctuation relations based on the dissipation function. The results for the integrated FT are presented in Figure 5.9a. The two sides of the integrated FT, $P(\Omega > 0)/P(\Omega < 0)$ and $\langle \exp(-a) \rangle_{\Omega>0}$, agree over the whole of the ramp. In addition, the plot of the FT at $t = 1s$ in Figure 5.9b shows strong agreement with the expected behaviour. This suggests that the FT is satisfied for $0 \leq t \leq \tau$ where the dissipation function is derived using stochastic dynamics for the ramp experiment. In Figure 5.9a, the ensemble average of the exponential of the negative of the dissipation function is plotted to demonstrate the PI. Despite some noise as the time goes towards 1s, the value of the average stays close to 1, the expected value for the PI.

The next set of results are those based on the normalised work function. In figures 5.11a and 5.11b we plot the distribution of the normalised work functions for the up ramp, $k(0) = 1.11$ pN/μm to $k(t) = 2.177$, and down ramp, $k(0) = 2.177$ pN/μm to $k(t) = 1.11$. It is interesting to note that these distributions are non-Gaussian, and not bounded by zero. To verify the WR we plot the ensemble average of the exponential of the normalised work function against the number of trajectories in Figure 5.13. It converges to 1, the expected value, verifying the WR for this experiment. Finally, for the normalised work function, figure 5.12 presents the CR for our system. In this plot there is far too much noise to in the data to say whether these results conform to the CR or not. This is surprising, as all the other results indicated agreement with the simulations.

The last experimental result is a plot of the ensemble average of the exponential of the Hatano-Sasa function with number of trajectories. As can be seen, the Hatano-Sasa relation very quickly converges to 1, and there is extremely little noise in the convergence. This confirms the Hatano-Sasa relation for the ramp experiment.

Figure 5.9: **Two figures showing FT results the for ramp experiment using a stochastically derived dissipation function.** In Figure 5.9a we plot dimensionless value vs time, for $P(\Omega < 0)/P(\Omega > 0)$ $(+)$, $\langle \exp(-\Omega) \rangle_{(\Omega>0)}$ $(\times)$, and $\langle \exp(-\Omega) \rangle$ $(\otimes)$ for the ramp experiment with a stochastically derived dissipation function, and in figure 5.9b, we plot $\ln(P(\Omega = A)/P(\Omega = -A)$ vs Ω for the ramp experiment at $t = \tau$ with the expected result for the FT (red) using the same dissipation function. These results were constructed with data from 2000 trajectories. In figure 5.9a, the two sides of the integrated FT agree over the whole period, and the PI average stays close to 1. In figure 5.9b, the experimental results conform to the prediction of the FT. This shows that the FT is satisfied at all times for the ramp experiment where a stochastically derived dissipation function is used.

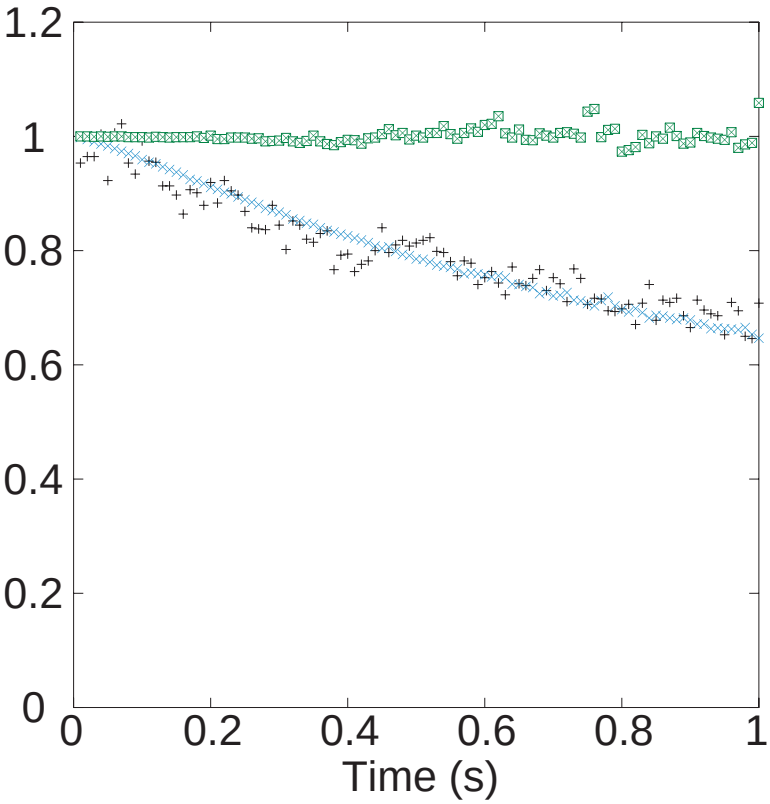

(a)

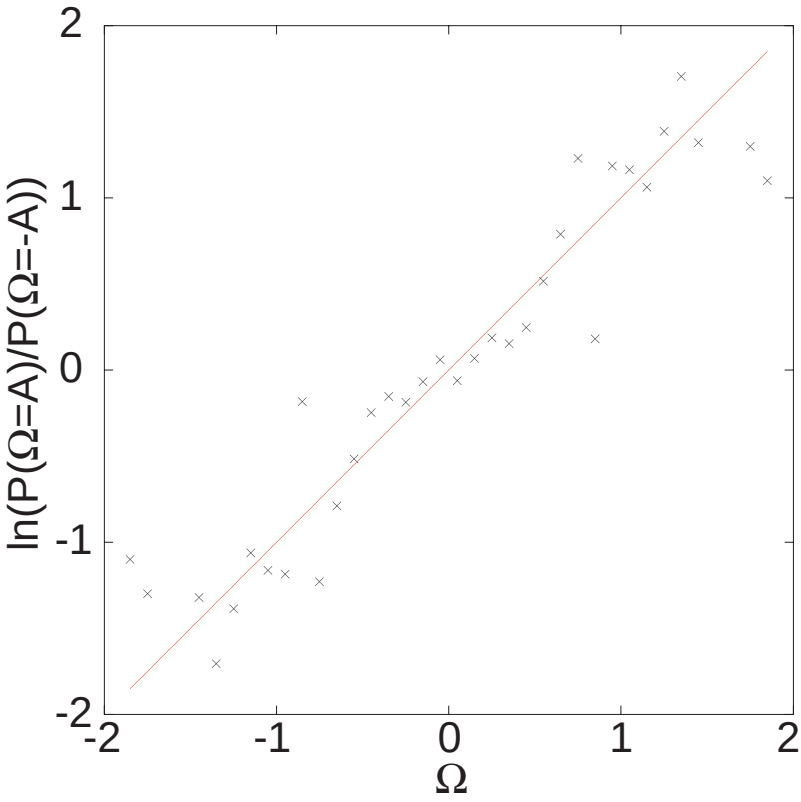

(b)

Figure 5.9

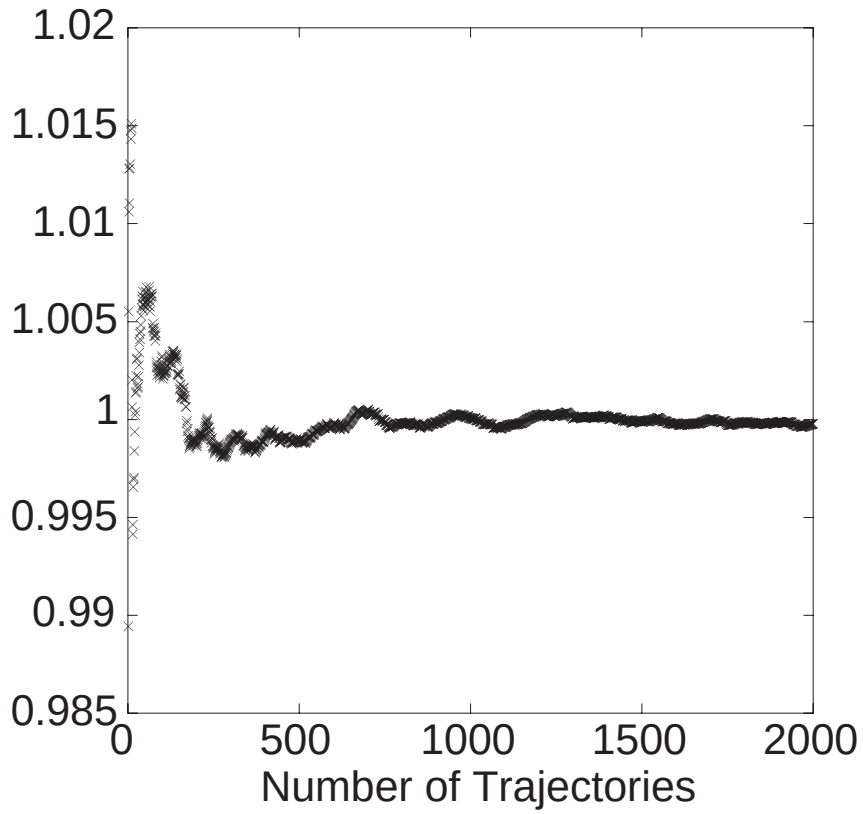

Figure 5.10: **Figure showing WR results for the ramp experiment with a stochastically derived normalised work function.** Dimensionless value vs number of trajectories for $\langle \exp(-\Delta W_d) \rangle$ ($\times$) over a 1 second change in trapping constants from $k(0) = 1.11$ pN/μm to $k(t) = 2.177$ pN/μm for the ramp experiment with a stochastically derived normalised work function. This converges to 1 confirming the WR for stochastically derived normalised work.

Figure 5.11: **Two figures showing the distribution of stochastically derived work for the ramp experiment.** In figure 5.11a we plot a histogram of stochastically derived normalised work trajectories over a 1 second change in trapping constants from $k(0) = 1.11$ pN/μm to $k(t) = 2.177$ pN/μm for the ramp experiment, and in figure 5.11b we plot a histogram of stochastically derived normalised work trajectories over a 1 second change in trapping constants from $k(0) = 2.177$ pN/μm to $k(t) = 1.11$ pN/μm for the ramp experiment. Both histograms contain 2000 trajectories. These distributions are strongly asymmetric and non-Gaussian, with non-zero variance and maximum probability density. This demonstrates that the system is not in the quasi-static or instantaneous limit, but in the finite time, non-equilibrium range that we wished to study. It is also interesting to note that these distributions are not all positive or all negative, this is quite different from the deterministically derived work, figure 5.4.

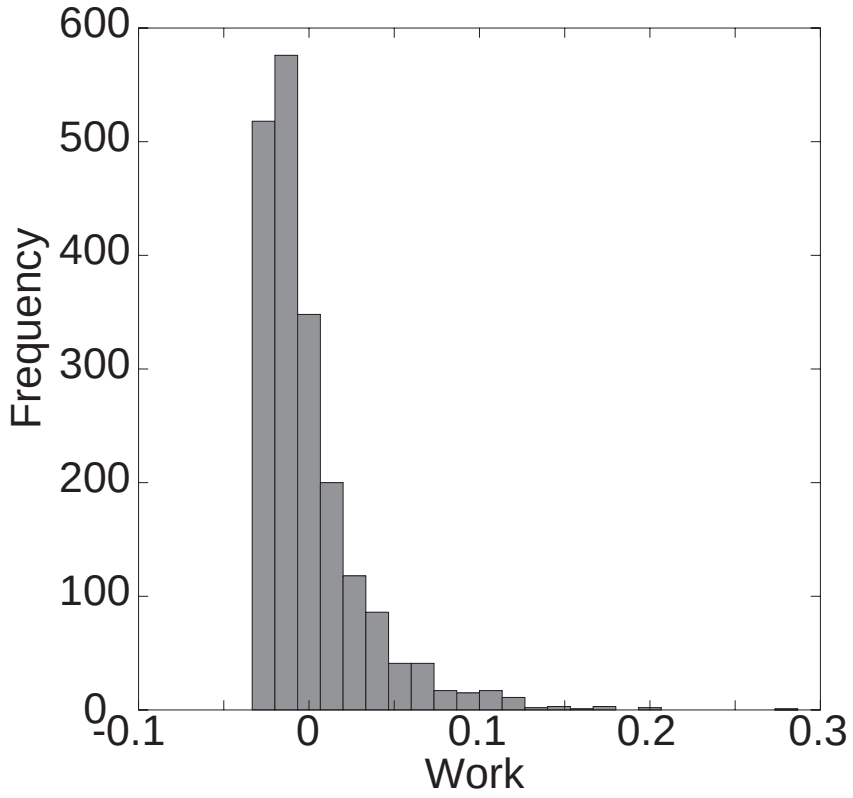

(a)

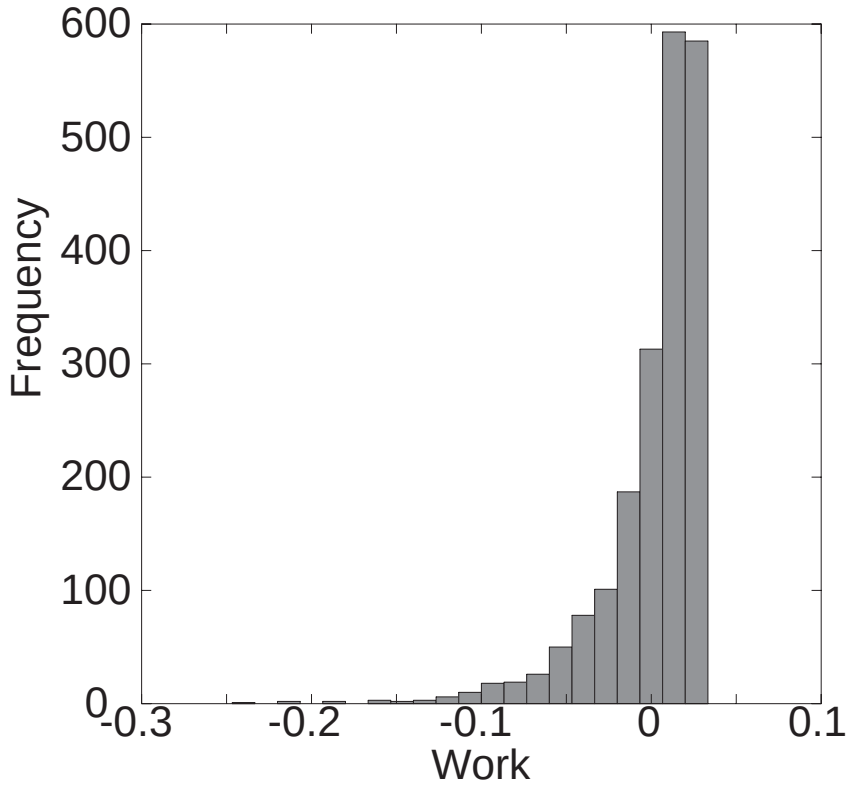

(b)

Figure 5.11

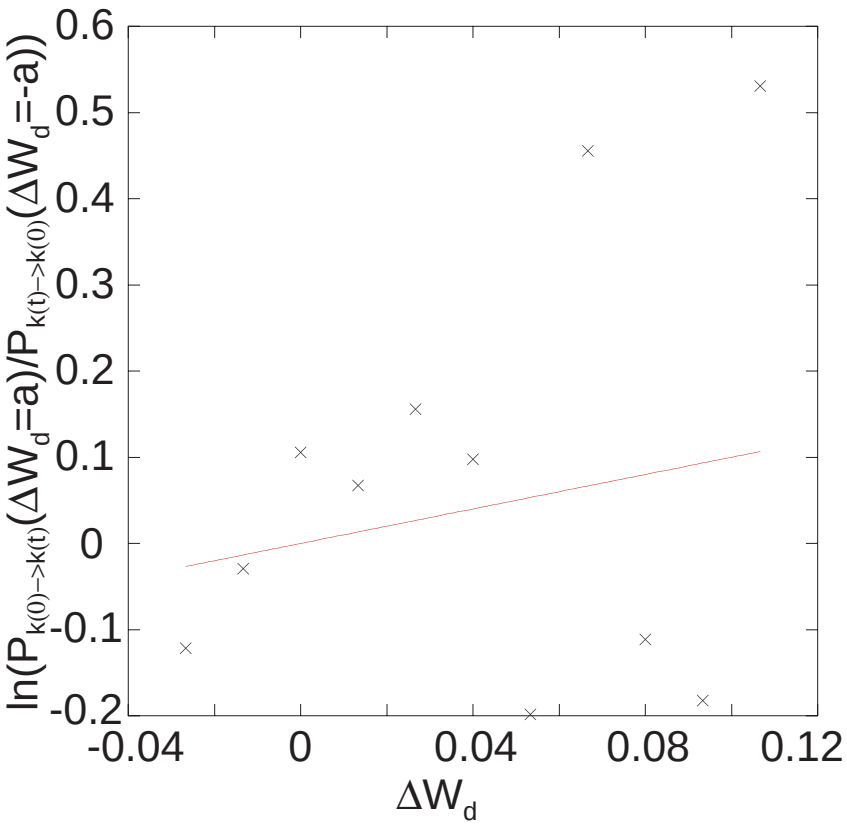

Figure 5.12: **Figure showing CR for the ramp experiment using a stochastically derived normalised work function.** $\ln[P_{k(0)\to k(t)}(\beta\Delta W_d = a)/P_{k(t)\to k(0)}(\beta\Delta W_d = -a)]$ vs (ΔW_d) with the expected result for the CR (red) for the ramp experiment using a stochastically derived normalised work function over two 1 second ramps with $k(0) = 1.11$ pN/μm to $k(t) = 2.177$ pN/μm. There is far too much spread in the data to identify a trend, so we are unable to tell if the CR is obeyed in this experiment for a stochastically derived normalised work function.

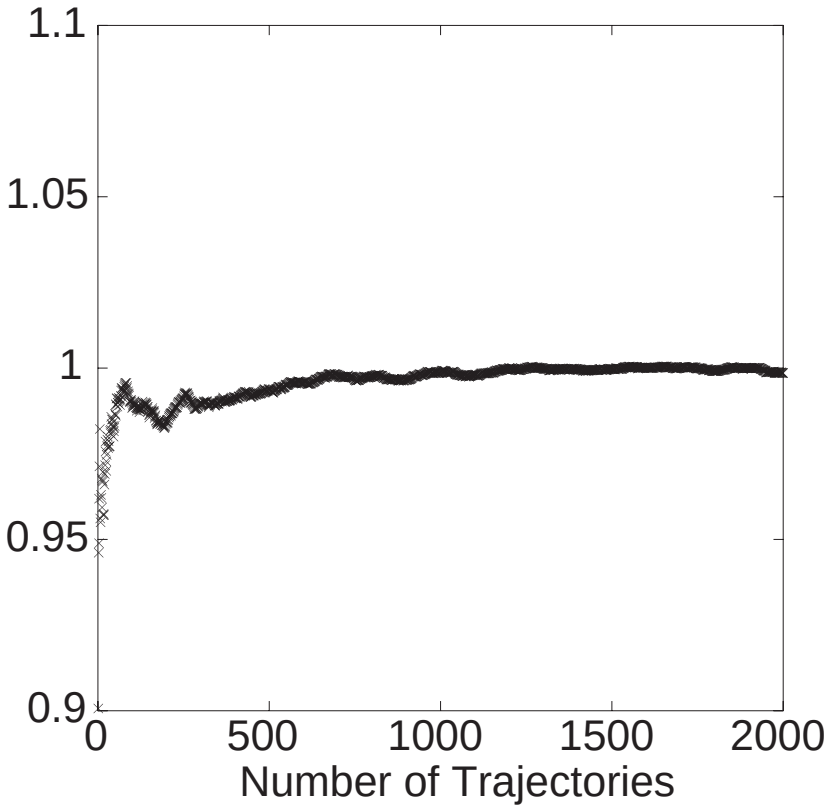

Figure 5.13: **Figure showing the Hatano-Sasa relation for the ramp experiment.** Dimensionless value vs number of trajectories for $\langle \exp(-Y) \rangle$ ($\times$) over a 1 second change in trapping constants from $k(0) = 1.11$ pN/μm to $k(t) = 2.177$ pN/μm for the ramp experiment with a stochastically derived Hatano-Sasa function. This converges to 1 confirming the Hatano-Sasa relation for the ramp experiment. It is worth noting the extremely small range of fluctuations in this average.

5.2.2 Simulation Results

We can perform stochastic simulations with comparable behaviour to our experiment. The advantage of these simulations over the experiment is that we can perform many more repetitions and get better statistics. In the experiment, the theorems that relied on averages such as the WR and PI performed as expected. The relations that were based on probability ratios, such as the FT and CR, while often consistent with expectation, showed some spread from the expected behaviour. In this section we present results from simulations with the same parameters as the experiment to demonstrate that this spread is due to a lack of sampling rather than a failure of the relations. The experimental parameters used for this simulation are designed to match those in the experiment, table 5.1, but with 3×10^7 trajectories performed.

We present results here for both stochastic and deterministic FT and CR, figures 5.14 and 5.15. With more samples we can see that these relations conform to our expectations, even where the experimental results were inconclusive, such as for stochastic Crooks, figure 5.15b. In all of these figures however, there is still some deviation at the extremes of the range of sampled data. This is due to the low probability of sampling these regions. As more samples are taken, the deviation will just move out further to the edges of the distribution, as we sample less and less probable regions where previously we had no samples at all.

5.3 Discussion

The ramp experiment tests and verifies all of the fluctuation relations under both stochastic and deterministic dynamics. In doing so, the ramp experiment provides information about the behaviour of some of the relations, and the interplay between the different dynamic frameworks.

The FT was the first of the fluctuation relations to be derived, and has been verified on numerous occasions. The ramp experiment provides information on when the FT can and can not be applied to a system. Under deterministic dynamics, the dissipation function is undefined except at the beginning and end of the experiment, and therefore the FT cannot be applied at intermediate times. In contrast, the

dissipation derived under stochastic dynamics is valid over intermediate times of the experiment, and therefore there is a practical benefit to using stochastic dynamics to derive the dissipation function over deterministic dynamics.

The ramp experiment was originally designed to verify the WR, and it successfully does so. The WR can be used to measure the free energy change for an experimental system, and is satisfied for both deterministically and stochastically derived work. The utility of the work relation comes from the fact that the partition functions for, and therefore the free energy difference between, the two equilibrium states are not required to be known analytically. However when applying stochastic dynamics to the ramp experiment, we do know the partition functions, making the use of the stochastic work to find the free energy change redundant. This is not a fault of the ramp experiment, as the system was chosen because it had a known free energy change. It does however make the WR redundant under stochastic dynamics for this system.

Analysing a system using different dynamics can solve difficulties in applying the fluctuation relations, as shown by the FT and WR results for the ramp experiment. However, not all systems can be easily analysed under multiple dynamic frameworks. For instance, a small change in the details of the ramp experiment, such as making the particle the same size as the solvent particles (as was done for the MD simulations), would mean that we would not be able to apply inertialess stochastic dynamics to the system. In this case, deterministic dynamics would be the only practical way to describe the system. The details of the system will decide what dynamics, and by extension what fluctuation relations, will be applicable.

The information provided by the ramp experiment was constrained by the number of trajectories available. With 2000 trajectories, all of the fluctuation relations could be demonstrated except the CR with a stochastic argument. Of the other relations, the least compelling results were those for the CR with a deterministic argument. This is interesting as there is nothing in the form of the CR to suggest that it should fare worse than the FT when it comes to convergence. Indeed, given that the FT compares the ratio of low probability trajectories with high probability trajectories in the same ensemble, while Crooks compares the ratio of what would be expected

Figure 5.14: **Two figures showing the FT and CR with deterministic arguments for stochastic ramp simulations.** In figure 5.14a we plot $\ln(P(\Omega = A)/P(\Omega = -A)$ vs Ω for a stochastic simulation of the ramp experiment at $t = 3\tau$ with the expected result for the FT (red) using a deterministically derived dissipation function and in figure 5.14b we plot $\ln[P_{k(0)\to k(t)}(\beta\Delta W = a)/P_{k(t)\to k(0)}(\beta\Delta W = -a)]$ vs $(\Delta W - \Delta A)$ with the expected result for the CR (red) for a stochastic simulation of the ramp experiment using a deterministically derived work function over two 1 second ramps with $k(0) = 1.11$ pN/μm to $k(t) = 2.177$ pN/μm. These figures both contain 3×10^7 trajectories, and both of these figures conform to the expected relationships. This verifies the FT at $t = 3\tau$, and the CR for the ramp experiment using deterministically derived functions.

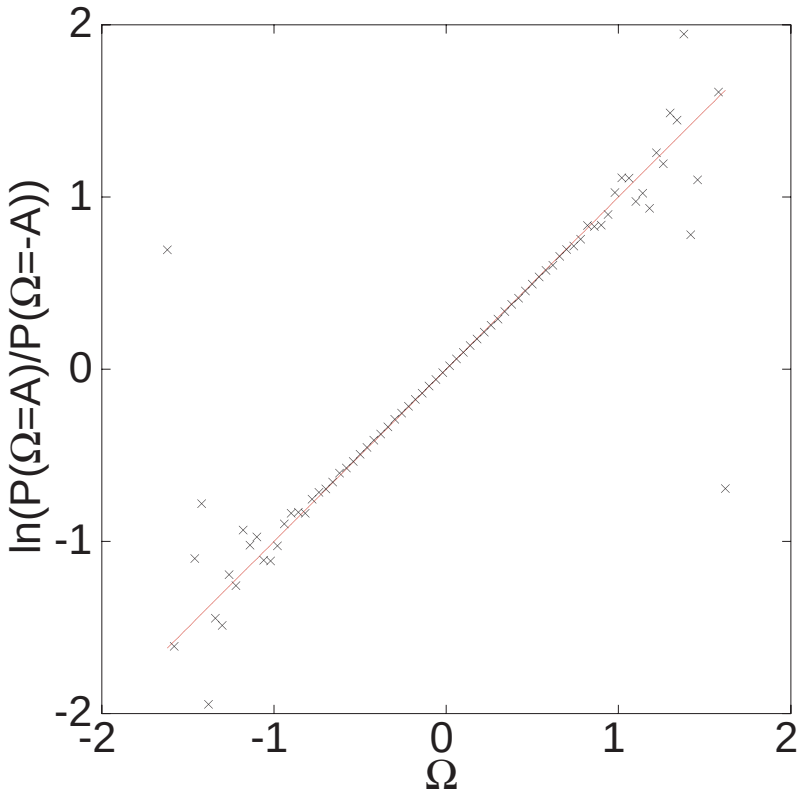

(a)

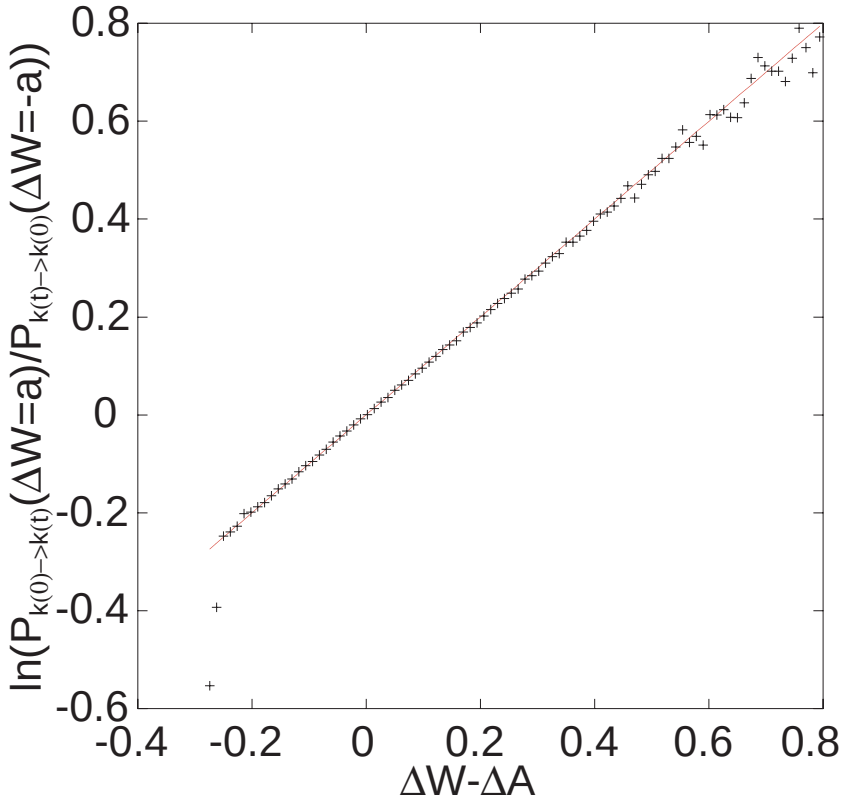

(b)

Figure 5.14

Figure 5.15: **Two figures showing the FT and CR with stochastic arguments for stochastic ramp simulations.** In figure 5.14a we plot $\ln(P(\Omega = A)/P(\Omega = -A)$ vs Ω for a stochastic simulation of the ramp experiment at $t = 3\tau$ with the expected result for the FT (red) using a stochastically derived dissipation function and in figure 5.14b we plot $\ln[P_{k(0)\to k(t)}(\beta\Delta W = a)/P_{k(t)\to k(0)}(\beta\Delta W = -a)]$ vs $(\Delta W - \Delta A)$ with the expected result for the CR (red) for a stochastic simulation of the ramp experiment using a stochastically derived work function over two 1 second ramps with $k(0) = 1.11$ pN/μm to $k(t) = 2.177$ pN/μm. These figures both contain 3×10^7 trajectories, and both of these figures conform to the expected relationships. This verifies the FT at $t = 3\tau$, and the CR for the ramp experiment using stochastically derived functions.

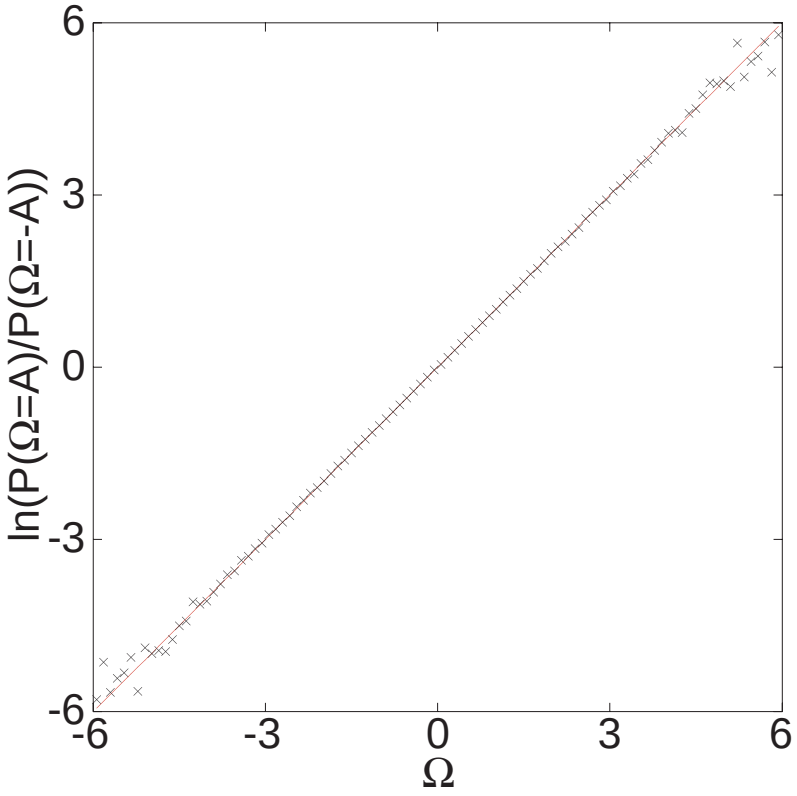

(a)

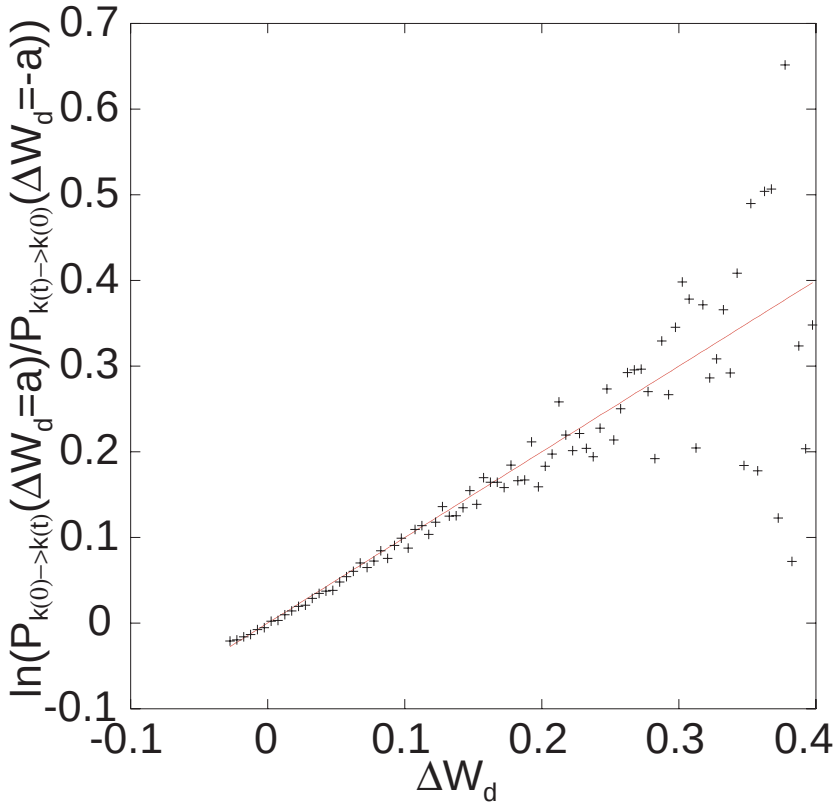

(b)

Figure 5.15

to be high probability trajectories in one ensemble with high probability trajectories in another ensemble, it might be expected that Crooks would present better with fewer samples. As can be seen under stochastic dynamics, the stochastic FT can be clearly demonstrated with only 2000 trajectories figure 5.9a, while Crooks takes many more, figure 5.15b.

The requirement for a large number of samples for the CR makes the WR a preferable method to Crooks for measuring the free energy change in this system. Not only does the WR produce a result with less samples than Crooks, but it also only requires the transformation between states to be carried out in one direction. When we compare the WR to the equilibrium sampling method however, the equilibrium sampling method is significantly faster in time. It is important to note that this experiment was designed to verify the WR. In order to fully compare the different methods experimentally, the ramp experiment would have to be repeated over a wide range of trapping constants, k_0 and k_1, and ramp times, τ.

Finally, it is worth making an observation about the different stochastic arguments. All of the stochastic arguments, normalised work, dissipation, and the argument to the Hatano-Sasa relation have the same ensemble average for the exponential of the function for this experiment. Where they differ is in the distribution of the functions: the dissipation obeys the FT, the normalised work the WR, and Hatano-Sasa has no comparable relation. Just because a random function has the right ensemble average does not mean that it has the right distribution to satisfy the associated fluctuation relation.

Bibliography

[1] G. M. Wang, E. M. Sevick, E. Mittag, D. J. Searles, D. J. Evans, *Phys. Rev. Lett.* **89**, 050601 (2002).

[2] G. M. Wang, J. C. Reid, D. M. Carberry, D. R. M. Williams, E. M. Sevick, D. J. Evans, *Phys. Rev. E* **71**, 046142 (2005).

[3] D. M. Carberry, J. C. Reid, G. M. Wang, E. M. Sevick, D. J. Searles, D. J. Evans, *Phys. Rev. Lett.* **92**, 140601 (2004).

[4] J. Liphardt, S. Dumont, S. Smith, I. T. Jr., C. Bustamante, *Science* **296**, 2832 (2002).

[5] F. Douarche, S. Ciliberto, A. Petrosyan, I. Rabbiosi, *Europhysics Letters* **70**, 593 (2005).

[6] M. Allen, D. J. Tildesley, *Computer Simulation of Liquids* (Oxford University Press, 1987).

Chapter 6

Discussion and Conclusion

The fluctuation theorem (FT) quantifies the fundamental behaviour of physical systems. The work relation (WR) provides a connection between a state function and a fluctuating variable. The primary aim of this thesis has been to explore the connection of these two theorems, and to understand their application to real physical systems. In doing this, we have produced a number of novel results:

- A general derivation of the two relations, section 2.1.
- The mathematical connection between the arguments of the FT and WR, section 2.1.
- A new fluctuation relation, the conjugate work relation, section 2.1.
- A stochastic definition of the arguments of the fluctuation relations for Langevin dynamics, section 3.2.2.
- A number of experimental demonstrations of the FT for stochastically derived dissipation functions, chapters 4 and 5.
- A demonstration of the FT for multiple stochastically derived dissipation functions in a single experiment, section 4.2.2.
- A demonstration of a non-asymptotic dissipation function applied to a non-equilibrium steady state, section 4.3.2.
- A verification of the WR against a known free energy change, section 5.1.1.

- A demonstration of the CR for an optical trapping system, section 5.1.1.
- A demonstration of all the fluctuation relations (FT, WR, PI, Crooks, CWR, Hatano-Sasa) in one experiment, chapter 5.
- A demonstration of the time symmetry in the external parameters required for the FT to be valid under deterministic dynamics, section 5.1.1.

These results broaden our understanding of the various fluctuation relations that can be applied in thermodynamic systems. The results in chapter 2, show that the fluctuation relations are a closely connected set of relations that are valid under extremely general conditions. In chapters 3 and 4, we took advantage of these general conditions to apply the FT to experimental systems in a new way, by using a dissipation function derived under stochastic dynamics. Finally, in chapter 5, we demonstrated the various relations in the context of a single experiment.

These results raise a number of avenues worthy of further research. A general approach to applying these fluctuation relations should lead to a number of new and interesting systems being quantified with these relations. In particular, the application of the fluctuation relations to systems that can be described by stochastic dynamics may enable probing of previously intractable problems, similar to its application in section 4.3.2. Also of interest is the utility of the various relations in measuring free energy differences. In this work we have shown that the WR and Crooks *can* measure free energy differences. When looking at new systems however, there is a question of whether we *should* use these relations, or whether others may be more appropriate. Hopefully this thesis will encourage others to examine these questions in the future.

Appendix A

Derivation of the Green's function for the ramp system

This derivation is by Dr. E.M. Sevick, and is used to derive stochastic arguments in chapter 5. It has been abridged, and any mistakes are in the reproduction, not the original.

A.0.1 For constant trap strength

For a constant trap strength, the particle motion follows the Langevin equation where the random force term is such that its mean is zero

$$\langle f(t) \rangle = 0 \tag{A.1}$$

and its time-correlation is

$$\langle f(t) f(t') \rangle = 2\xi k_B T \delta(t - t') \tag{A.2}$$

The distribution of x is Gaussian at all times as displacements suffered by the particle are simply a linear combination of Gaussian terms, *i.e.*, the random forces, $f(t)$. That is, we can write down a general from of the Green function as

$$G(x; x_0, t) = \frac{1}{\sqrt{2\pi B(t)}} \exp\left[-\frac{(x - A(t))^2}{2B(t)}\right] \tag{A.3}$$

where

$$A(t) = \langle x(t) \rangle \tag{A.4}$$

and

$$B(t) = \langle (x(t) - A(t))^2 \rangle \tag{A.5}$$

So the aim is to solve the Langevin equation for $A(t)$ and $B(t)$. Rewrite the Langevin equation in the form

$$\frac{dx}{dt} + \frac{1}{\tau}x = \frac{f(t)}{\xi}. \tag{A.6}$$

We can solve this by introducing an integrating factor. For any equation of the form

$$\frac{dy}{dx} + P(x)y = Q(x), \tag{A.7}$$

you can introduce an integrating factor of the form $\mu(x) = \exp\left[\int dx P(x)\right]$:

$$\begin{aligned}
\mu(x)\frac{dy}{dx} + \mu(x)P(x)y &= \mu(x)Q(x) && \text{(A.8)}\\
\frac{d}{dx}(y\mu(x)) &= \mu(x)Q(x) && \text{(A.9)}\\
y\mu(x) &= \int dx \mu(x)Q(x) && \text{(A.10)}\\
y &= \frac{(\int dx \mu(x)Q(x) + C)}{\mu(x)} && \text{(A.11)}
\end{aligned}$$

where C is a constant of integration to be determined by an initial condition. Thus, an appropriate integrating factor for the Langevin equation is $\mu(t) = \exp[t\tau]$ so that a solution with initial condition $x(t=0) = x_0$ is

$$\begin{aligned}
x(t) &= \exp[-t/\tau](x_0 + \frac{1}{\xi}\int_0^t dt' \exp[t'/\tau] f(t')) && \text{(A.12)}\\
&= x_0 \exp[-t/\tau] + \frac{1}{\xi}\int_0^t dt' \exp[-(t-t')/\tau] f(t'). && \text{(A.13)}
\end{aligned}$$

Now we need to express the mean, $\langle x(t) \rangle \equiv A(t)$:

$$\begin{aligned}
\langle x(t) \rangle &= x_0 \exp[-t/\tau] + \frac{1}{\xi}\int_0^t dt' \exp[-(t-t')/\tau] \langle f(t') \rangle && \text{(A.14)}\\
&= x_0 \exp[-t/\tau]. && \text{(A.15)}
\end{aligned}$$

Now to find $B(t) = \langle (x(t) - A(t))^2 \rangle$, you can see that

$$x(t) - A(t) = \frac{1}{\xi} \int_0^t dt' \exp[-\frac{(t-t')}{\tau}] f(t') \tag{A.16}$$

so that

$$[x(t) - A(t)] \times [x(t) - A(t)] = \frac{1}{\xi} \int_0^t \exp[-\frac{(t-t')}{\tau}] f(t') \times \frac{1}{\xi} \int_0^t \exp[-\frac{(t-t'')}{\tau}] f(t'') \tag{A.17}$$

or

$$\begin{aligned} B(t) &= \frac{1}{\xi^2} \int_0^t dt' \int_0^t dt'' \exp[-\frac{(2t-t'-t'')}{\tau}] \langle f(t') f(t'') \rangle & \text{(A.18)} \\ &= \frac{1}{\xi^2} \int_0^t dt' \exp[-\frac{2(t-t')}{\tau}] \times 2\xi k_B T & \text{(A.19)} \\ &= \frac{k_B T}{k} \times (1 - \exp[-\frac{2t}{\tau}]) & \text{(A.20)} \end{aligned}$$

Inserting these expressions for $A(t)$ and $B(t)$ into the general Gaussian form of the Green function gives the resulting function for a trap of constant strength.

A.0.2 For time-varying trap strength

All of the steps above can be followed to derive a new Green function for a time-dependent trapping constant. We cast the Langevin equation as:

$$\frac{dx}{dt} + \frac{k(t)}{\xi} x = \frac{1}{\xi} f(t), \tag{A.21}$$

and use an integrating factor

$$\mu(t) = \exp[\int_0^t ds \frac{k(s)}{\xi}]. \tag{A.22}$$

Following Prabhakar [R. Prabhakar], we express the Green's function in terms of this integrating factor, μ. In our problem, we want to use a linear ramp function for trap strength: $k(t) = k_0 + \dot{k}t$. But for now we will keep the problem cast in general terms. So, multiplying the integration factor, $\mu(s)$, through the Langevin expression

yields

$$\frac{d}{ds}(x\mu(s)) = \frac{\mu(s)f(s)}{\xi} \tag{A.23}$$

$$\int d(x\mu(s)) = \frac{1}{\xi}\int ds\mu(s)f(s) \tag{A.24}$$

$$x\mu(t) = \frac{1}{\xi}\int ds\mu(s)f(s) + C \tag{A.25}$$

$$x(t) = \frac{1}{\mu(t)}(\frac{1}{\xi}\int ds\mu(s)f(s) + C) \tag{A.26}$$

Using the initial condition $x(t=0) = x_0$ and substituting in for the integrating factor,

$$x(t) = \frac{1}{\mu(t)}(\frac{1}{\xi}\int_0^t ds\mu(s)f(s) + x_0\mu(0)) \tag{A.27}$$

Once again, as the mean random force is zero,

$$A(t) \equiv \langle x(t)\rangle = x_0\frac{\mu(0)}{\mu(t)} \tag{A.28}$$

and as $B(t) \equiv \langle (x(t) - A(t))^2\rangle$,

$$\begin{aligned}
[x(t) - A(t)] \times [x(t) - A(t)] &= \frac{1}{\mu(t)\xi}\int_0^t ds\mu(s)f(s) \times \frac{1}{\mu(t)\xi}\int_0^t ds'\mu(s')f(s') \\
&= \frac{1}{(\mu(t)\xi)^2}\int_0^t\int_0^t dsds'\mu(s)\mu(s')f(s)f(s') \\
B(t) &= \frac{1}{(\mu(t)\xi)^2}\int_0^t\int_0^t dsds'\mu(s)\mu(s')\langle f(s)f(s')\rangle \\
&= \frac{2\xi k_BT}{(\mu(t)\xi)^2}\int_0^t ds\mu^2(s)
\end{aligned}$$

So the Green's function appears as

$$\begin{aligned}
G(x;x_0,t) &= \sqrt{\frac{\xi}{4\pi k_BT\int_0^t ds\frac{\mu^2(s)}{\mu^2(t)}}} \\
&\times \exp\left[-\frac{\xi}{4k_BT\int_0^t ds\frac{\mu^2(s)}{\mu^2(t)}}(x - x_0\frac{\mu(0)}{\mu(t)})^2\right]
\end{aligned}$$

Now, this function IS indeed properly formulated. But it states that the variance in x vanishes in the limit of t, or δt as we will later assign it, going to 0. This is correct.

Appendix B

The FT with a non-Gaussian starting distribution.

The harmonic potential in the optical trapping system produces a Gaussian distribution of particle positions at equilibrium. While we have demonstrated experimentally that the FT applies where the distribution of the dissipation function is non-Gaussian, we have not shown that it applies to systems with a non-Gaussian distribution of system co-ordinates. In this section, we present a model system based on optical trapping but with a non-Gaussian initial distribution. With this system, known as the tan distribution system, we will demonstrate the FT using a stochastic simulation.

The tan distribution system is based on the optical trapping system. We have a colloid particle suspended in solution that is subject to a potential that generates a non-Gaussian distribution function. At $t = 0$, we instantaneously change the potential to a harmonic potential of trapping constant k, and measure the particle position as the system relaxes. This simulation is the as the capture experiment except for a different initial distribution.

The starting point for the tan distribution system is the starting distribution of particle positions:

$$P(\mathbf{r}_0) = \frac{1}{1 + \mathbf{r}_0^2}, \tag{B.1}$$

as we do not need to know the potential to derive the dissipation function, or to

Table B.1: Parameters for the tan distribution experiment

k	$0.5pN/\mu m$
τ	1s
Trajectories	1000000

carry out our simulation. This distribution was chosen as it can be sampled quickly using a random number generator;

$$\mathbf{r}_0 = \tan(\pi * iseed/2) \tag{B.2}$$

where $iseed$ is our random number produced by our quasi random number generator, $0 < iseed < 1$. A second random number is used to choose the sign of $\mathbf{r}_0$, with equal probability of a positive or negative value.

The simulation begins at the point where the potential is changed to a harmonic, therefore the only equations of motion are those for a stochastic particle in a trap of strength k. This gives us the same Greens function as was used in the capture experiment, equation 4.6. This, combined with our starting distribution, can be substituted in equation 3.28, to generate our dissipation function:

$$\Omega = \ln\left(\frac{1+\mathbf{r}_t^2}{1+\mathbf{r}_0^2}\right) - \frac{k}{2k_BT}(\mathbf{r}_t - \mathbf{r}_0). \tag{B.3}$$

The first term comes from the distribution, while the second term comes from the dynamics. For our simulations we worked in scaled units so that our values of k were in pico-Newtons per micro-metre and our distances were in micro-metres. These correspond with the experimental scales for an optical tweezers experiment. The parameters are presented in table B.1.

In Figure B.1a, we present an integrated form of the FT, and demonstrate the agreement of the FT at all times for this system. The asymptotic behaviour of this plot suggests that the system has relaxed almost to the new equilibrium by 1s. The reason this plot does not asymptote to zero however, is that there is always a finite chance of negative dissipation. In Figures B.1b and B.1c we present the FT directly at a point in the transient regime, 0.05s, and a point in the equilibrium regime,

1s. All of these results demonstrate the FT for our system, despite the lack of an exponential distribution for the colloid particle or the dissipation function.

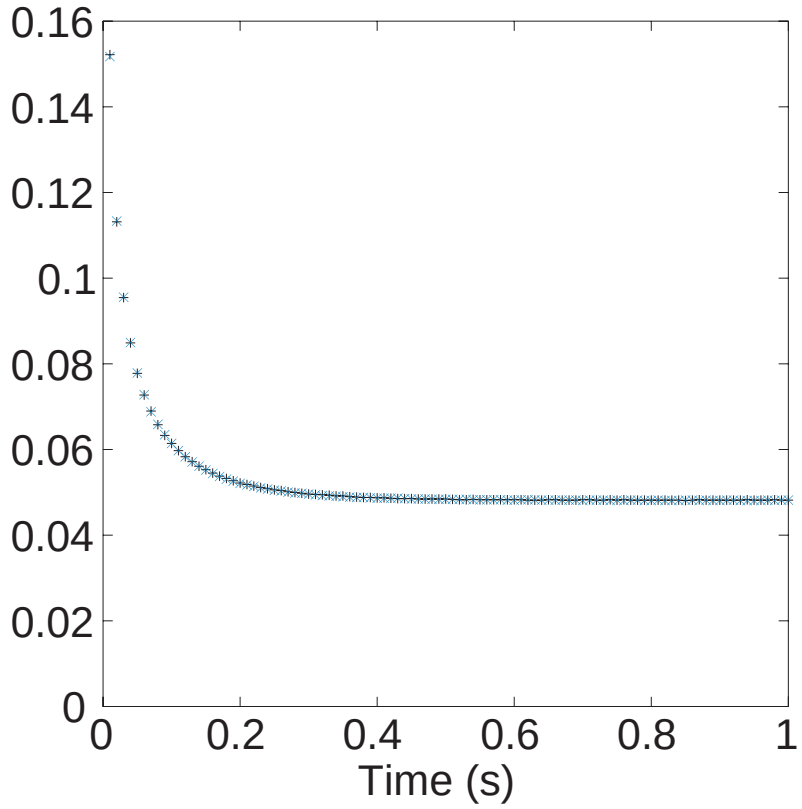

(a)

Figure B.1: **Three figures showing FT and integrated FT results for the tan distribution experiment.** In figure B.1a, we plot dimensionless value vs time, t, for $P(\Omega < 0)/P(\Omega > 0)$ $(+)$ and $\langle \exp(-\Omega) \rangle_{(\Omega>0)}$ $(\times)$ for the tan distribution experiment, and in figures B.1b and B.1c we plot $\ln(P(\Omega = A)/P(\Omega = -A)$ vs Ω for the tan distribution experiment with the expected result for the FT (red) for times of $t = 0.05$s and $t = 1$s respectively. In figure B.1a the two curves are co-incident, demonstrating the integrated form of the FT, and in figures B.1b and B.1c the data strongly agrees with the prediction of the FT. This shows that the FT is obeyed even where there is a non-Gaussian starting distribution.

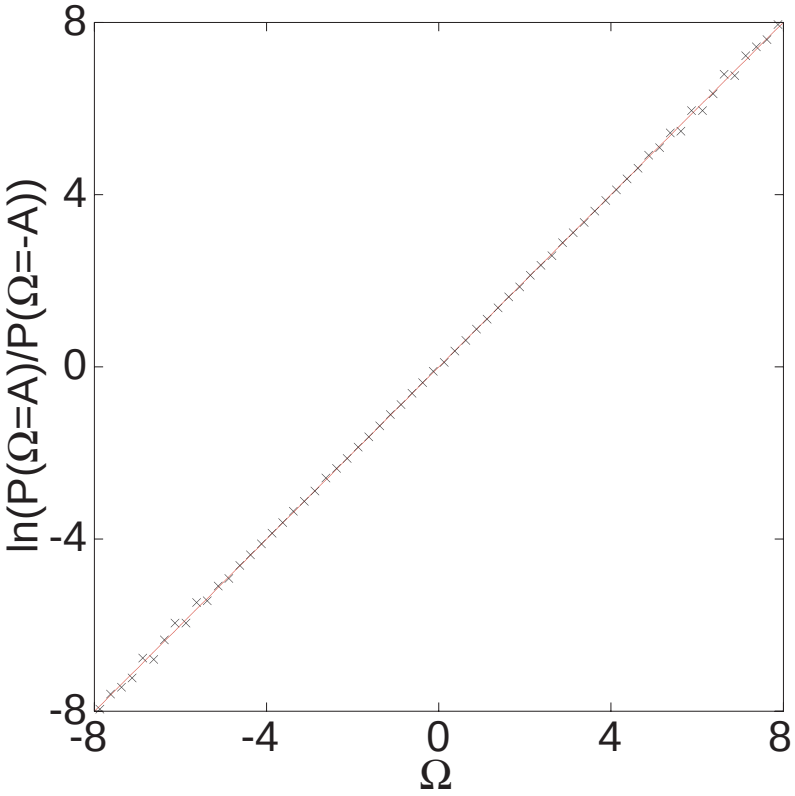

(b)

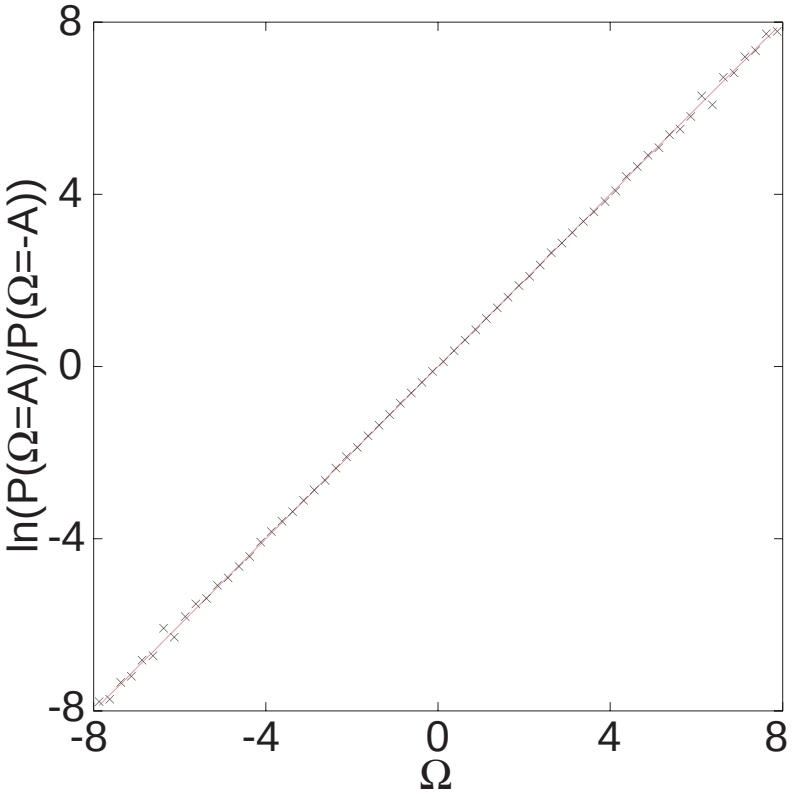

(c)

Figure B.1

Appendix C

List of Common Abbreviations/Symbols

CR: CR

CWR: Conjugate Work Relation

FT: Fluctuation Theorem

MD: Molecular Dynamics Simulation

PI: Partition Identity

WR: Work Relation

k: Trapping Constant

z: Partition Function

$\Delta W_{(d)}$: Work (Normalised)

λ: Time Dependent External Parameter

Ω: The Dissipation Function

$\omega_{(d)}$: Conjugate Work (Normalised)